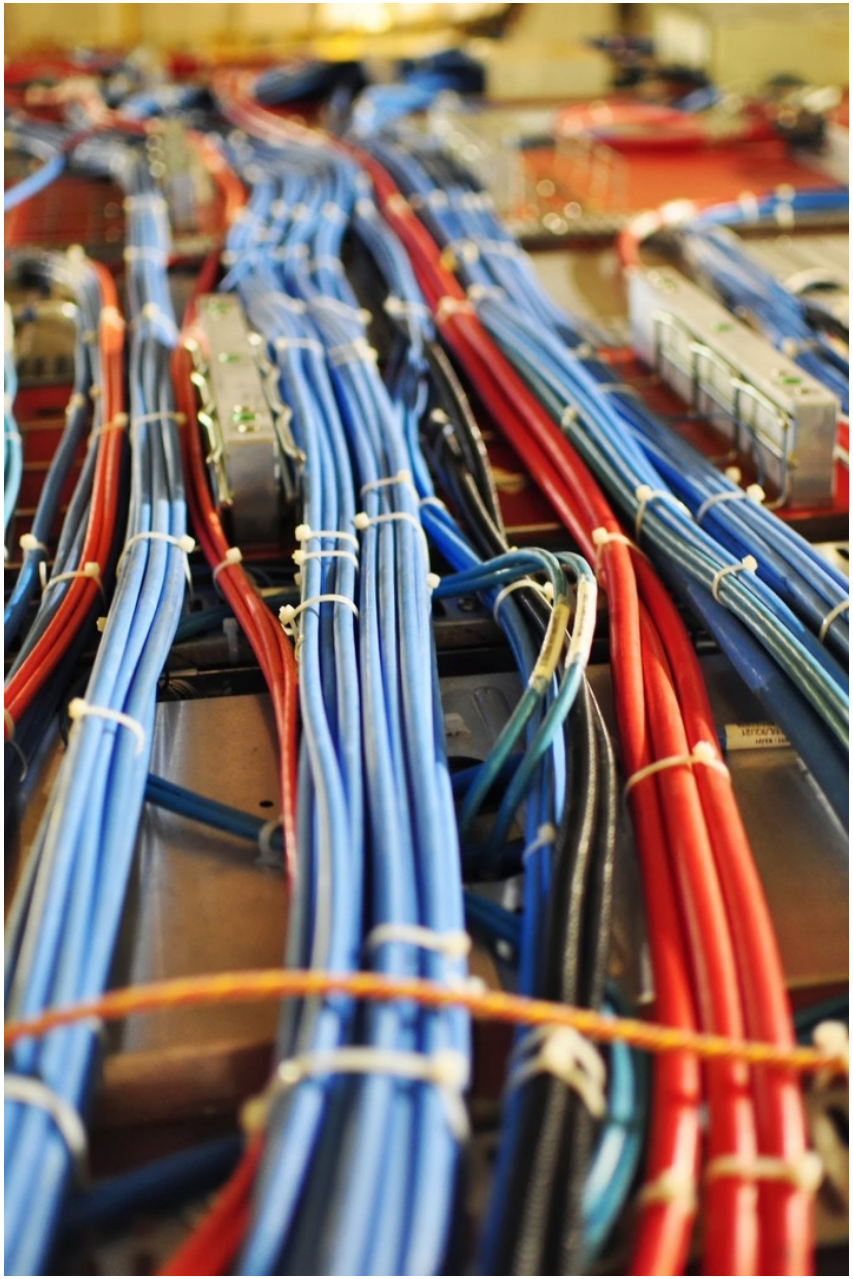

2. Muon detectors and performance

Piet Verwilligen

INFN Sezione di Bari

Capita Selecta in HEP
Vrije Universiteit Brussel
April 9-10, 2014

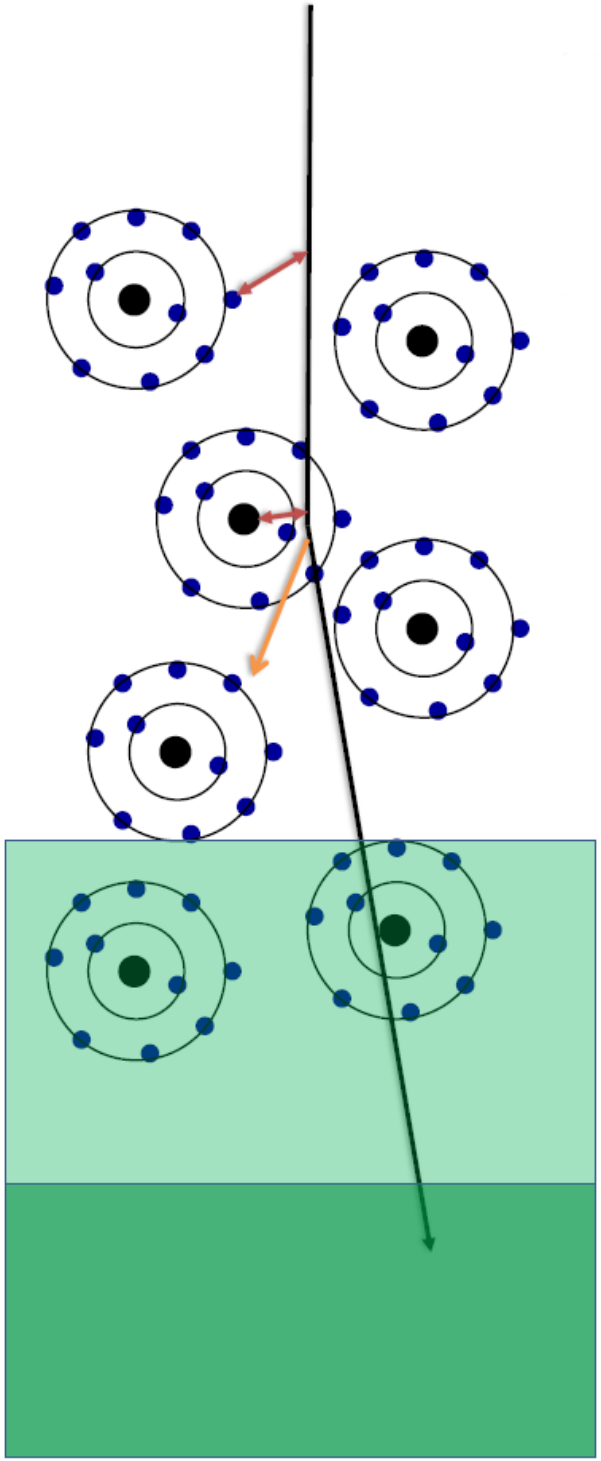

Interaction of Particles with Matter

Electromagnetic Interaction of Particles with Matter

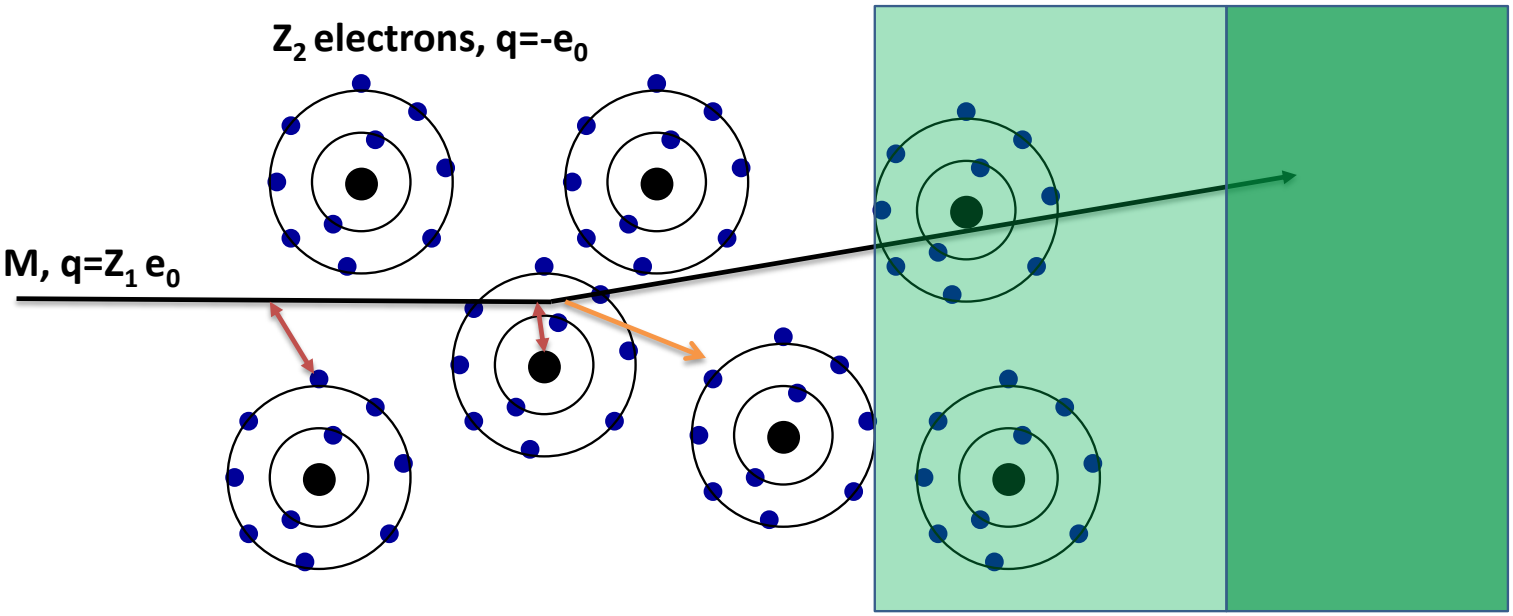

Interaction with the atomic electrons. The incoming particle loses energy and the atoms are excited or ionized.

Interaction with the atomic nucleus. The particle is deflected (scattered) causing multiple scattering of the particle in the material. During this scattering a Bremsstrahlung photon can be emitted.

In case the particle's velocity is larger than the velocity of light in the medium, the resulting EM shockwave manifests itself as Cherenkov Radiation. When the particle crosses the boundary between two media, there is a probability of the order of 1% to produced and X ray photon, called Transition radiation.

Particle Detection Principle

In order to detect a particle

- it must interact with the material of the detector
- transfer energy in some recognizable fashion

i.e. The detection of particles happens via their energy loss in the material it traverses ...

Possibilities:

Charged particles	Ionization, Bremsstrahlung, Cherenkov ...
Hadrons	Nuclear interactions
Photons	Photo/Compton effect, pair production
Neutrinos	Weak interactions

Energy loss by multiple reactions

Total energy loss via single interaction → charged particles

Particle Interactions

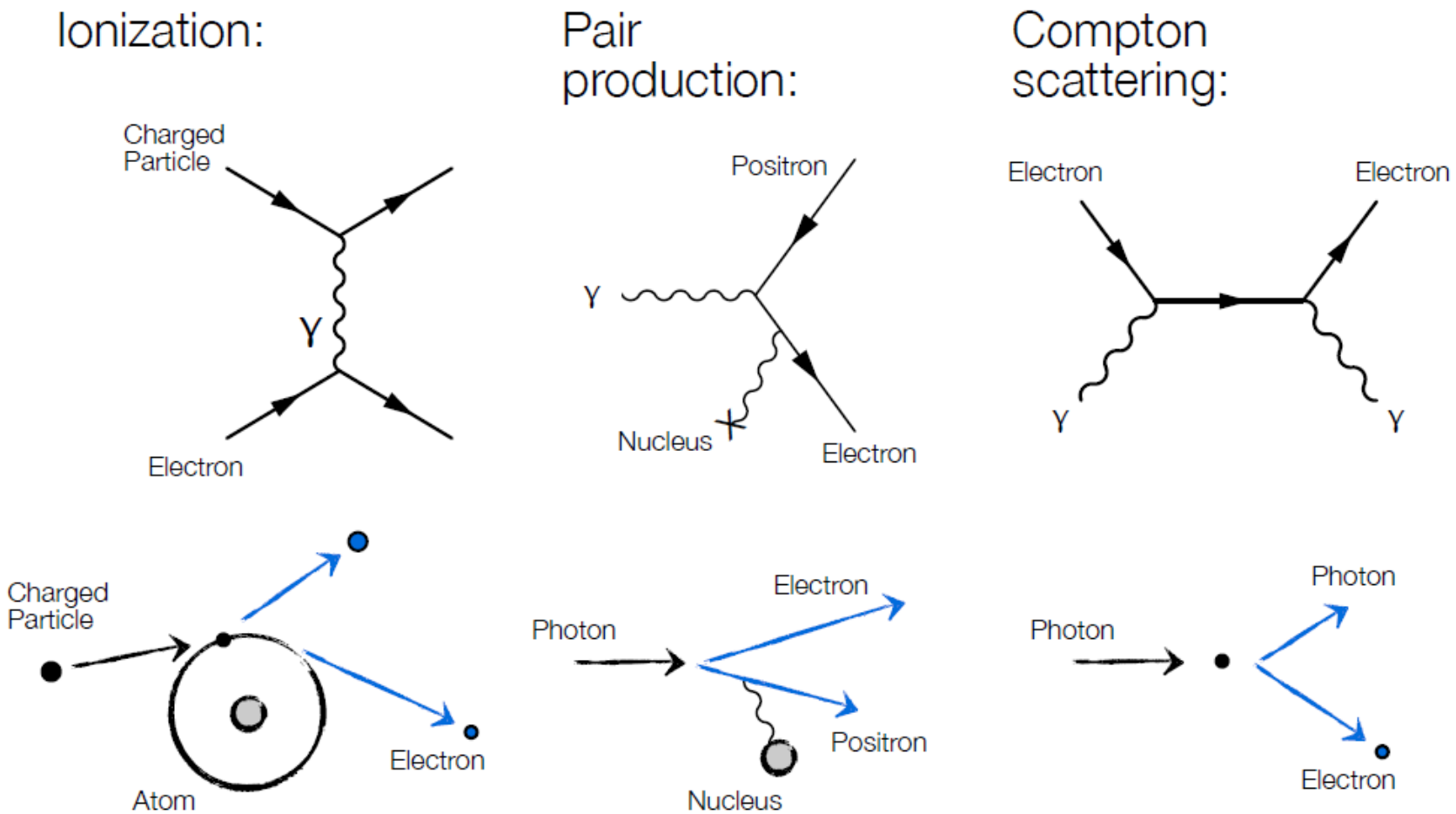

H.-C. Schultz-Coulon & J. Stachel — http://www.kip.uni-heidelberg.de/~coulon/Lectures/Detectors/

Energy Loss by Ionization

For now assume: $Mc^2 \gg m_e c^2$

i.e. energy loss for heavy charged particles
[dE/dx for electrons more difficult; later ...]

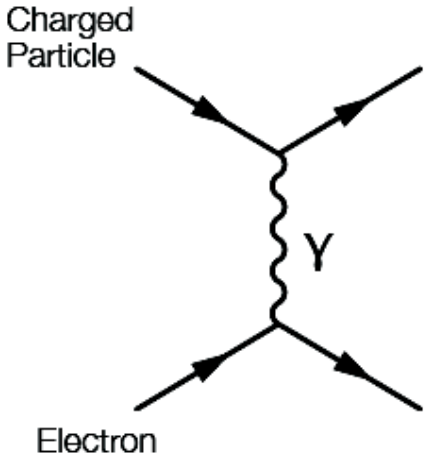

Interaction dominated
by elastic collisions with electrons ...

Bethe-Bloch Formula

$$-\left\langle \frac{dE}{dx} \right\rangle = K z^2 \frac{Z}{A} \frac{1}{\beta^2} \left[\frac{1}{2} \ln \frac{2 m_e c^2 \beta^2 \gamma^2 T_{\max}}{I^2} - \beta^2 - \frac{\delta(\beta\gamma)}{2} \right]$$

$\propto 1/\beta^2 \cdot \ln(\text{const} \cdot \beta^2\gamma^2)$

Understanding Bethe-Bloch

$1/\beta^2$-dependence:

Remember:

$$\Delta p_\perp = \int F_\perp dt = \int F_\perp \frac{dx}{v}$$

i.e. slower particles feel electric force of atomic electron for longer time ...

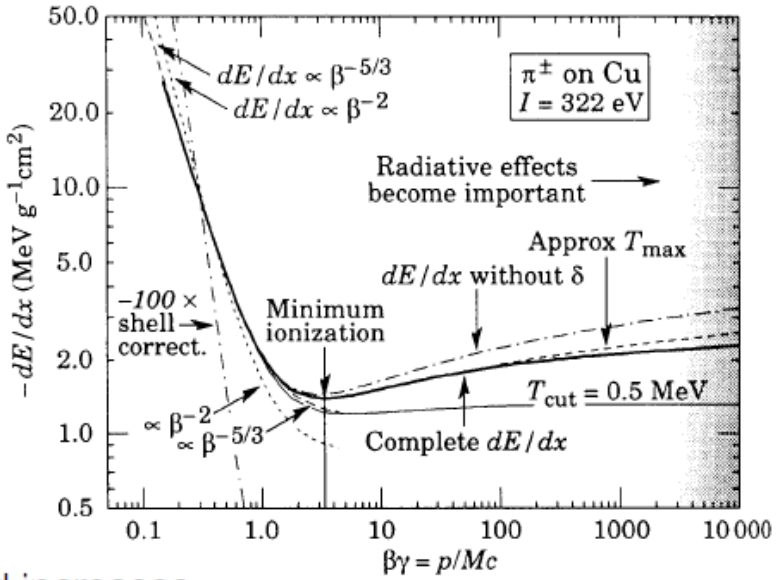

Relativistic rise for $\beta\gamma > 4$:

High energy particle: transversal electric field increases due to Lorentz transform; $E_y \rightarrowtail \gamma E_y$. Thus interaction cross section increases ...

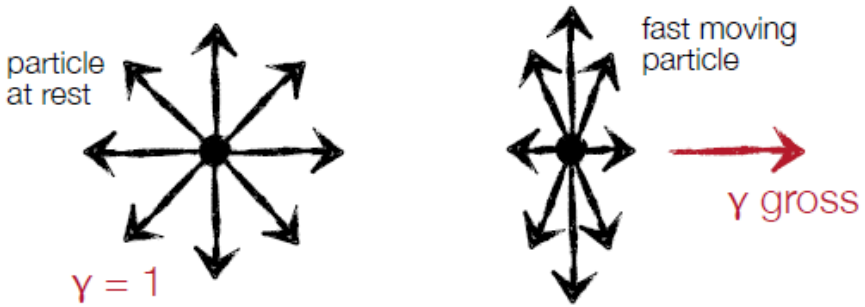

Corrections:

low energy : shell corrections

high energy : density corrections

Understanding Bethe-Bloch

Density correction:

Polarization effect ...
[density dependent]

→ Shielding of electrical field far from particle path; effectively cuts of the long range contribution ...

More relevant at high γ ...
[Increased range of electric field; larger b_{max}; ...]

For high energies:

$$\delta/2 \to \ln(\hbar\omega/I) + \ln\beta\gamma - 1/2$$

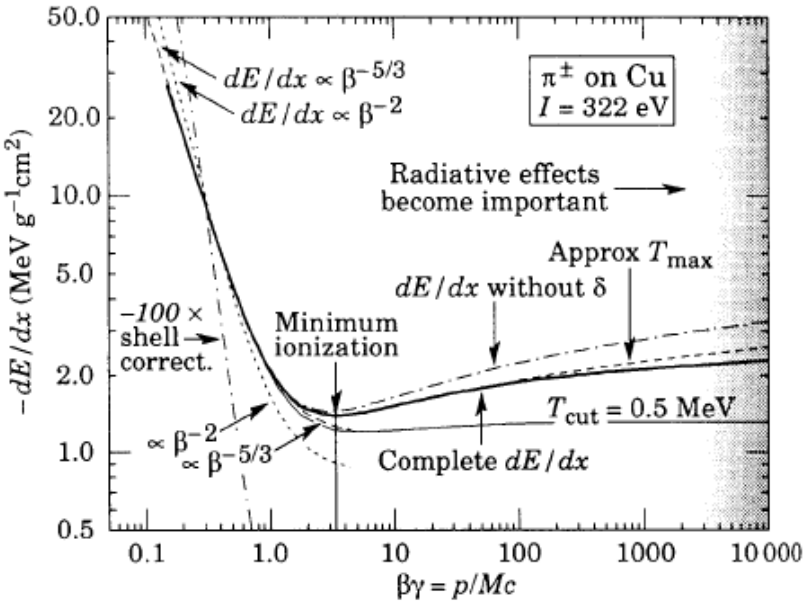

Shell correction:

Arises if particle velocity is close to orbital velocity of electrons, i.e. βc ~ v_e.

Assumption that electron is at rest breaks down ...
Capture process is possible ...

Density effect leads to saturation at high energy ...

Shell correction are in general small ...

Bremsstrahlung

Bremsstrahlung arises if particles
are accelerated in Coulomb field of nucleus

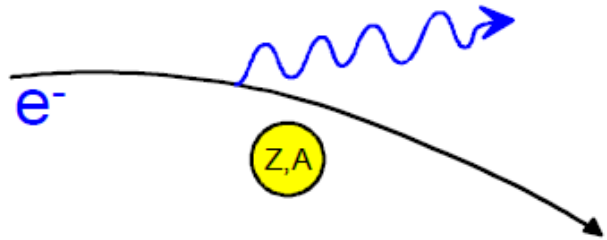

$$\frac{dE}{dx} = 4\alpha N_A \frac{z^2 Z^2}{A} \left(\frac{1}{4\pi\epsilon_0}\frac{e^2}{mc^2}\right)^2 E \ln\frac{183}{Z^{\frac{1}{3}}} \propto \frac{E}{m^2}$$

i.e. energy loss proportional to $1/m^2$ ➙ main relevance for electrons ...

... or ultra-relativistic muons

Consider electrons:

$$\frac{dE}{dx} = 4\alpha N_A \frac{Z^2}{A} r_e^2 \cdot E \ln\frac{183}{Z^{\frac{1}{3}}}$$

$$\frac{dE}{dx} = \frac{E}{X_0} \quad \text{with} \quad X_0 = \frac{A}{4\alpha N_A Z^2 r_e^2 \ln\frac{183}{Z^{\frac{1}{3}}}}$$

[Radiation length in g/cm²]

➙ $E = E_0 e^{-x/X_0}$

After passage of one X_0 electron has lost all but $(1/e)^{th}$ of its energy

[i.e. 63%]

Bremsstrahlung

Critical energy:

$$\left.\frac{dE}{dx}(E_c)\right|_{\text{Brems}} = \left.\frac{dE}{dx}(E_c)\right|_{\text{Ion}}$$

$$\left(\frac{dE}{dx}\right)_{\text{Tot}} = \left(\frac{dE}{dx}\right)_{\text{Ion}} + \left(\frac{dE}{dx}\right)_{\text{Brems}}$$

Approximation:

$$E_c^{\text{Gas}} = \frac{710\ \text{MeV}}{Z + 0.92}$$

$$E_c^{\text{Sol/Liq}} = \frac{610\ \text{MeV}}{Z + 1.24}$$

Example Copper:

Ec ≈ 610/30 ≈ 20

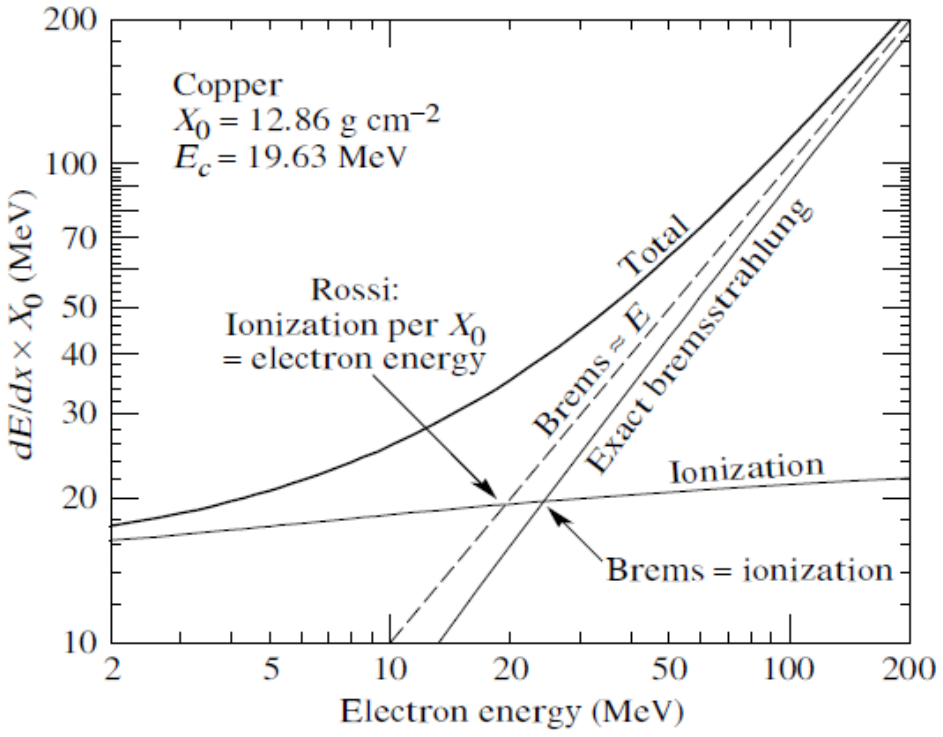

Energy loss summary for Muons

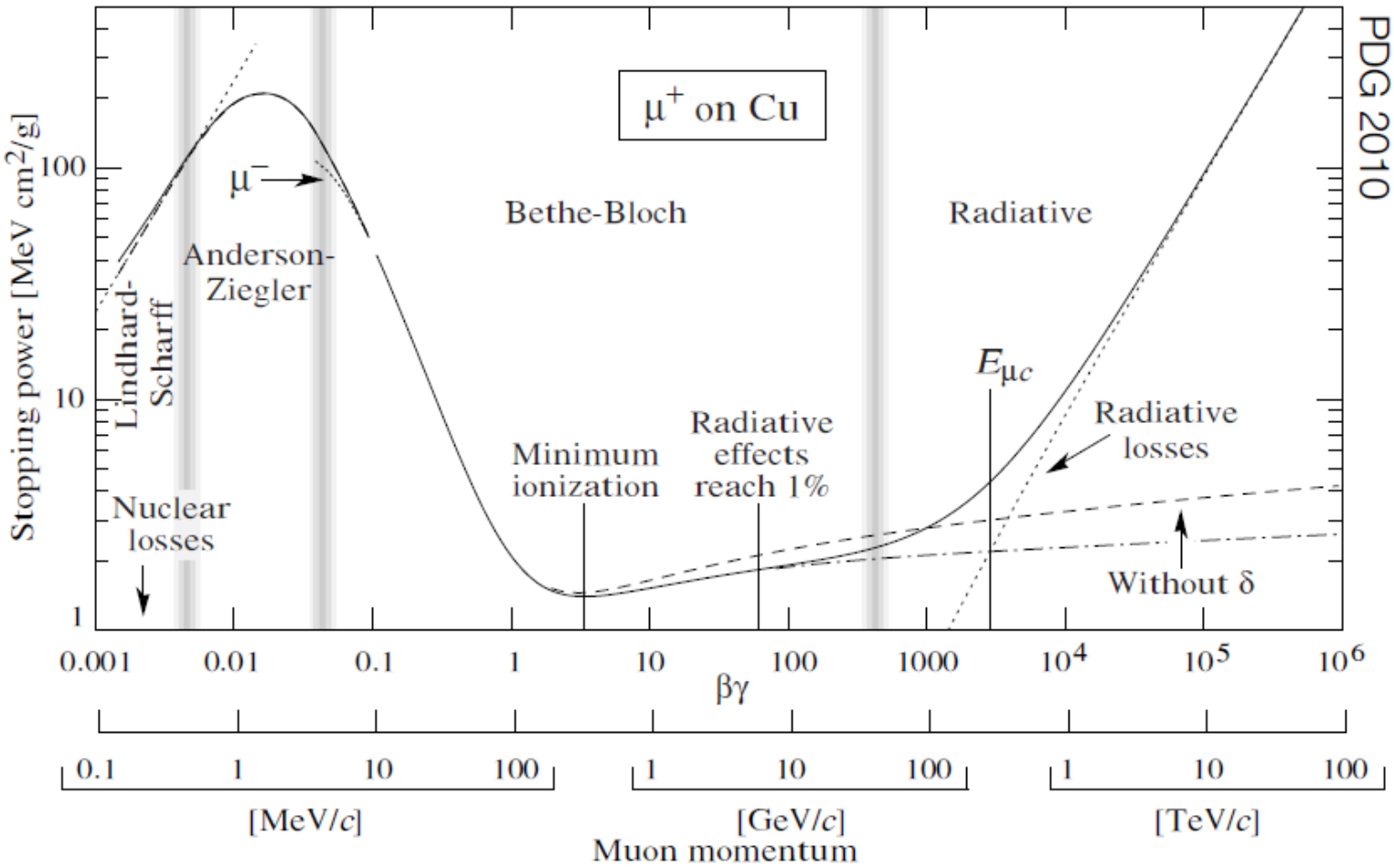

Gas Ionization

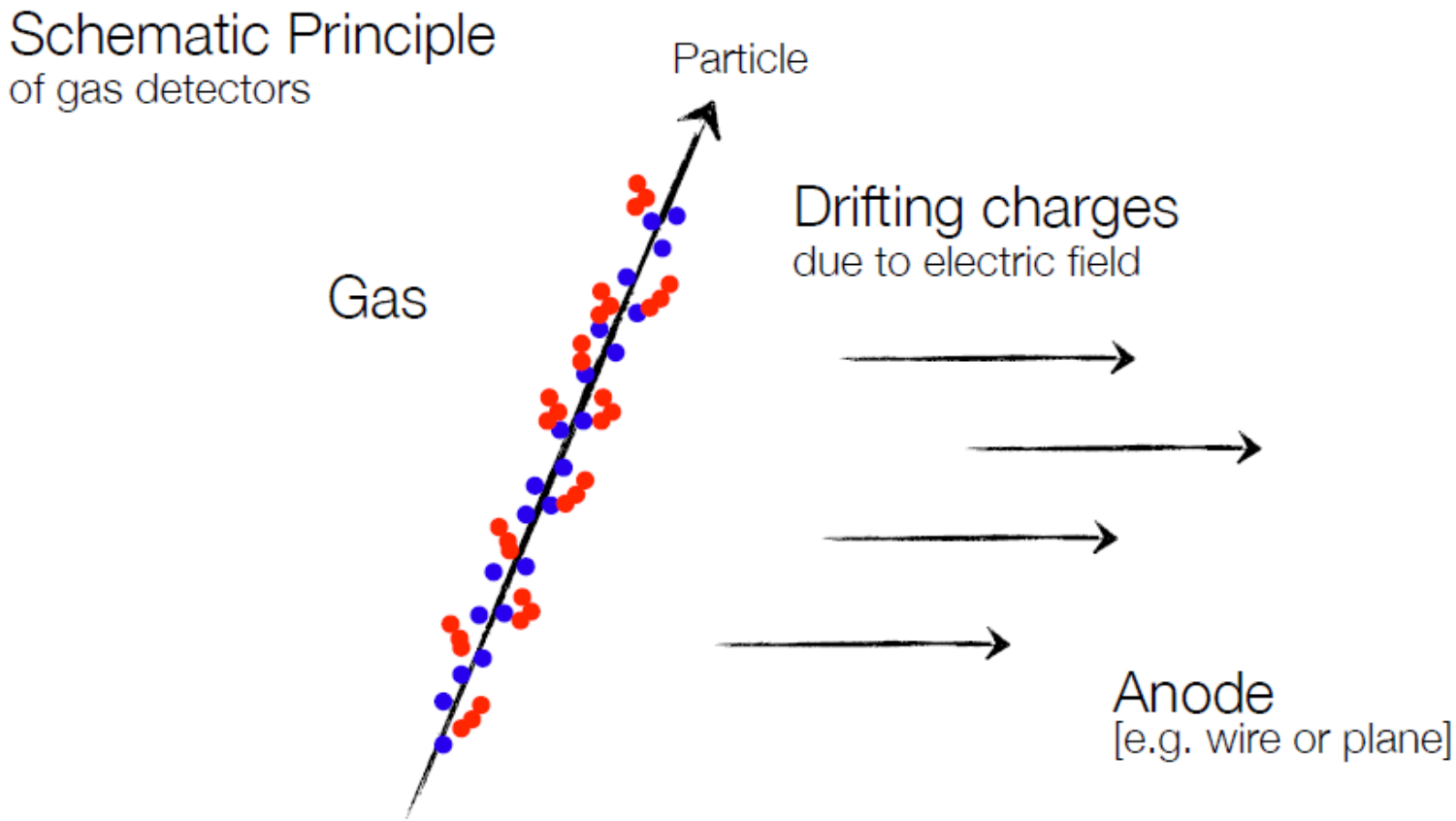

- Primary Ionization
- Secondary Ionization (due to δ-electrons)

H.-C. Schultz-Coulon & J. Stachel — http://www.kip.uni-heidelberg.de/~coulon/Lectures/Detectors/

Gas Ionization

CHARGE MULTIPLICATION IN UNIFORM FIELD

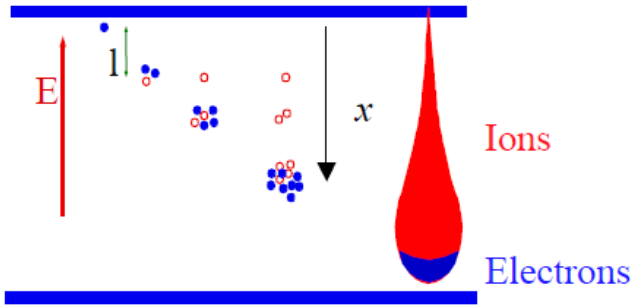

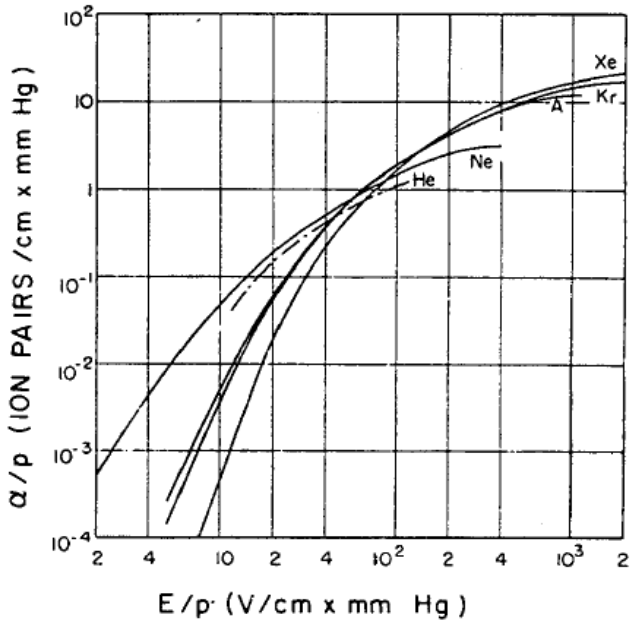

S.C. Brown, Basic Data of Plasma Physics (MIT Press, 1959)

Mean free path for ionization:

$$\lambda = \frac{1}{N\sigma} \qquad N: \textit{molecules/cm}^3$$

Townsend coefficient:

$$\alpha = \frac{1}{\lambda} \qquad \textit{Ionizing collisions/cm} \qquad \frac{\alpha}{P} = f\left(\frac{E}{P}\right)$$

Incremental increase of the number of electrons in the avalanche:

$$dn = n\,\alpha\,dx$$

Multiplication factor (Gain): $M(x) = \frac{n}{n_0} = e^{\alpha x}$

Maximum Avalanche size before discharge (Raether limit):

$$Q_{MAX} \approx 10^7 \text{ e}$$

H. Raether, Electron Avalanches and Breakdown in Gases (Butterworth 1964)

Gas Ionization

PARALLEL PLATE COUNTERS:

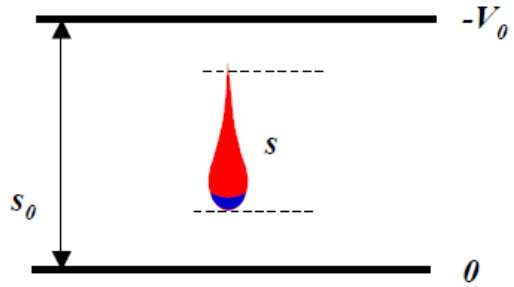

Increase in the number of charges after a path ds:

$$dn = n\alpha ds \qquad n = n_0 e^{\alpha s}$$

Charge induced by electrons: $dq^- = -en_0 e^{\alpha s}\frac{ds}{s_0}$

$$q^-(s) = \frac{en_0}{\alpha s_0}(e^{\alpha s} - 1) \approx \frac{en_0}{\alpha s_0}e^{\alpha s} = \frac{en_0}{\alpha s_0}e^{\alpha w^- t}$$

$$i^-(t) = \frac{dq^-}{dt} = \frac{en_0 w^-}{s_0}e^{\alpha w^- t} = \frac{en_0}{T^-}e^{\alpha w^- t}$$

Current signal induced by ions:

$$i^+(t) = \frac{en_0}{T^+}\left(e^{\alpha w^- t} - e^{\alpha w^* t}\right) \quad 0 \le t \le T^-$$

$$i^+(t) = \frac{en_0}{T^+}\left(e^{\alpha s} - e^{\alpha w^* t}\right) \quad T^- \le t \le T^+$$

$$\frac{1}{w^*} = \frac{1}{w^+} + \frac{1}{w^-}$$

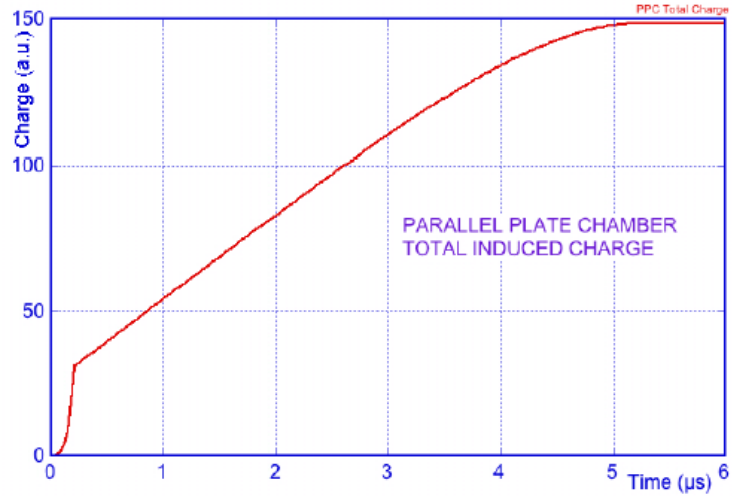

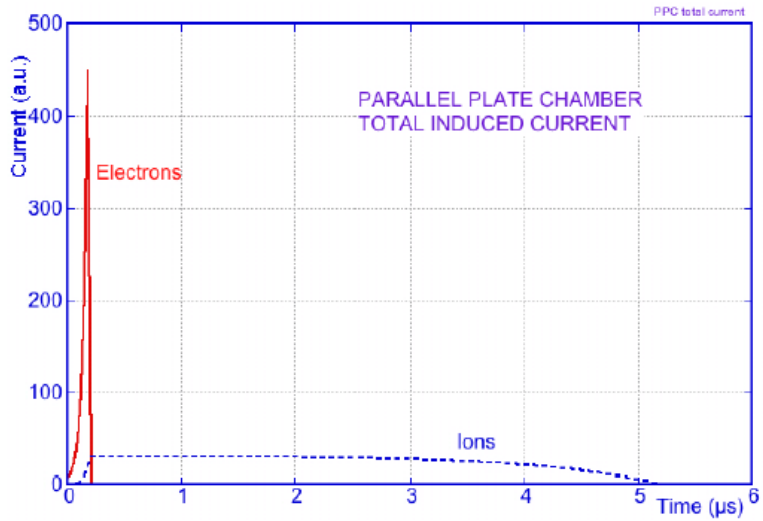

Gas Ionization

THIN ANODE WIRE

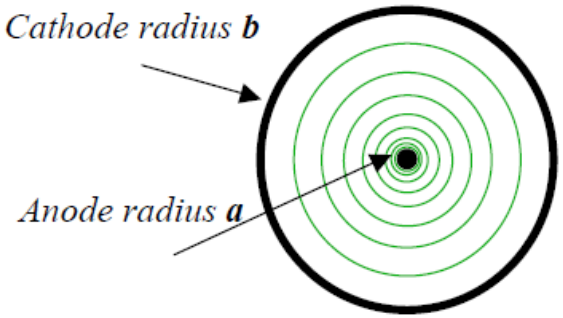

ELECTRIC FIELD AND POTENTIAL:

$$E(r) = \frac{CV_0}{2\pi\varepsilon_0}\frac{1}{r}$$

$$V(r) = \frac{CV_0}{2\pi\varepsilon_0}\ln\frac{r}{a}$$

$$C = \frac{2\pi\varepsilon_0}{\ln(b/a)}$$ capacitance per unit length

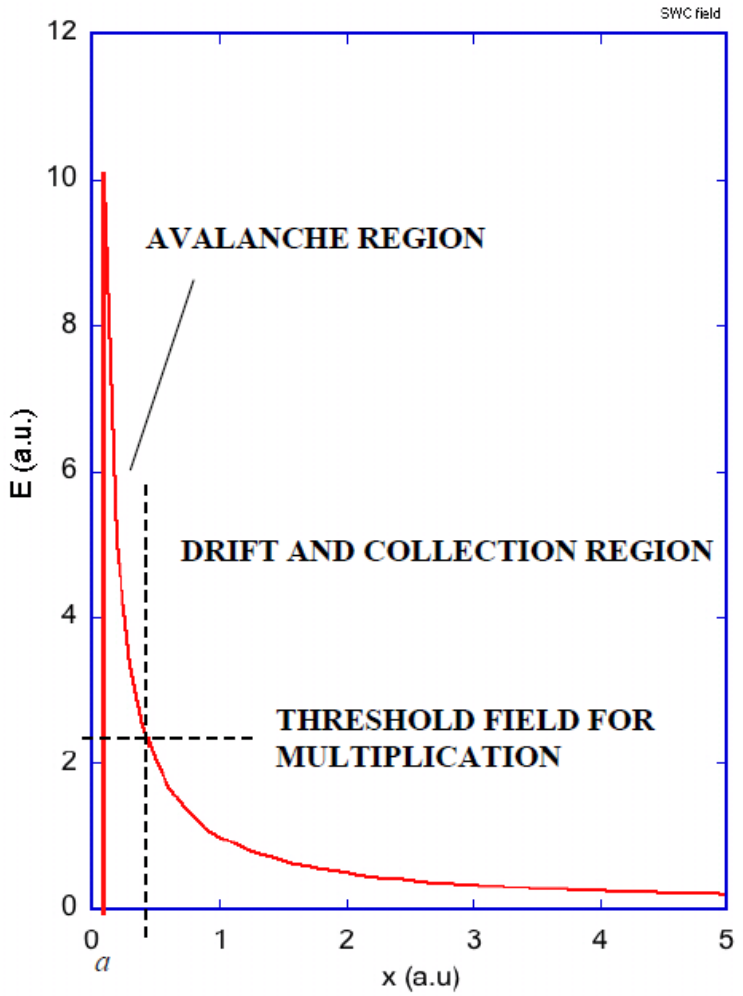

Gas Ionization

AVALANCHE DEVELOPMENT:

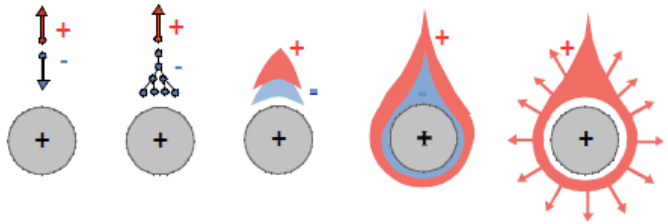

CHARGE SIGNAL INDUCTION:

$$q^- = \frac{Q}{V_0}\int_a^{a+\lambda}\frac{dV}{dr}dr = -\frac{QC}{2\pi\varepsilon_0}\ln\frac{a+\lambda}{a}$$

$$q^+ = \frac{Q}{V_0}\int_{a+\lambda}^{b}\frac{dV}{dr}dr = -\frac{QC}{2\pi\varepsilon_0}\ln\frac{b}{a+\lambda}$$

$$q = q^- + q^+ = -\frac{QC}{2\pi\varepsilon_0}\ln\frac{b}{a} = -Q$$

λ: distance of avalanche start

$$\frac{q^-}{q^+} = \frac{\ln(a+\lambda)-\ln a}{\ln b-\ln(a+\lambda)} \approx 0.01$$

99% of signal due to positive ions

$$q(t) = -\frac{QC}{2\pi\varepsilon_0}\ln\left(1+\frac{\mu^+ CV_0}{2\pi\varepsilon_0 a^2}t\right) = -\frac{QC}{2\pi\varepsilon_0}\ln\left(1+\frac{t}{t_0}\right)$$

CHARGE SIGNAL: POSITIVE ION TAIL

RC differentiation for faster response

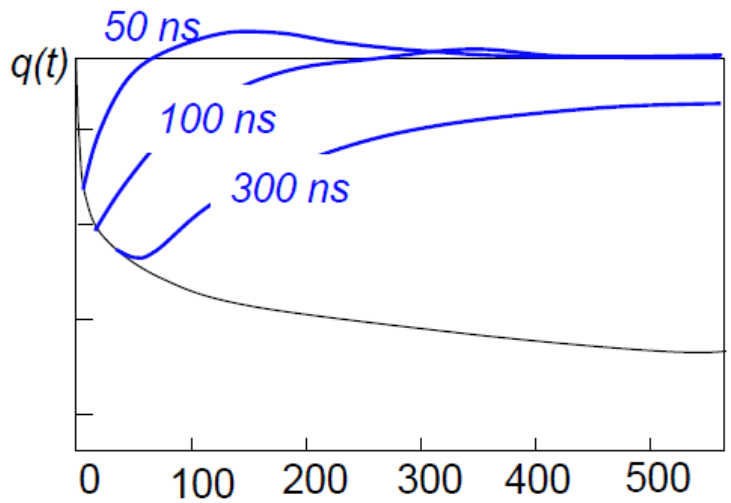

S. C. Curran and J. D. Craggs, Counting Tubes (Butterworth 1949)

F. Sauli, Principles of Operation of Multiwire Proportional and Drift Chambers (CERN 77-09)

Gas Ionization

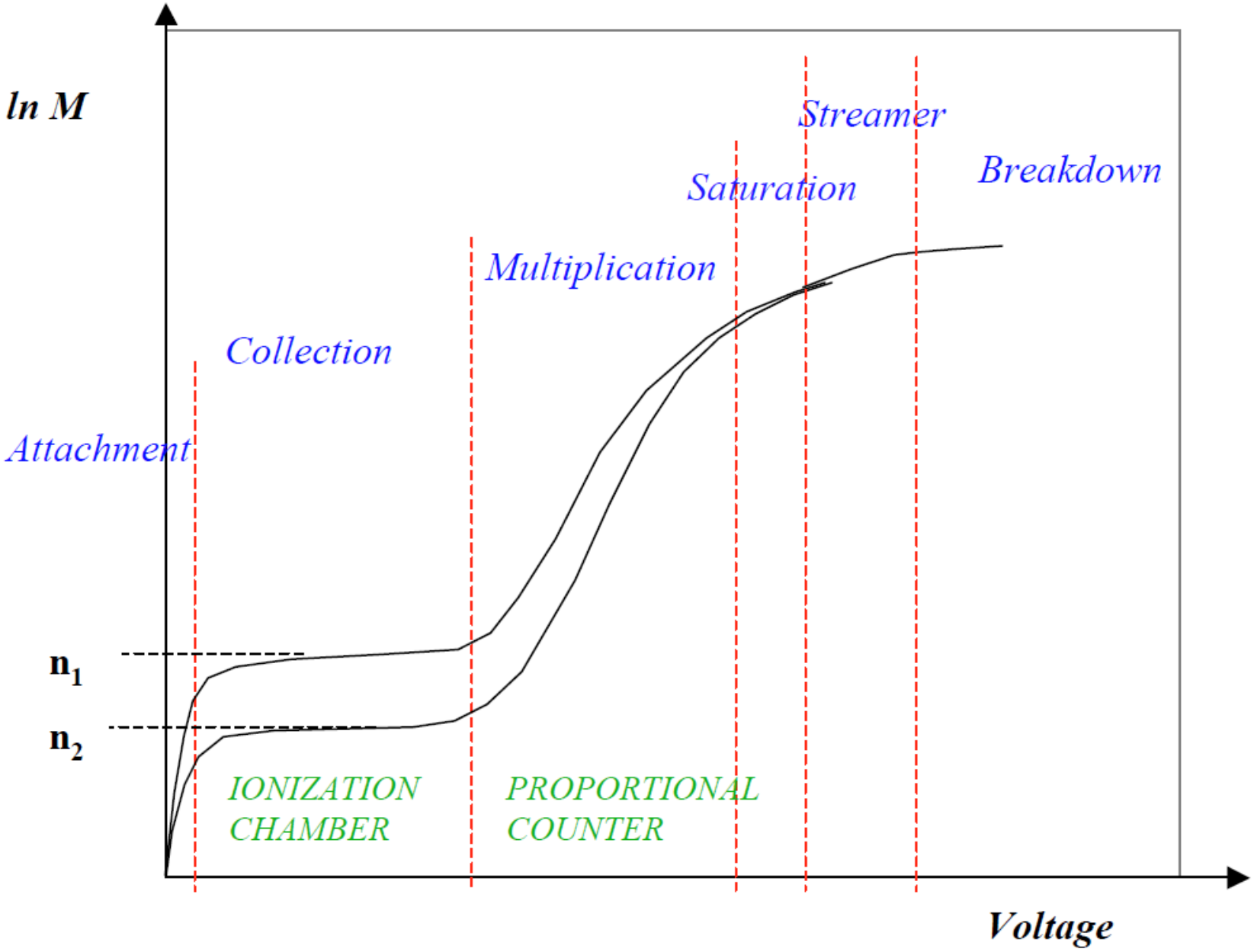

Gas Ionization

Molecular tracking

- Example:
  - CSC-like structure,
  - Ar 80 % CO_2 20 %,
  - 10 GeV μ.
- The electron is shown every 100 collisions, but has been tracked rigourously.

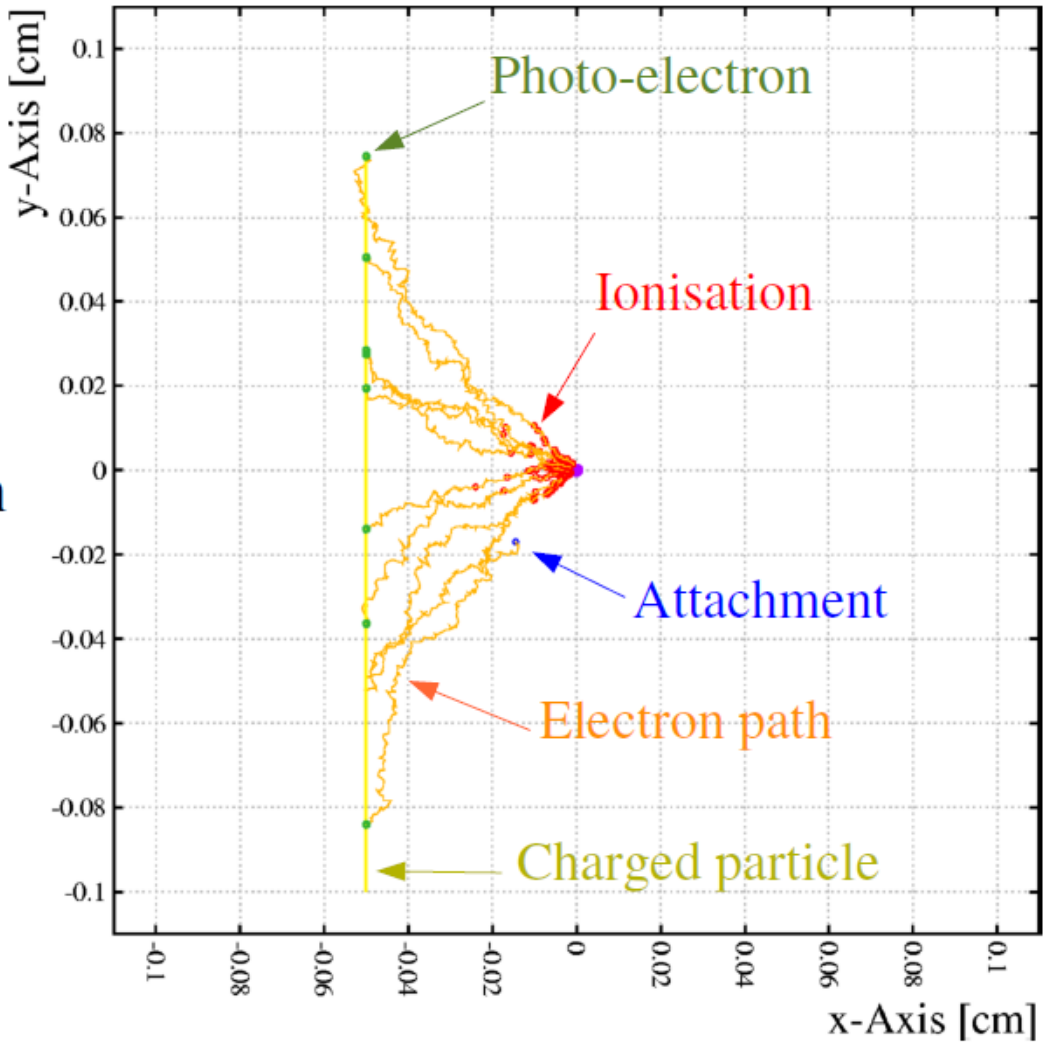

Multiple Scattering

The 'Rutherford scattering' of the incoming particle on the nuclei, that is also the reason for Bremsstrahlung, results in multiple small angle scattering scattering of the particles when traversing material.

The statistical analysis of the small angle scattering together with inclusion of the shielding effects by the electrons results in simple expressions for the multiple scattering angles of particles.

$$\frac{d\sigma}{d\Omega} = \left(\frac{1}{4\pi\varepsilon_0}\frac{Z_1(Z_2 - F)e_0^2}{2pv}\right)^2 \frac{1}{\sin^4\theta/2}$$

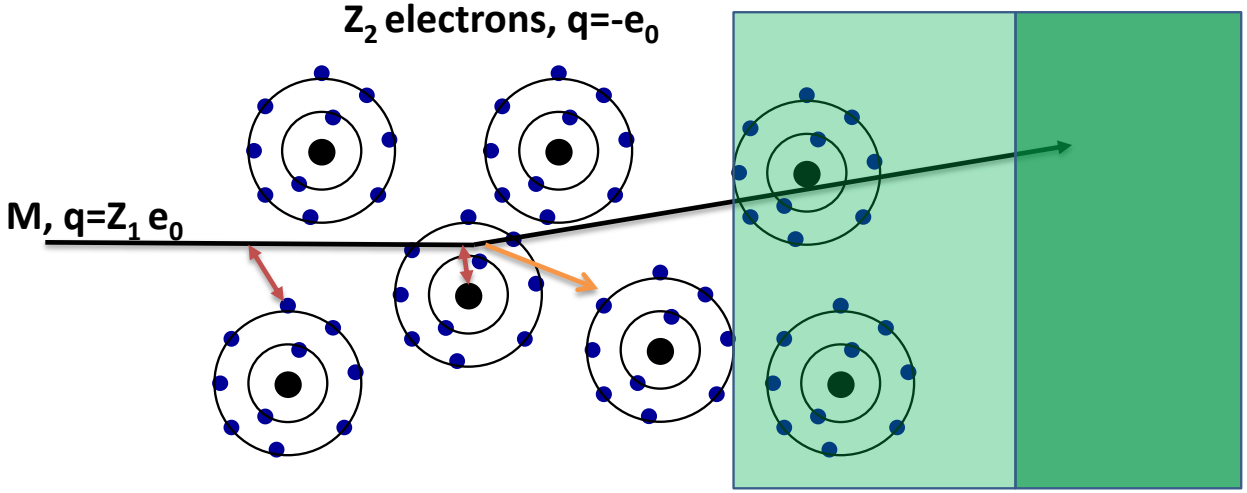

Electromagnetic Interaction of Particles with Matter

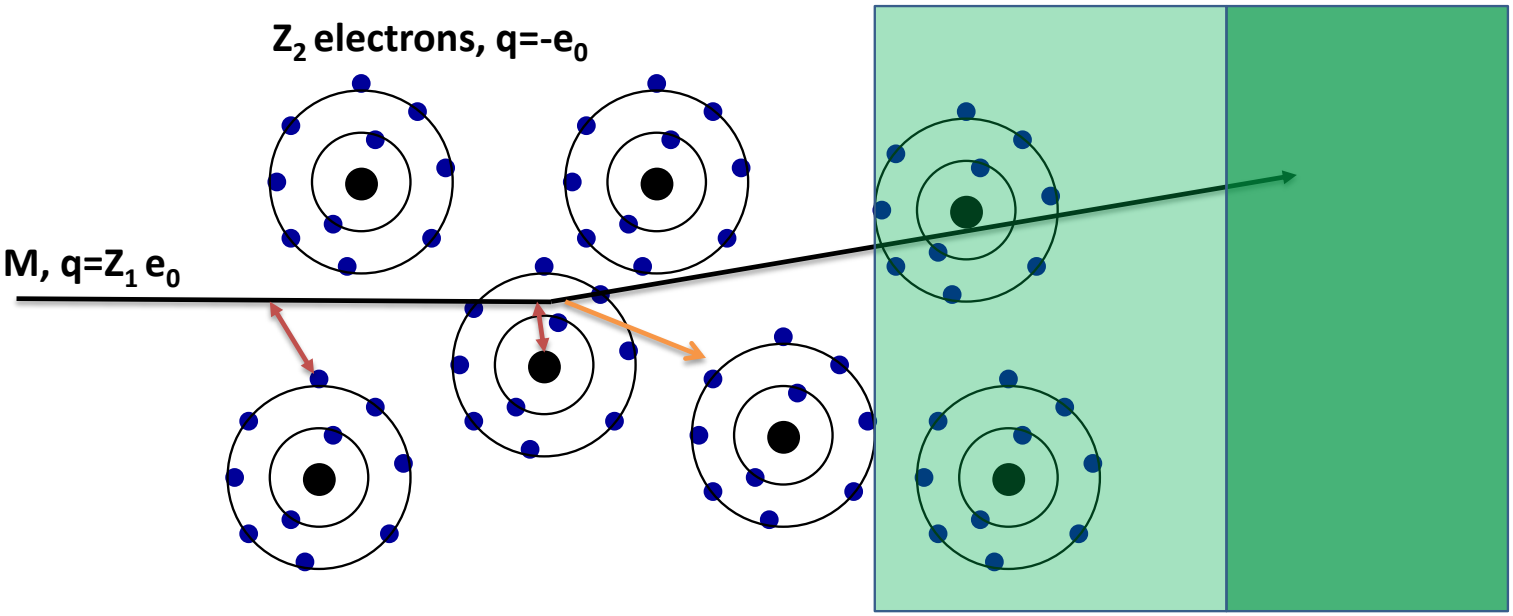

Now that we know all the Interactions we can talk about Detectors !

Interaction with the atomic electrons. The incoming particle loses energy and the atoms are excited or ionized.

Interaction with the atomic nucleus. The particle is deflected (scattered) causing multiple scattering of the particle in the material. During this scattering a Bremsstrahlung photon can be emitted.

In case the particle's velocity is larger than the velocity of light in the medium, the resulting EM shockwave manifests itself as Cherenkov Radiation. When the particle crosses the boundary between two media, there is a probability of the order of 1% to produced and X ray photon, called Transition radiation.

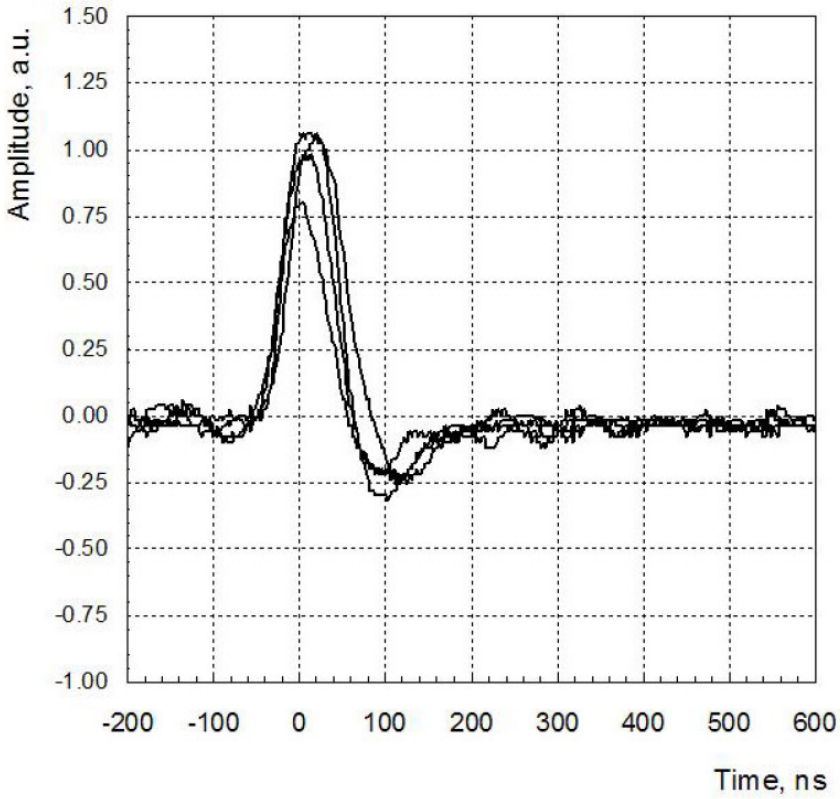

Signal Creation in Particle Detectors

Principle of Signal Induction by Moving Charges

A point charge q at a distance z_0

Above a grounded metal plate 'induces' a surface charge.

The total induced charge on the surface is –q.

Different positions of the charge result in different charge distributions.

The total induced charge stays –q.

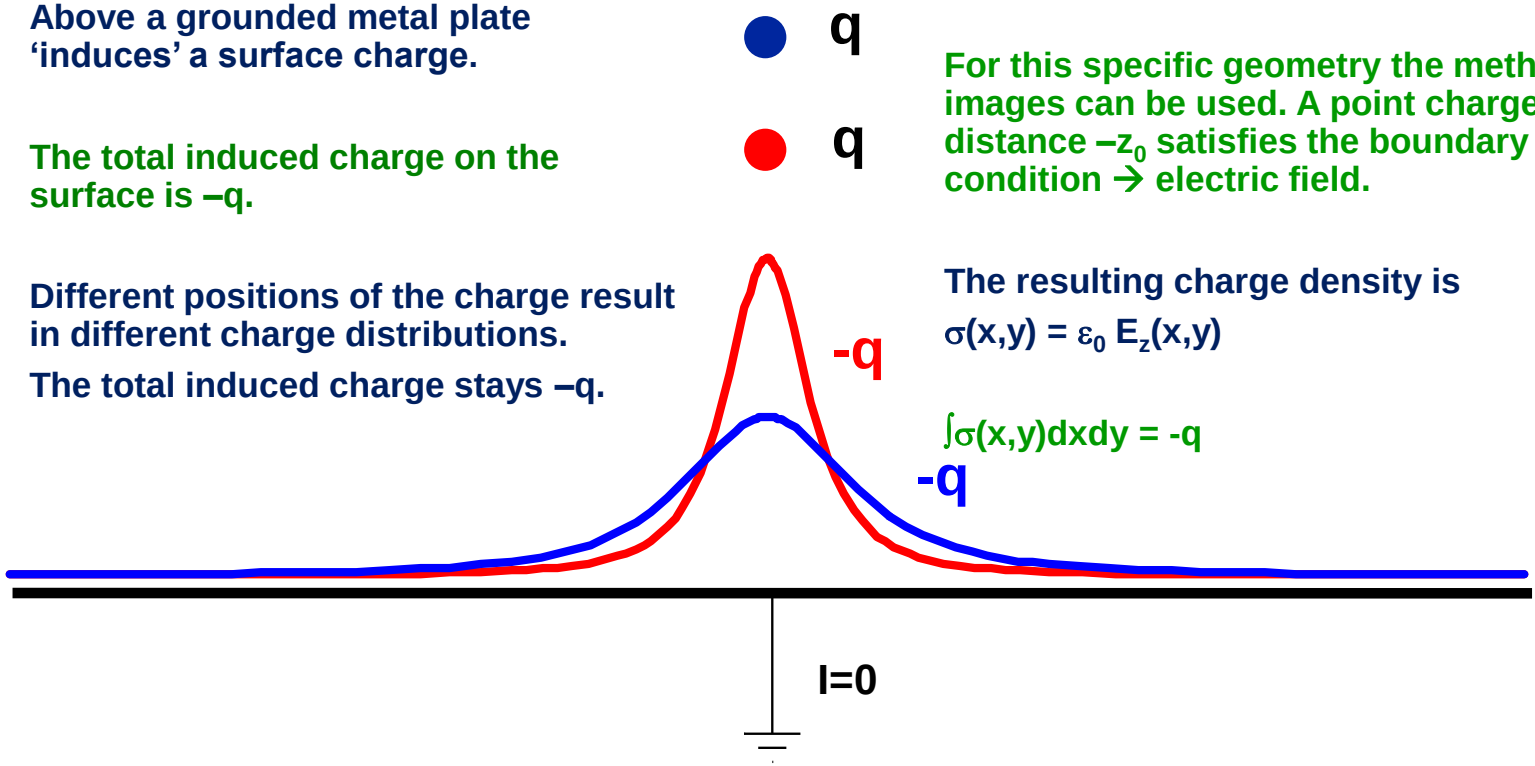

The electric field of the charge must be calculated with the boundary condition that the potential φ=0 at z=0.

For this specific geometry the method of images can be used. A point charge –q at distance $-z_0$ satisfies the boundary condition → electric field.

The resulting charge density is

$\sigma(x,y) = \varepsilon_0 E_z(x,y)$

$\int\sigma(x,y)dxdy = -q$

$$E_z(x,y) = -\frac{qz_0}{2\pi\varepsilon_0(x^2+y^2+z_0^2)^{\frac{3}{2}}} \qquad E_x = E_y = 0 \qquad \sigma(x,y) = \varepsilon_0 E_z(x,y) \qquad Q = \int_{-\infty}^{\infty}\int_{-\infty}^{\infty}\sigma(x,y)dxdy = -q$$

Principle of Signal Induction by Moving Charges

If we segment the grounded metal plate and if we ground the individual strips the surface charge density doesn't change with respect to the continuous metal plate.

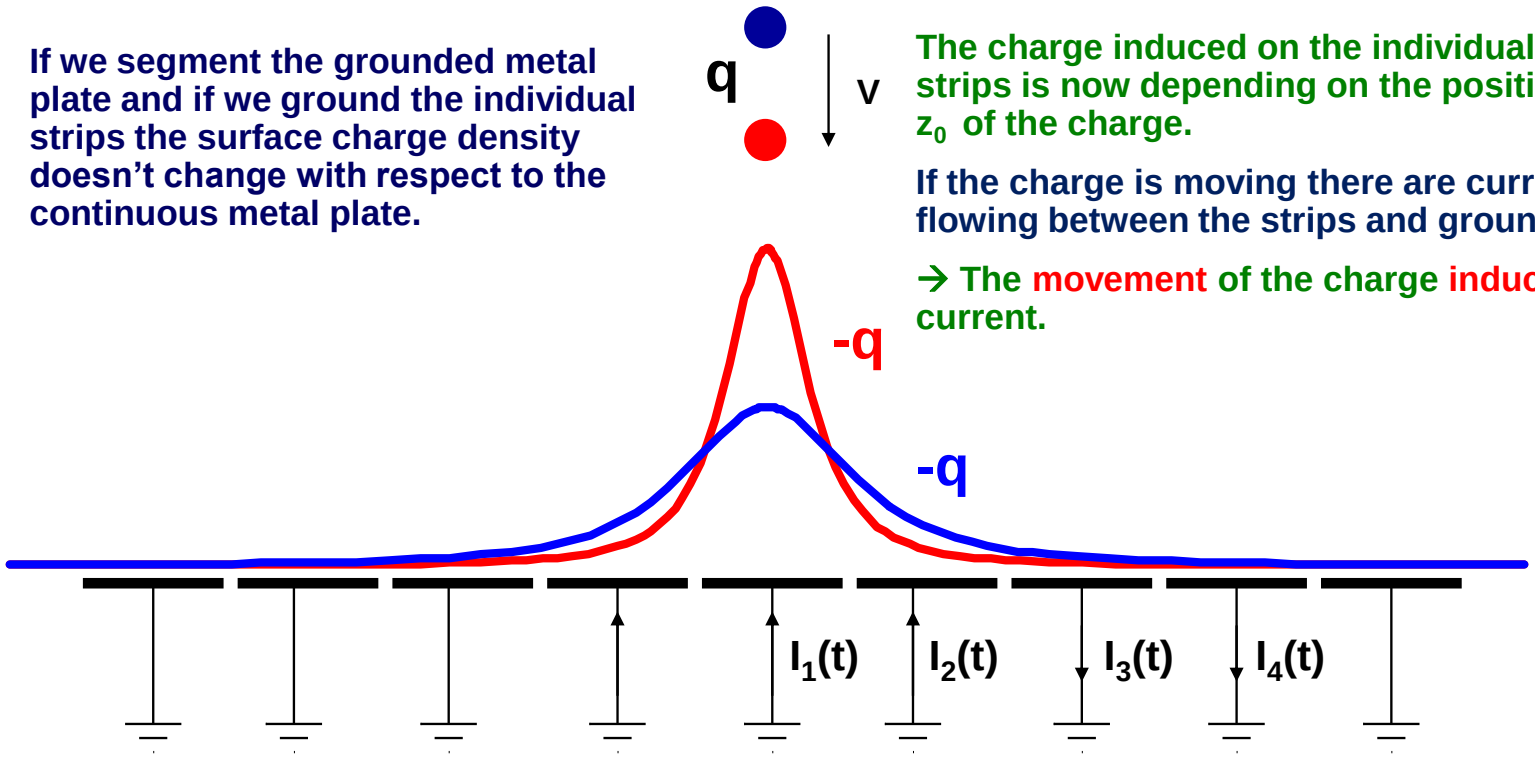

The charge induced on the individual strips is now depending on the position z_0 of the charge.

If the charge is moving there are currents flowing between the strips and ground.

→ The movement of the charge induces a current.

$$Q_1(z_0) = \int_{-\infty}^{\infty}\int_{-w/2}^{w/2} \sigma(x,y)dxdy = -\frac{2q}{\pi}\arctan\left(\frac{w}{2z_0}\right)$$

$$z_0(t) = z_0 - vt$$

$$I_1^{ind}(t) = -\frac{d}{dt}Q_1[z_0(t)] = -\frac{\partial Q_1[z_0(t)]}{\partial z_0}\frac{dz_0(t)}{dt} = \frac{4qw}{\pi[4z_0(t)^2 + w^2]}\,v$$

Signal Theorems

Placing charges on metal electrodes results in certain potentials of these electrodes. A different set of charges results in a different set of potentials. The reciprocity theorem states that

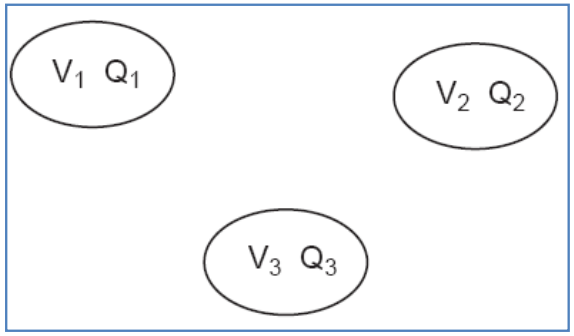

$$\sum_{n=1}^{N} Q_n \overline{V}_n = \sum_{n=1}^{N} \overline{Q}_n V_n$$

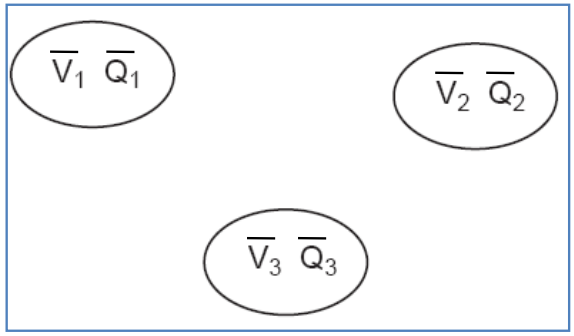

Using this theorem we can answer the following general question: What are the signals created by a moving charge on metal electrodes that are connected with arbitrary discrete (linear) components ?

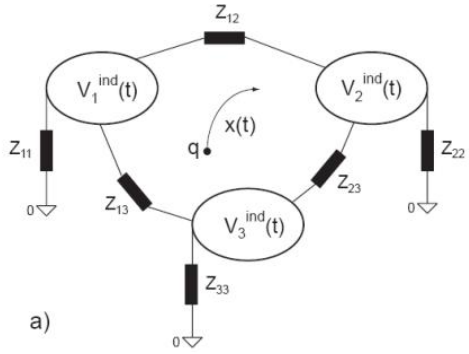

Signal Theorems

What are the charges induced by a moving charge on electrodes that are connected with arbitrary linear impedance elements ?

One first removes all the impedance elements, connects the electrodes to ground and calculates the currents induced by the moving charge on the grounded electrodes.

The current induced on a grounded electrode by a charge q moving along a trajectory x(t) is calculated the following way (Ramo Theorem):

One removes the charge q from the setup, puts the electrode to voltage V_0 while keeping all other electrodes grounded. This results in an electric field $E_n(x)$, the Weighting Field, in the volume between the electrodes, from which the current is calculated by

$$I_n(t) = -\frac{q}{V_0}\vec{E_n}[\vec{x}(t)]\frac{d\vec{x}(t)}{dt} = -\frac{q}{V_0}\vec{E_n}[\vec{x}(t)]\vec{v}(t)$$

These currents are then placed as ideal current sources on a circuit where the electrodes are 'shrunk' to simple nodes and the mutual electrode capacitances are added between the nodes. These capacitances are calculated from the weighting fields by

$$c_{nm} = \frac{\varepsilon_0}{V_w}\oint_{\boldsymbol{A}_n} \boldsymbol{E}_m(\boldsymbol{x})d\boldsymbol{A} \qquad C_{nn} = \sum_m c_{nm} \qquad C_{nm} = -c_{nm} \quad n \neq m$$

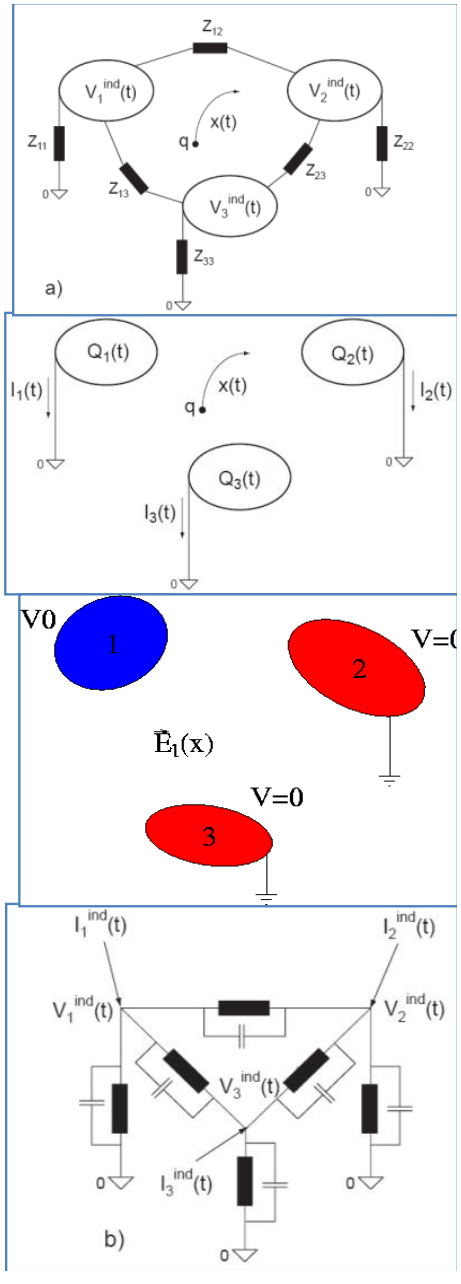

Signal Theorems

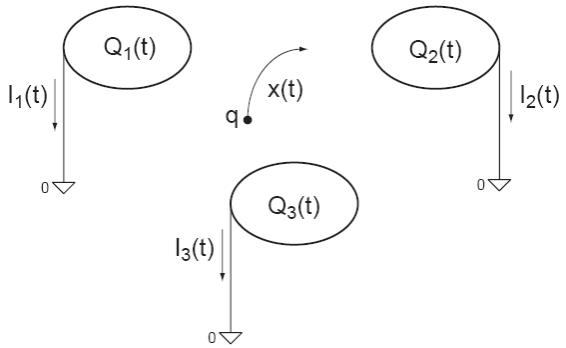

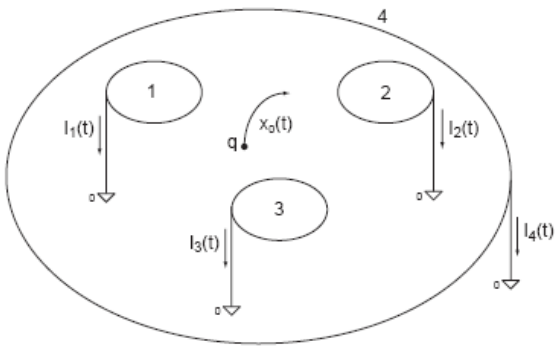

The following relations hold for the induced currents:

1) The charge induced on an electrode in case a charge in between the electrode has moved from a point x_0 to a point x_1 is

$$Q_n^{ind} = \int_{t_0}^{t_1} I_n^{ind}(t)dt = -\frac{q}{V_w}\int_{t_0}^{t_1} \boldsymbol{E}_n[\boldsymbol{x}(t)]\,\dot{\boldsymbol{x}}(t)dt = \frac{q}{V_w}[\psi_n(\boldsymbol{x}_1) - \psi_n(\boldsymbol{x}_0)]$$

and is independent on the actual path.

2) Once ALL charges have arrived at the electrodes, the total induced charge in the electrodes is equal to the charge that has ARRIVED at this electrode.

3) In case there is one electrode enclosing all the others, the sum of all induced currents is zero at any time.

Signals in a Parallel Plate Geometry

E.g.: Elektron-ion pair in gas
or Electron-ion pair in a liquid
or Electron-hole pair in a solid

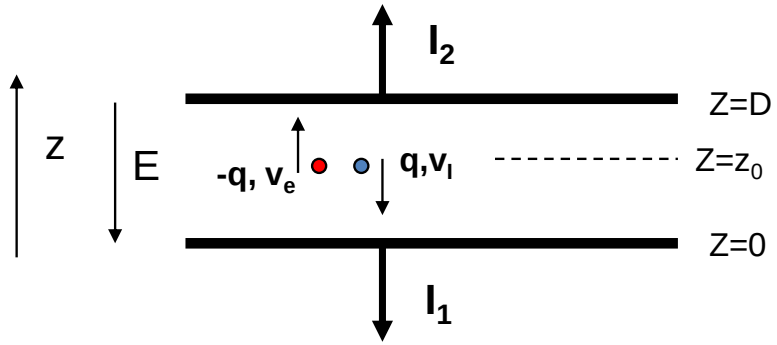

$E_1=V_0/D$
$E_2=-V_0/D$

$I_1= -(-q)/V_0*(V_0/D)*v_e - q/V_0\ (V_0/D)\ (-v_I)$
$= q/D*v_e+q/D*v_I$
$I_2=-I_1$

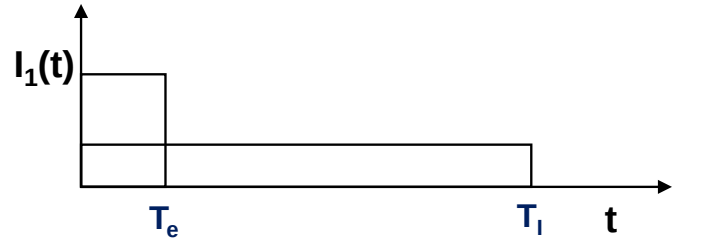

$Q^{tot}_1= \int I_1 dt = q/D*v_e\ T_e + q/D*v_I*T_I$
$= q/D*v_e*(D-z_0)/v_e + q/D*v_I*z_0/v_I$
$= q(D-z_0)/D + qz_0/D =$
$q_e+q_I=q$

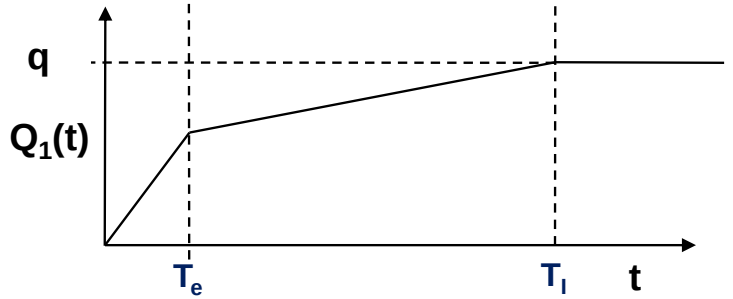

The total induced charge on a specific electrode, once all the charges have arrived at the electrodes, is equal to the charge that has arrived at this specific electrode.

Signals in a Parallel Plate Geometry

In case the electrodes are not grounded but connected by arbitrary active or passive elements one first calculates the currents induced on the grounded electrodes and places them as ideal current sources on the equivalent circuit of the electrodes.

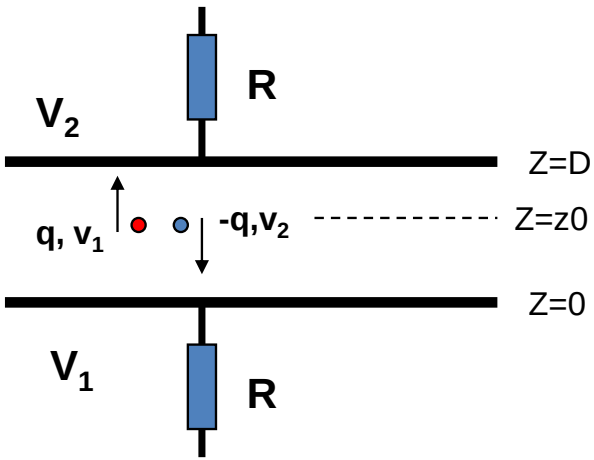

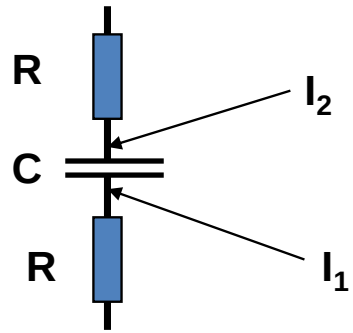

Cathode Strip Chamber detector

Multi Wire Proportional Chambers (MWPC)

Tube, Geiger- Müller, 1928

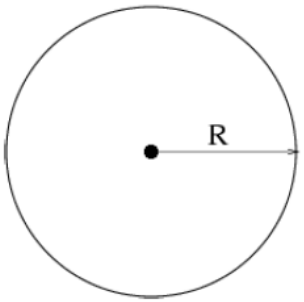

Multi Wire Geometry, in H. Friedmann 1949

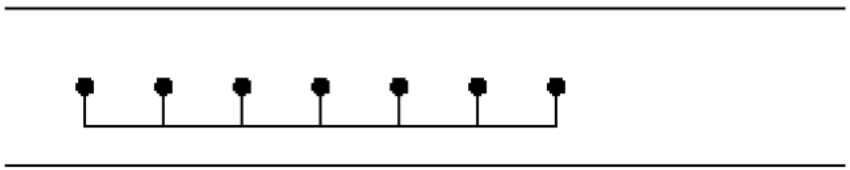

G. Charpak 1968, Multi Wire Proportional Chamber,
readout of individual wires and proportional mode working point.

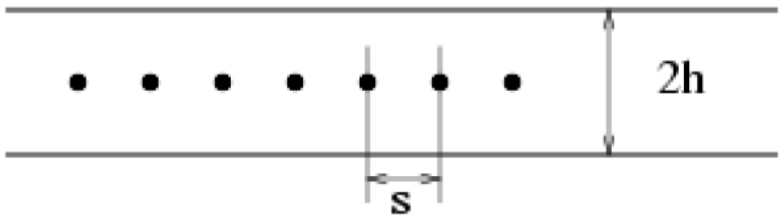

Multi Wire Proportional Chambers (MWPC)

Individual wire readout: A charged particle traversing the detector leaves a trail of electrons and ions. The wires are on positive HV. The electrons drift to the wires in the electric field and start to form an avalanche in the high electric field close to the wire. This induces a signal on the wire which can be read out by an amplifier.

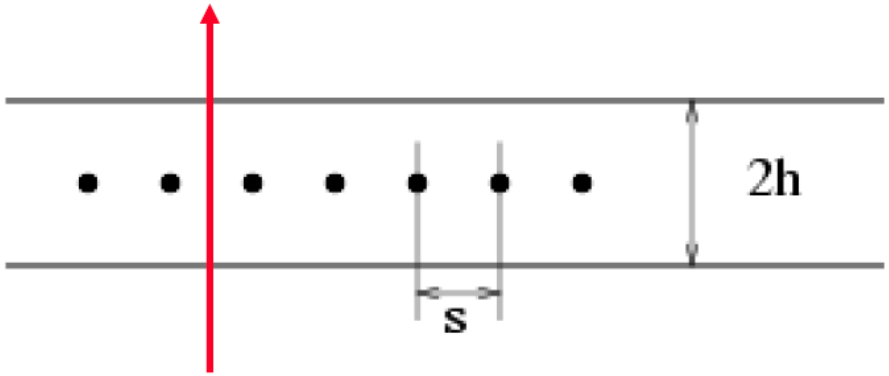

Measuring this drift time, i.e. the time between passage of the particle and the arrival time of the electrons at the wires, made this detector a precision positioning device.

Multi Wire Proportional Chambers (MWPC)

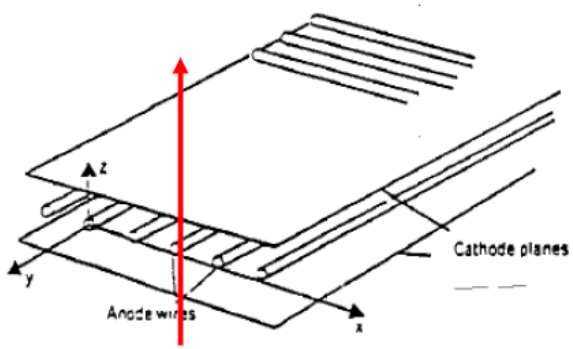

Abbildung 2.27: *Vieldrahtproportionalkammer.*

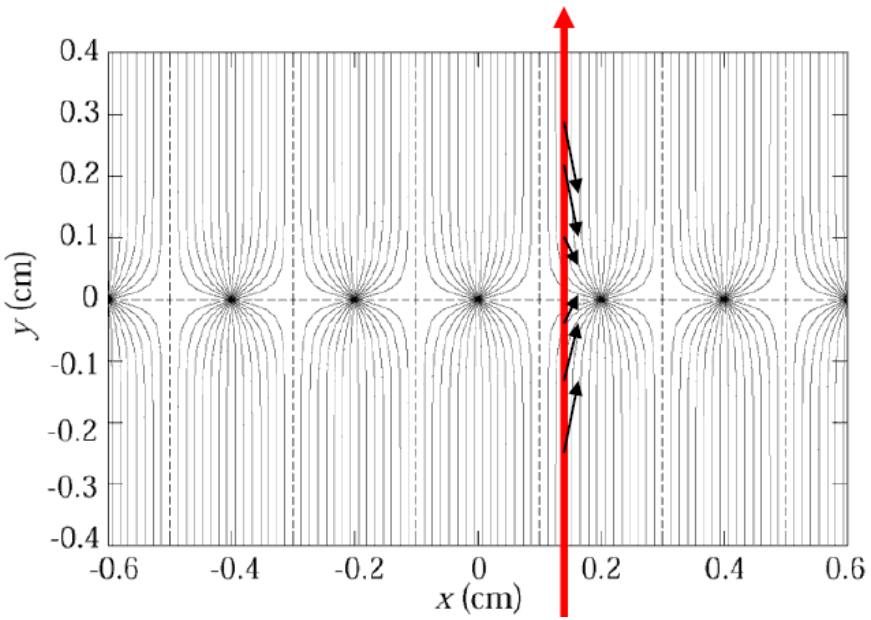

Classic geometry (Crossection), Charpak 1968 :

One plane of thin sense wires is placed between two parallel plates.

Typical dimensions:

Wire distance 2-5mm, distance between cathode planes ~10mm.

Electrons (v≈5cm/μs) are collected within ≈ 100ns. The ion tail can be eliminated by electronics filters → pulses of <100ns length.

For 10% occupancy → every μs one pulse

→ 1MHz/wire rate capabiliy !

→ Compare to Bubble Chamber with 10 Hz !

Multi Wire Proportional Chambers (MWPC)

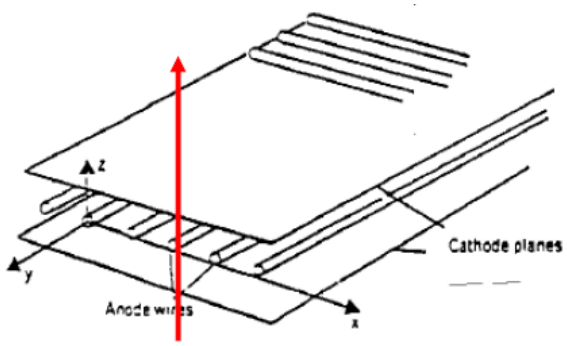

Abbildung 2.27: *Vieldrahtproportionalkammer.*

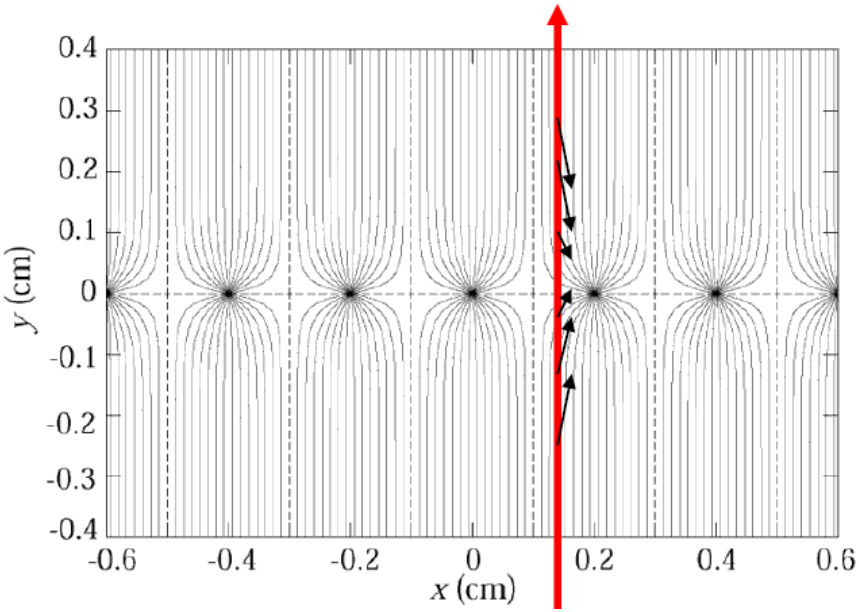

In order to eliminate the left/right ambiguities: Shift two wire chambers by half the wire pitch.

For second coordinate:

→Another chamber at 90^0 relative rotation

→Signal propagation to the two ends of the wire.

→Pulse height measurement on both ends of the wire. Because of resisitvity of the wire, both ends see different charge.

Segmenting of the cathode into strips or pads:

The movement of the charges induces a signal on the wire AND on the cathode. By segmentation of the cathode plane and charge interpolation, resolutions of 50µm can be achieved.

Multi Wire Proportional Chambers (MWPC)

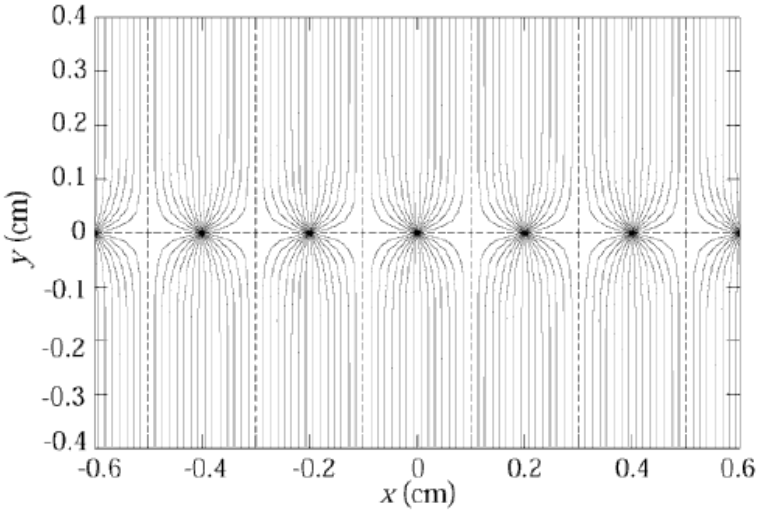

Cathode strip:

Width (1σ) of the charge distribution ≈ distance between Wires and cathode plane.

'Center of gravity' defines the particle trajectory.

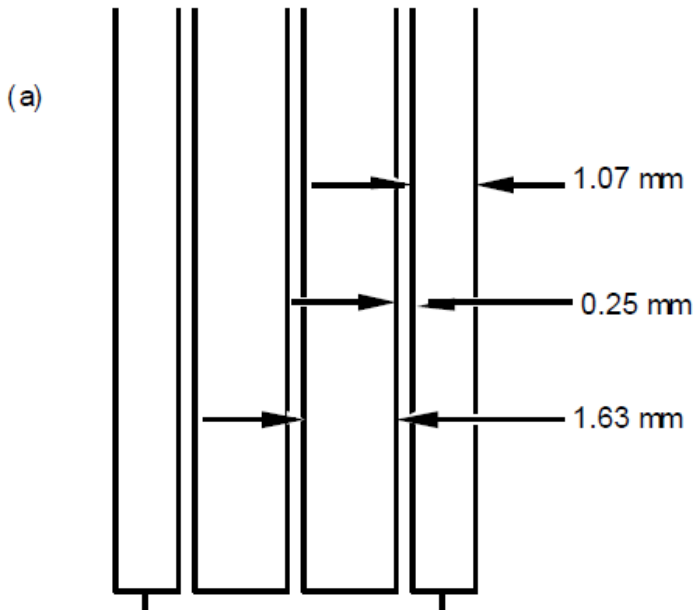

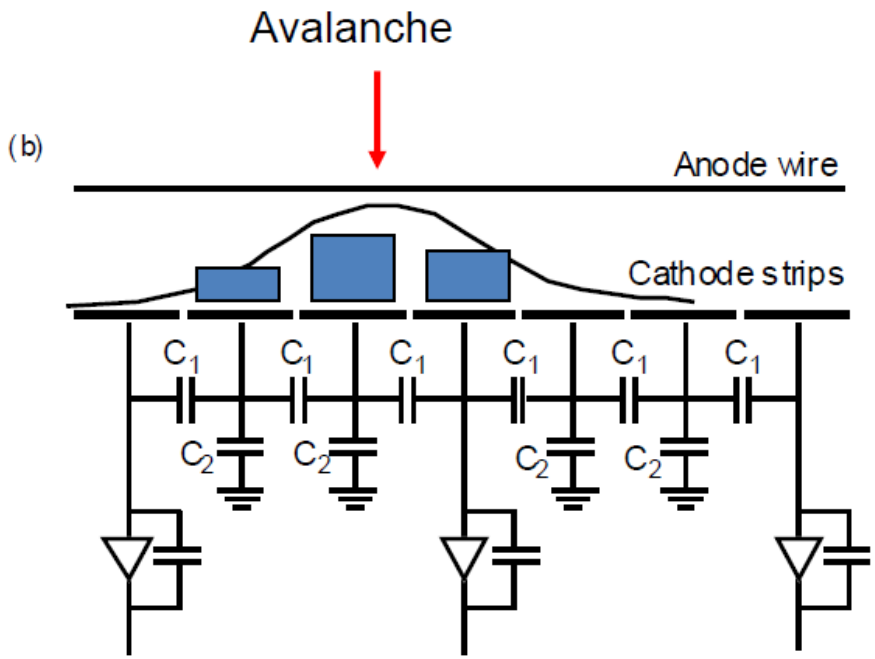

Cathode Strip Chamber (CSC)

MWPC OPERATION

- How MWPCs operate
  Gas ionized by passage of charged particle.
  Detect signals on anodes and cathodes.

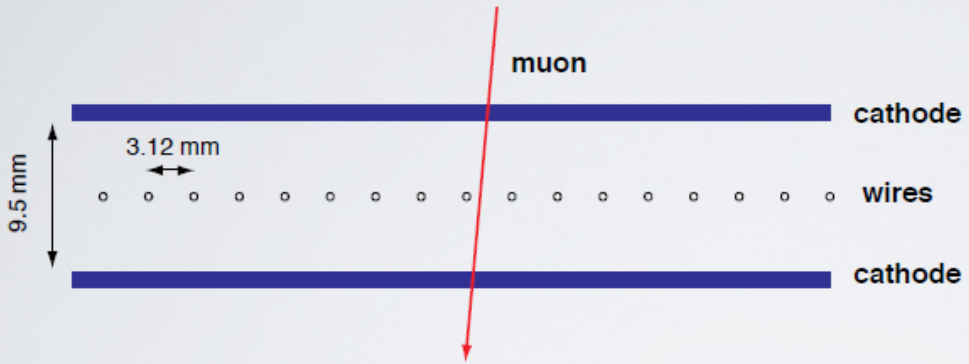

The CMS CSC geometry

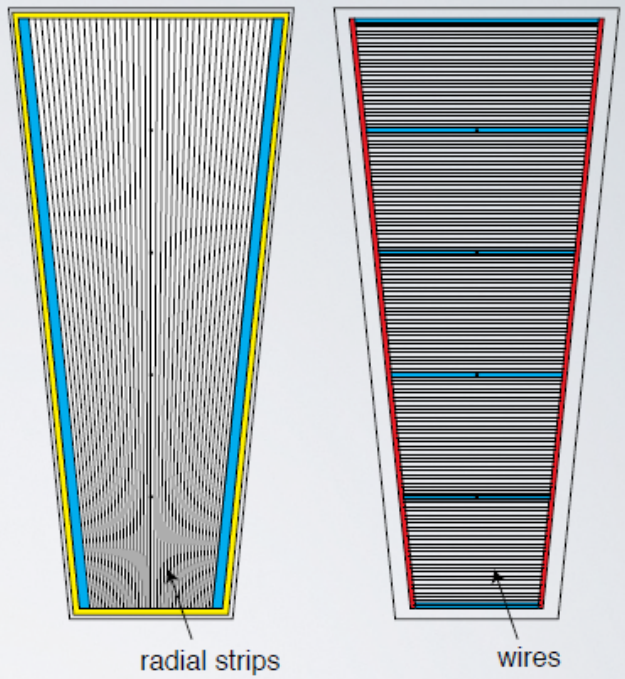

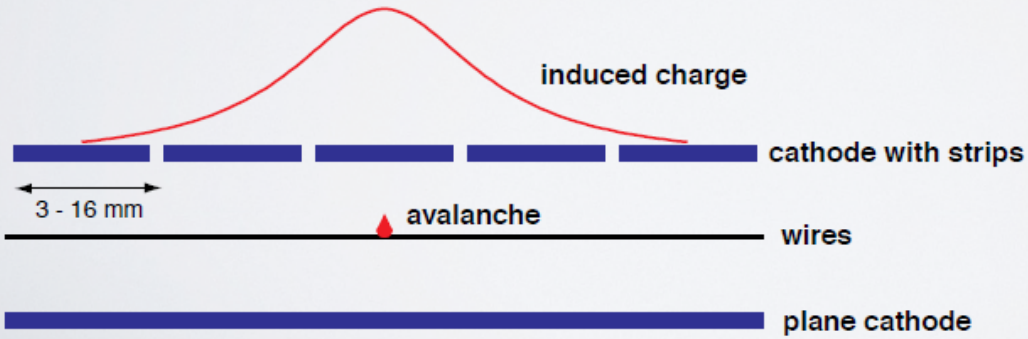

Georges Charpak's detector group
at CERN in 1960's & 70's

Cathode Strip Chamber (CSC)

- The Gatti et al. distribution is a semi-empirical function that describes the induced charge distribution on cathode strips: $\Gamma(\lambda) = k_1[(1 - \tanh^2(k_2\lambda))/(1 + k_3\tanh^2(k_2\lambda))]$

$\lambda = x/D$

Here it is compared to strip widths characteristic of the CSC system [anode-to-cathode spacing D=4.8 mm]

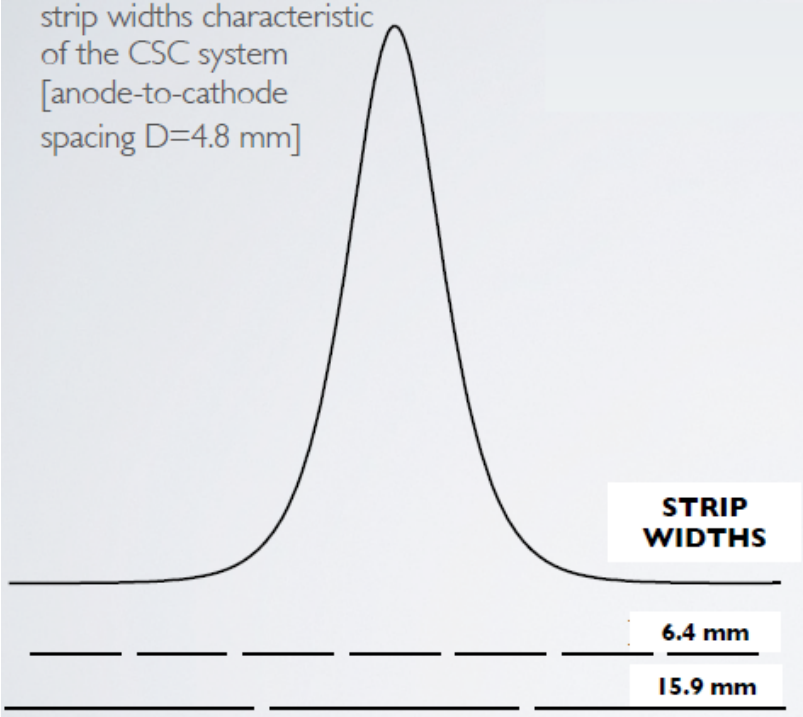

NUCLEAR INSTRUMENTS AND METHODS 163 (1979) 83-92 ; © NORTH-HOLLAND PUBLISHING CO.

OPTIMUM GEOMETRY FOR STRIP CATHODES OR GRIDS IN MWPC FOR AVALANCHE LOCALIZATION ALONG THE ANODE WIRES*

E. GATTI, A. LONGONI
Istituto di Fisica del Politecnico, Milan, Italy
H. OKUNO+
Brookhaven National Laboratory, Upton, New York, U.S.A.
and
P. SEMENZA
Politecnico, Milan, Italy

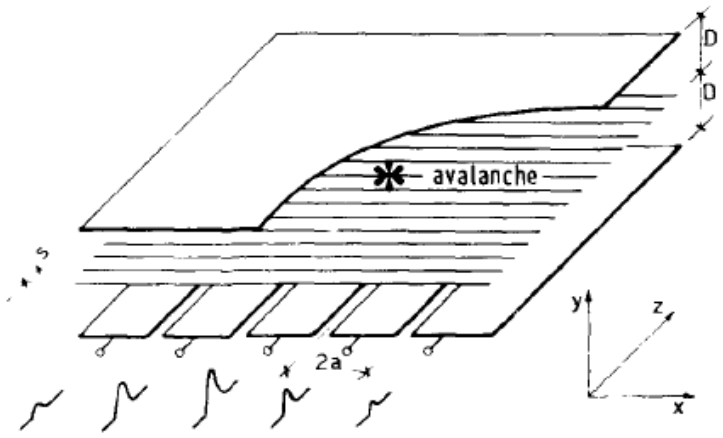

Fig. 1. MWPC with readout cathode strips.

E. Gatti, A. Longoni, H. Okuno, P. Semenza – Nucl. Instr. and Meth., 163 (1979), 83–92
http://www.sciencedirect.com/science/article/pii/0029554X79900351

The strip widths in the system are in the range 6.6 mm innermost ME1/2 to 16.0 mm outermost ME234/2 chambers. ME1/1 has smaller widths, 3.2–7.6 mm and a-to-c spacing 3.5 mm

Cathode Strip Chamber (CSC)

The CMS CSC Design

- 7 16 mm trapezoidal pannels (PolyCarb + FR4) forming 6 gas gaps (9.5 mm)
- anode wires run azimuthally and provide measurement of radial coordinate (r)
- 0.50 μm wires spaced at 3.2 mm (3.6 kV)
- wires grouped by 10–15
- Gas Mixture: $Ar/CO_2/CF_4$ :: 40/50/10 (insensitive for Temperature variations)
- cathode strips are trapezoidal and provide measurement of azimuthal coordinate (ϕ)
- strip pitch 8.4 – 16 mm (4.75 mm below wire)
- strips staggered by half strip

V. Barashko et al. / Nuclear Instruments and Methods in Physics Research A 589 (2008) 383–397 385

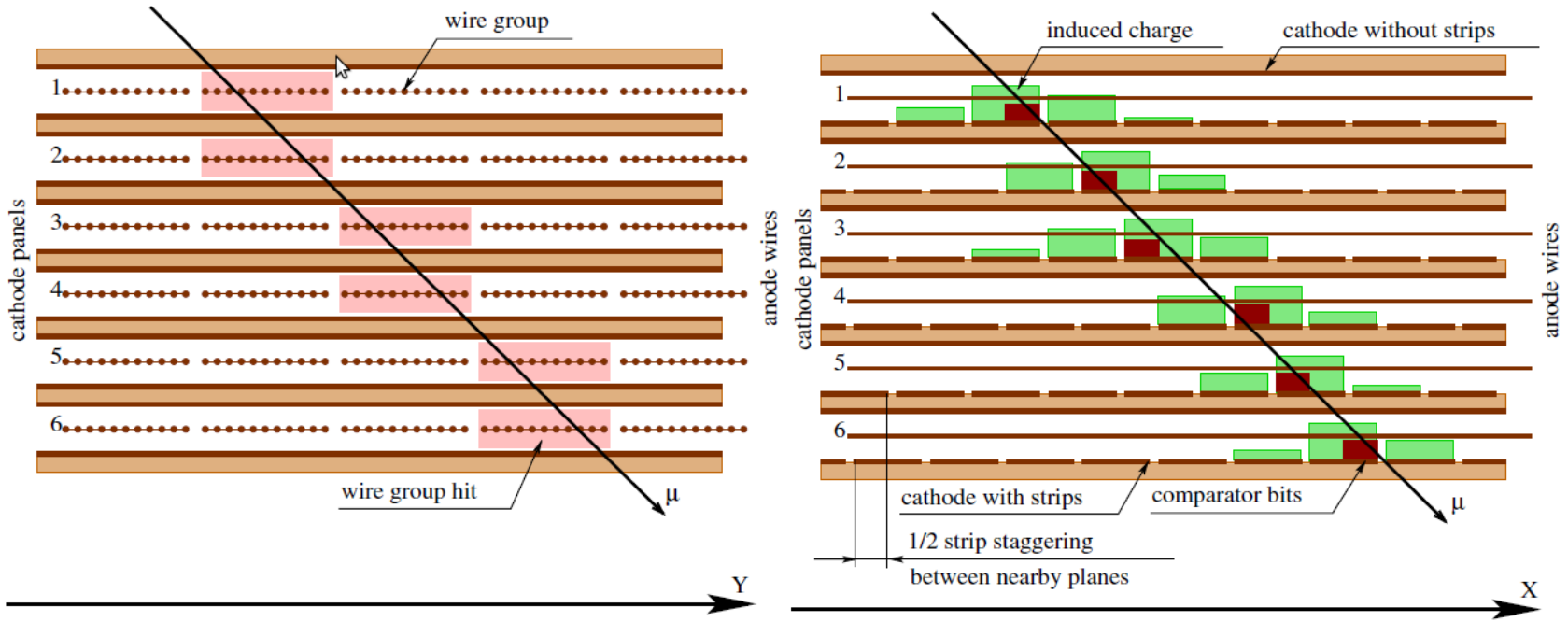

Fig. 3. Left: A pattern of wire group hits left behind by a muon passing through a chamber. Right: A pattern of induced charges on strips and half-strip hits left behind by a muon.

Anode Wire Signal

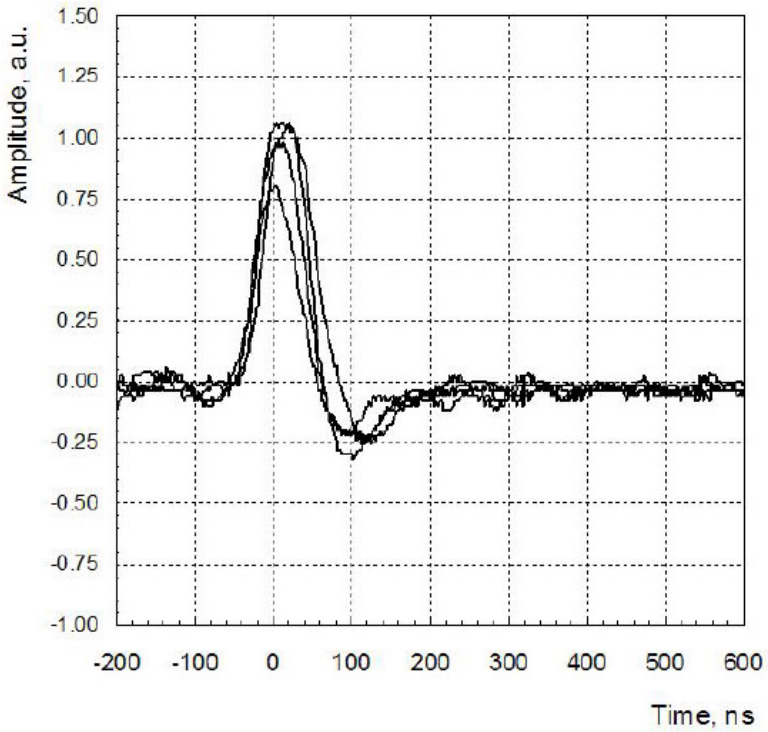

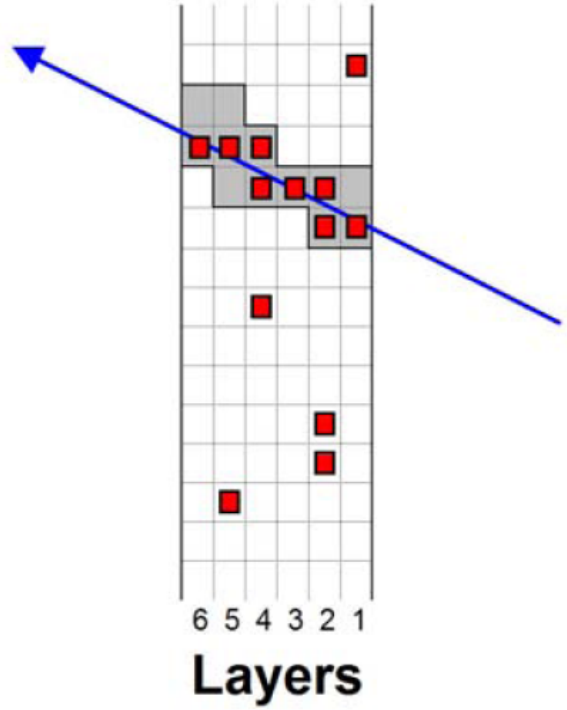

Figure 7.55: Left panel: muon signals as seen at the AFEB amplifier output. Right panel: a schematic event display showing anode signals in the 6 planes of a CSC (small dark squares). The ALCT board FPGA logic is programmed to scan the chamber and search for hits falling inside predefined patterns (grey cells) consistent with muons originating from the interaction point. Hits must be present in at least 4 planes for an ALCT pattern to be found.

Cathode Strip Signal

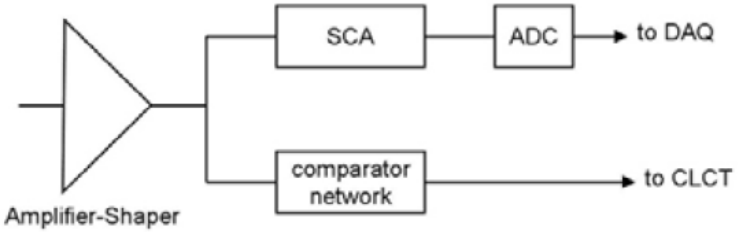

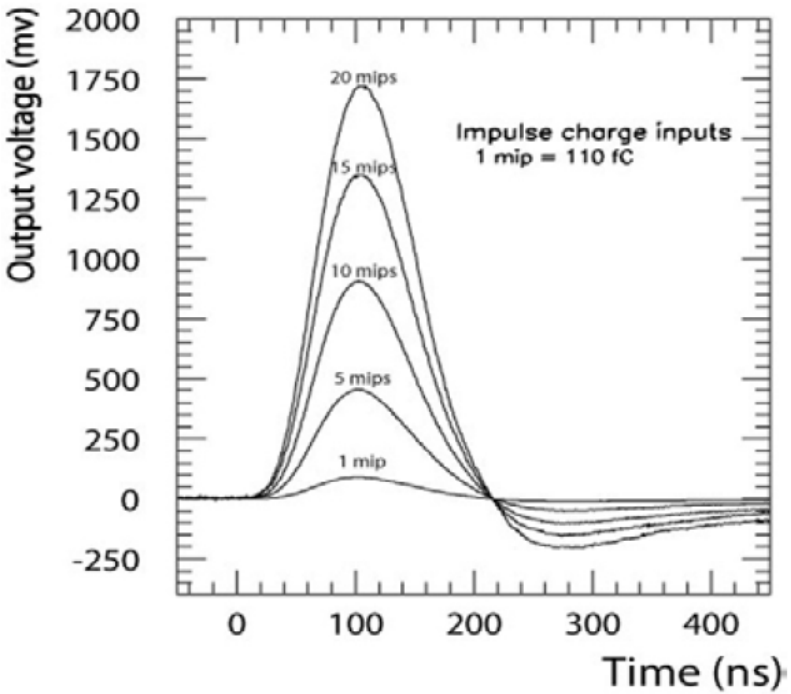

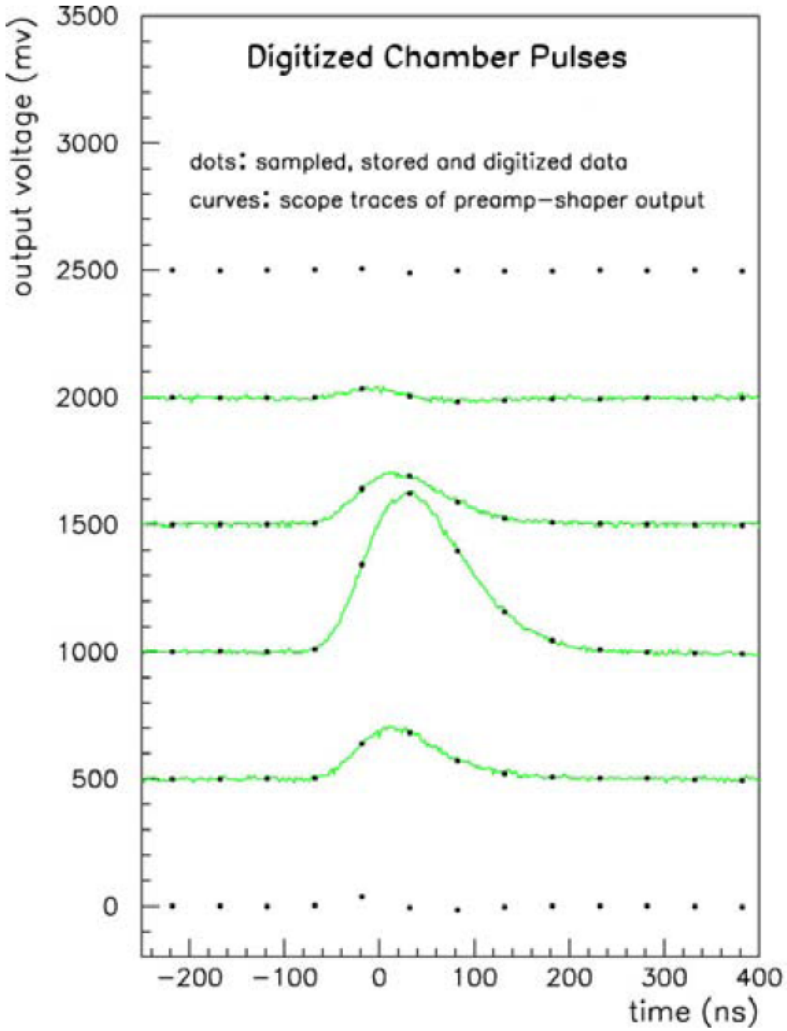

Cathode Strip Signal Comparator

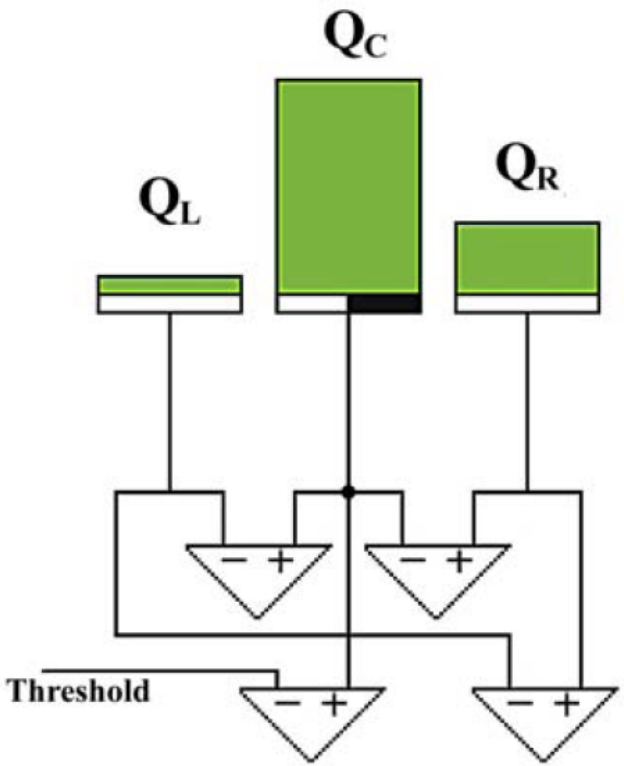

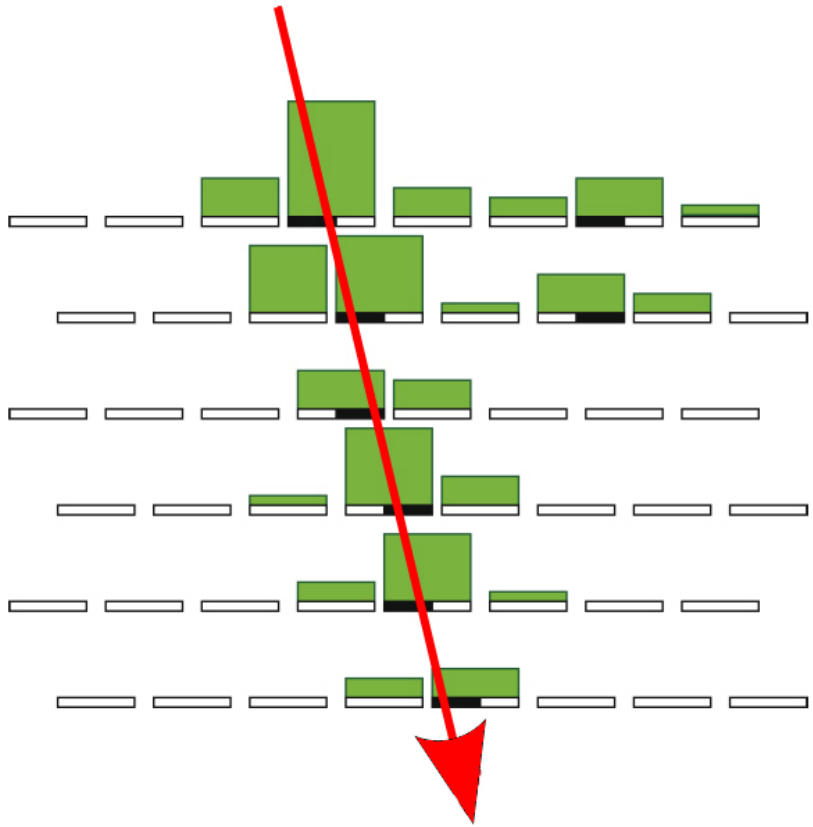

CSC Electronics Overview

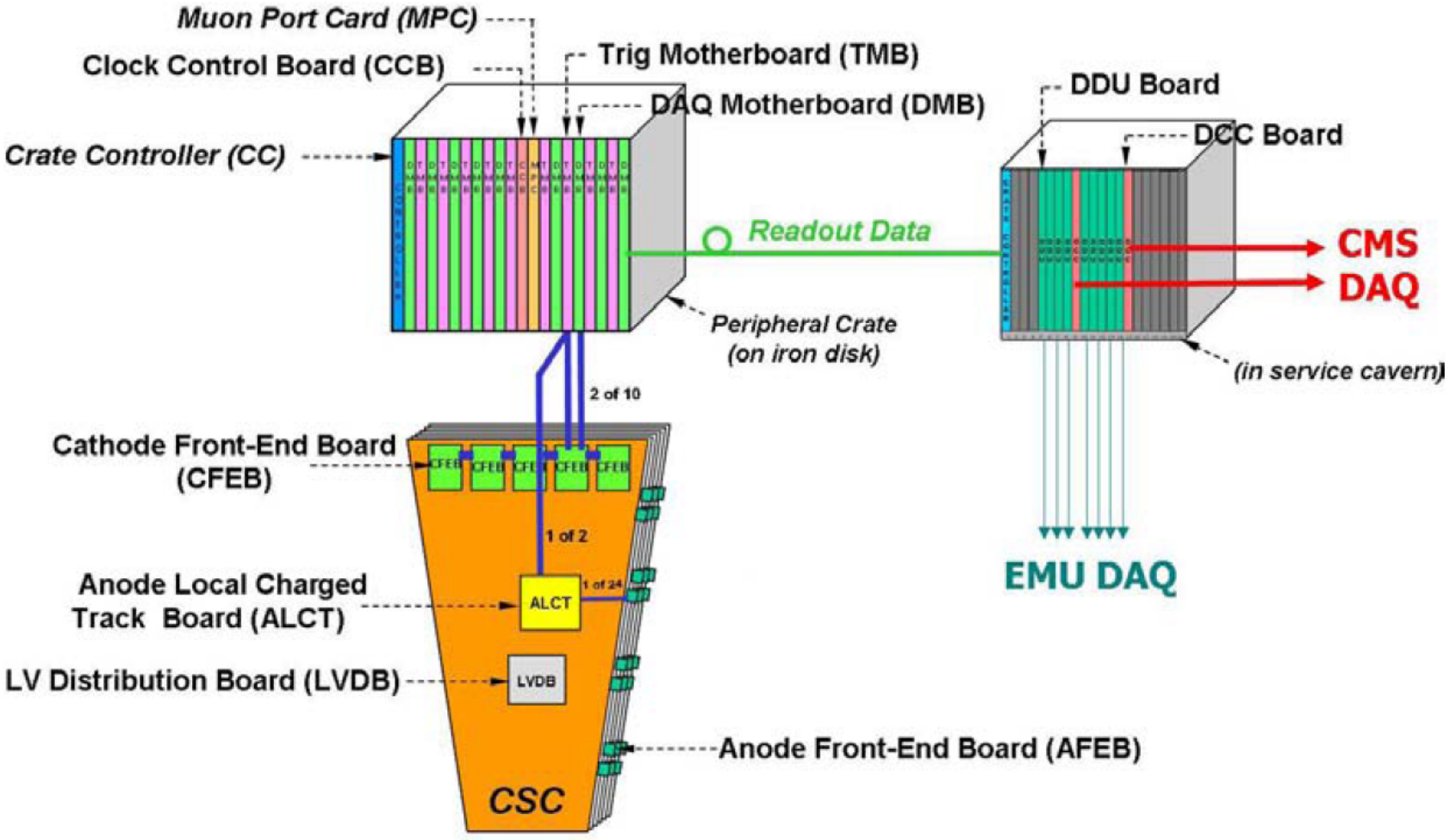

CMS CSC System

CSC System in numbers:

- 2 Endcaps, each 4 stations
- $0.9 < |\eta| < 2.4$
- 540 CSC chambers
- 2M wires in 180k anode wire channels
- 220k cathode strip channels
- $> 50\,\mathrm{m}^3$ gas, 9000 HV channels
- operated at 3.6 kV
- all chambers overlap in ϕ except ME1/3

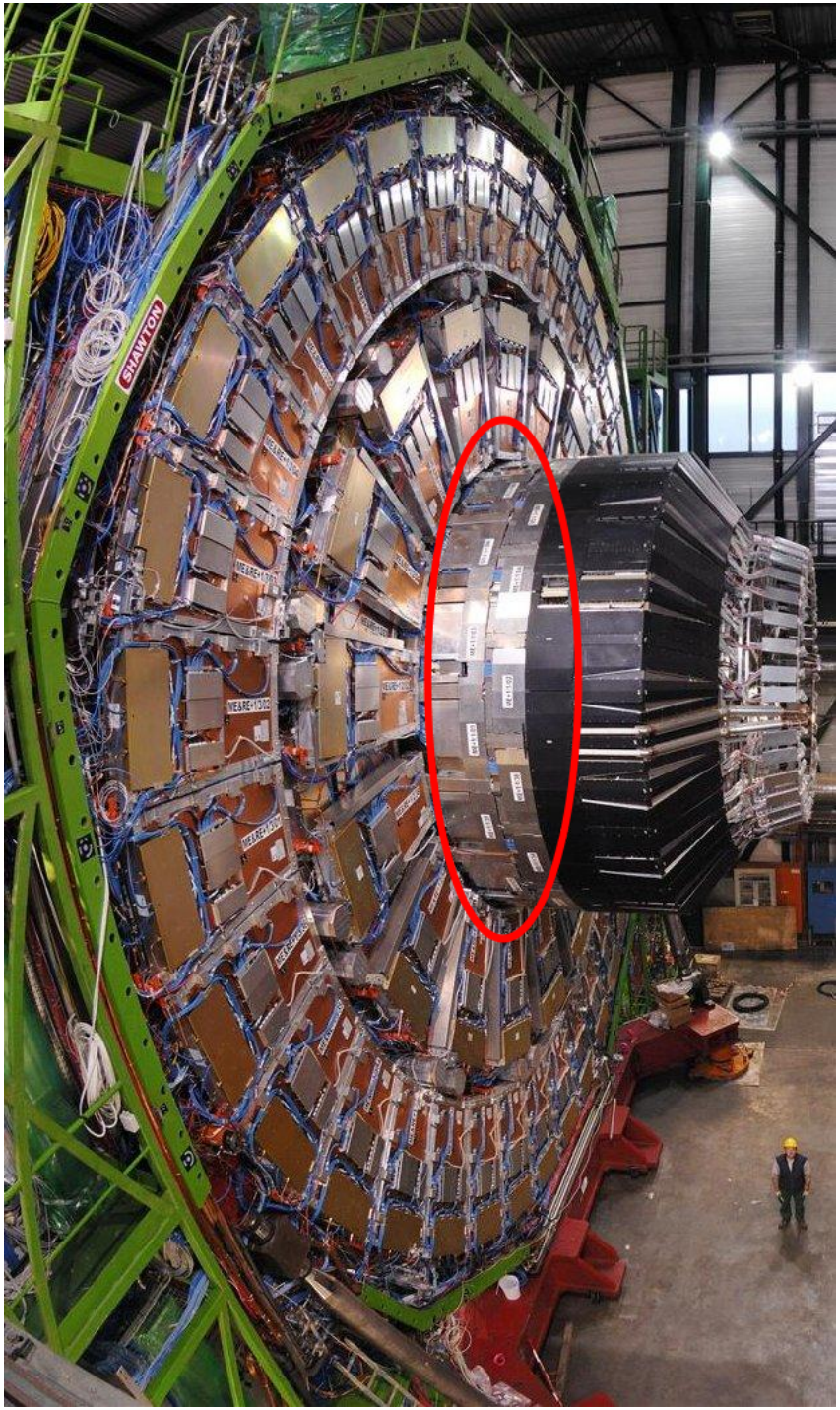

A special case :: ME1/1

- Chambers in the CMS Solenoid
- Strong Uniform Magnetic Field (4T)
- 7 mm gas gap, 2.5 mm wire spacing
- 30 μm wires operated at 2.9 kV
- ME1/1b ($|\eta| < 2.1$)
- ME1/1a ($|\eta| < 2.4$)
- 3 strips "ganged" in 1 ch in ME1/1a
- wires tilted with $\alpha_L = 29^\circ$

ME1/1a channel ganging

ME1/1A ganged strips

To compensate for lack of money and space.
We treat ME1/1A as a separate chamber (layers) labelled as C=1, R=4 (i.e. pseudo-ring 4).
How the ganging of strips to channels works, and how this can lead to ambiguities in reconstruction:

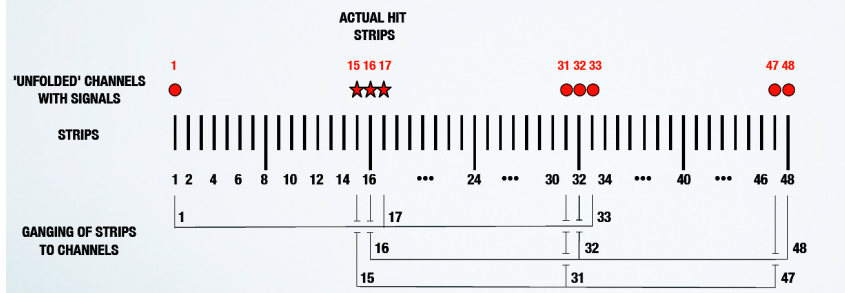

Lorentz Angle

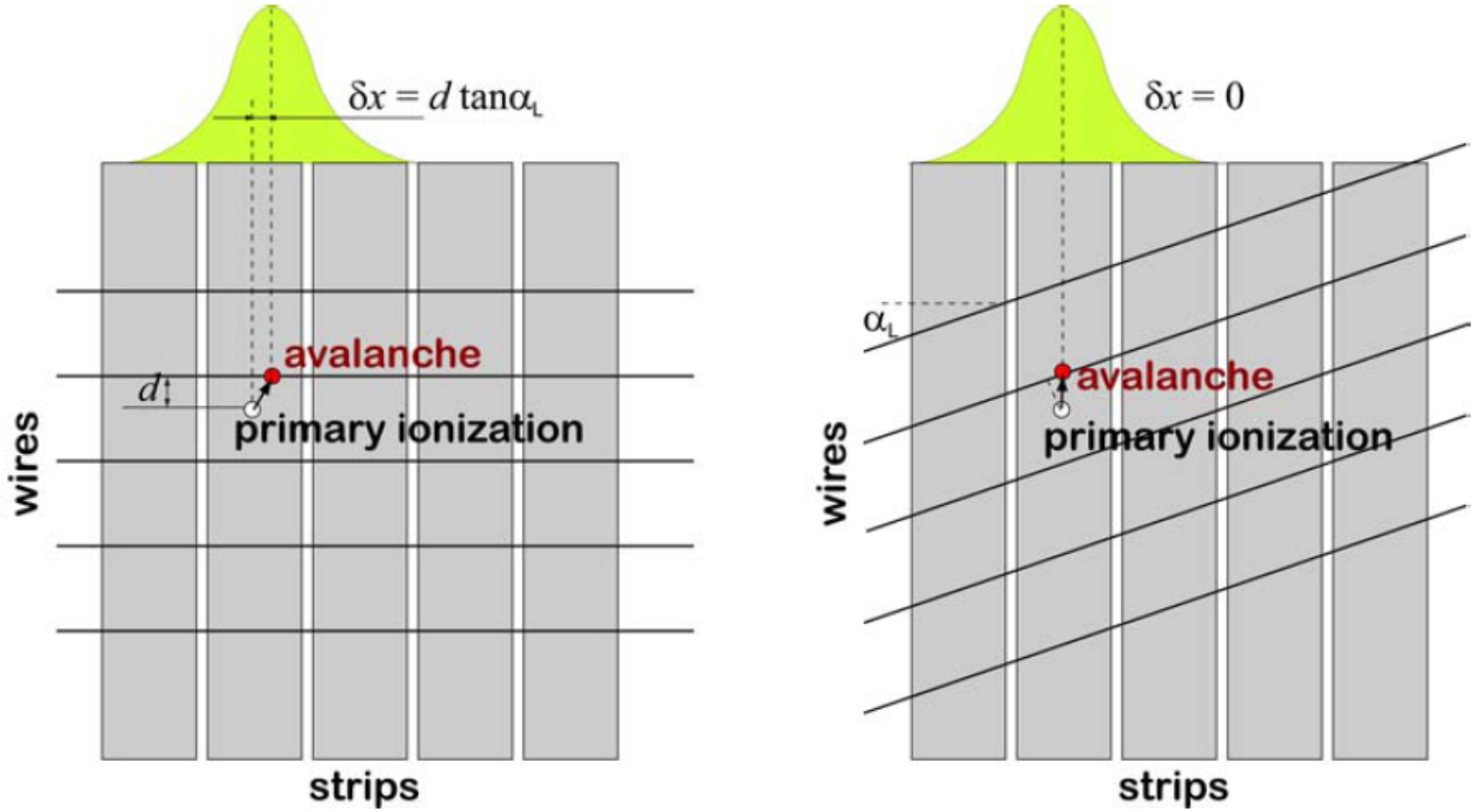

Figure 7.53: Left panel: if the ME1/1 wires were not tilted, ionisation electrons, as they drift toward the anode wires in the strong magnetic field normal to the plane of the drawing, would be carried sideways by the Lorentz force. The direction and size of the shift would depend on whether the electrons drift upwards or downwards and on how far away they were from the wires to begin with. These sideways displacements would spread the charge over the anode wires. Right panel: by tilting the wires at the Lorentz angle α_L, all ionisation electrons arrive near the same point.

Drift Tube detector

From MWPC to Drift Chambers: Field Shaping

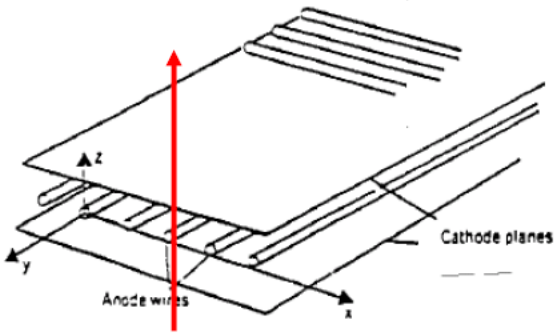

Abbildung 2.27: *Vieldrahtproportionalkammer.*

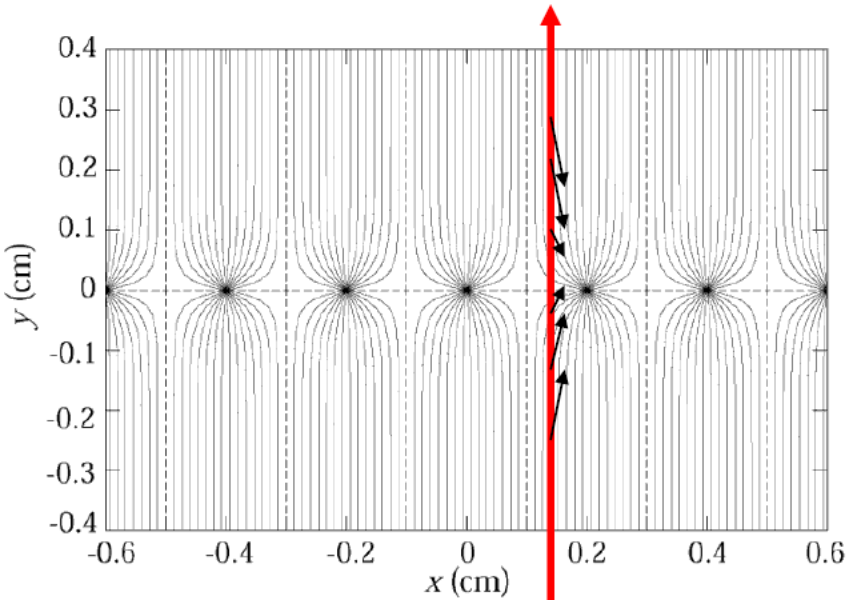

MWPC WITH A FIELD-SHAPING WIRE BETWEEN ANODES, TO AVOID LOW-FIELD REGIONS

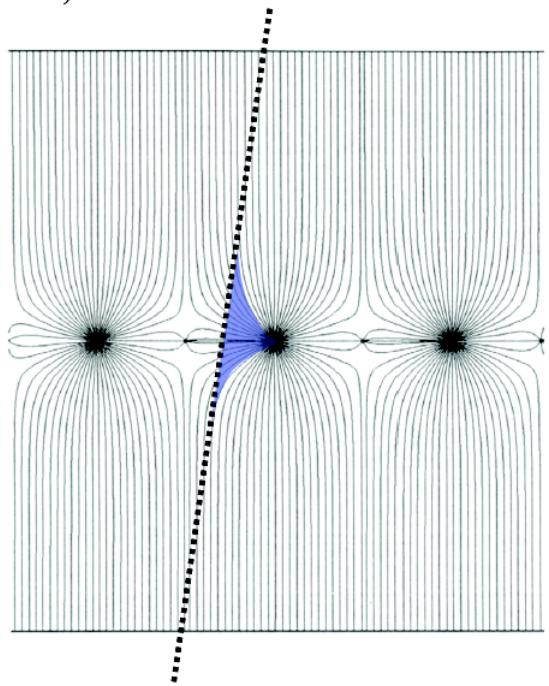

A. H. Walenta, J. Heintze and B. Scürlein, Nucl. Instr. and Meth. 92(1971)373

Drift Chambers

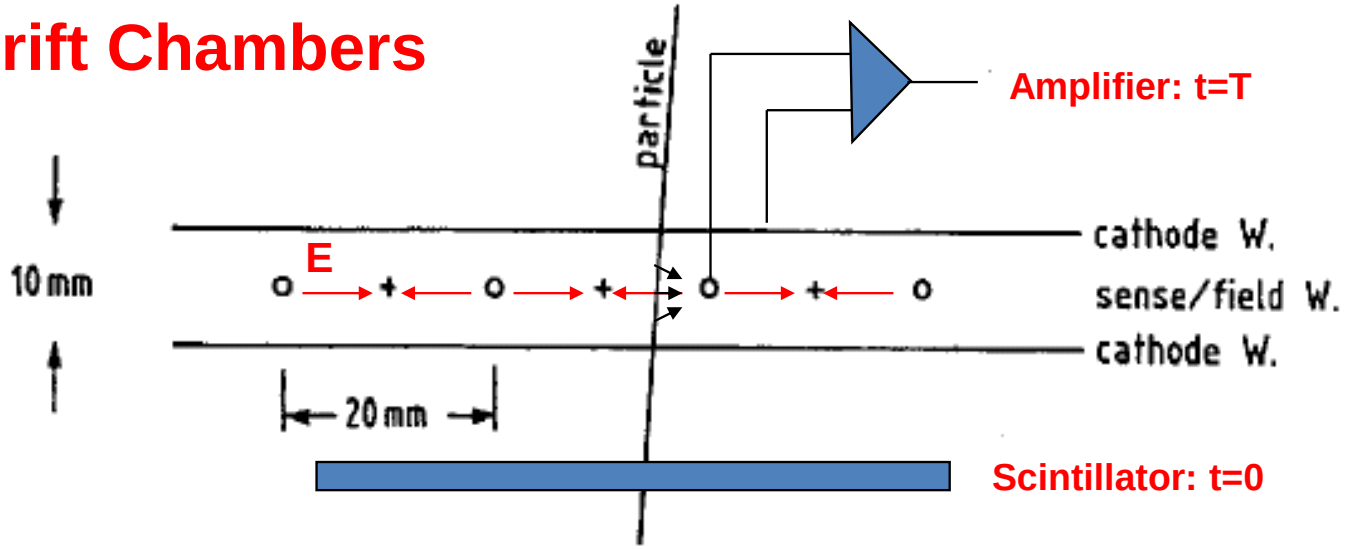

In an alternating sequence of wires with different potentials one finds an electric field between the 'sense wires' and 'field wires'.

The electrons are moving to the sense wires and produce an avalanche which induces a signal that is read out by electronics.

The time between the passage of the particle and the arrival of the electrons at the wire is measured.

The drift time T is a measure of the position of the particle !

By measuring the drift time, the wire distance can be increased (compared to the Multi Wire Proportional Chamber) → save electronics channels !

Drift Chambers, typical Geometries

Electric Field ≈ 1kV/cm

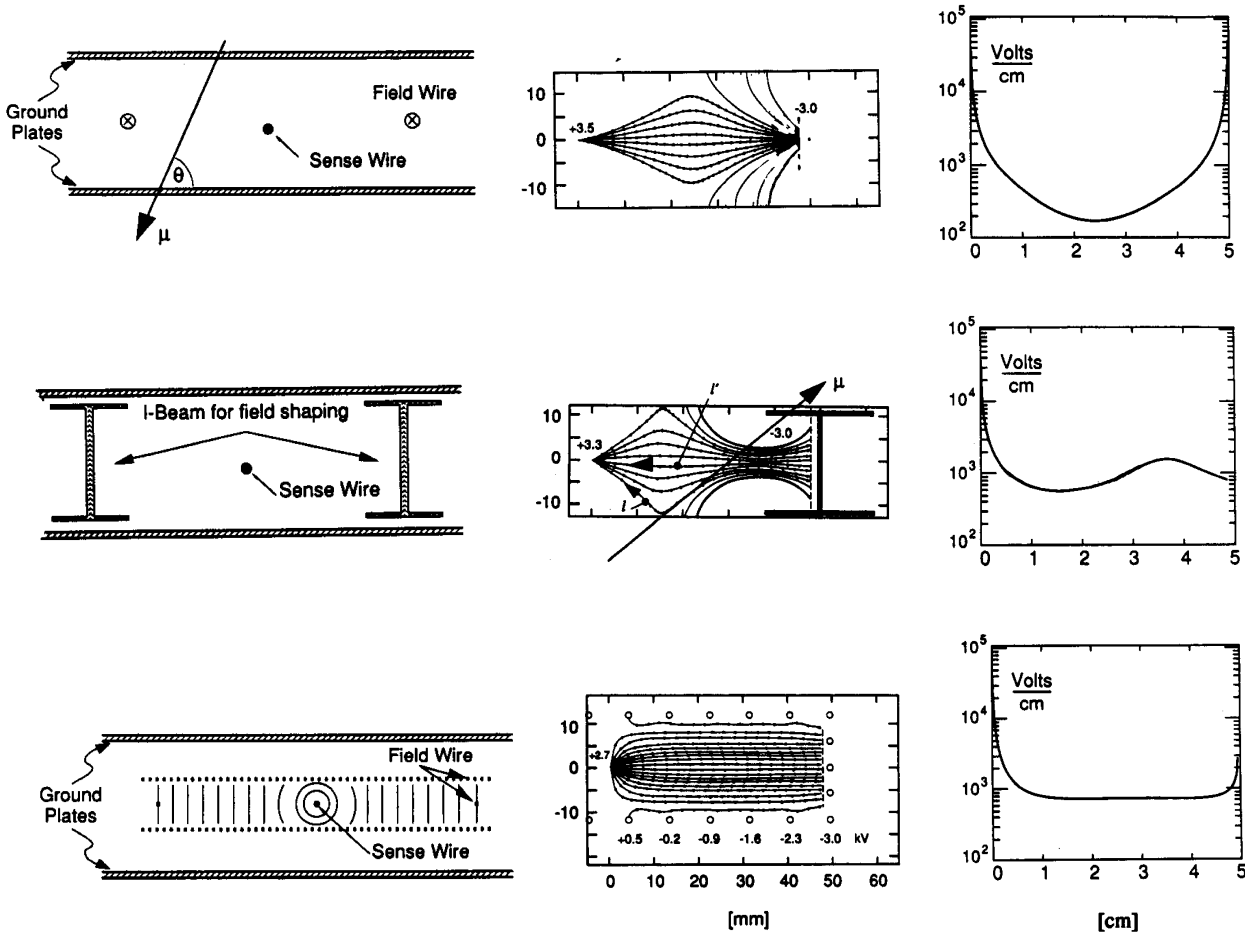

W. Klempt, Detection of Particles with Wire Chambers, Bari 04

CMS Drift Tube Cell

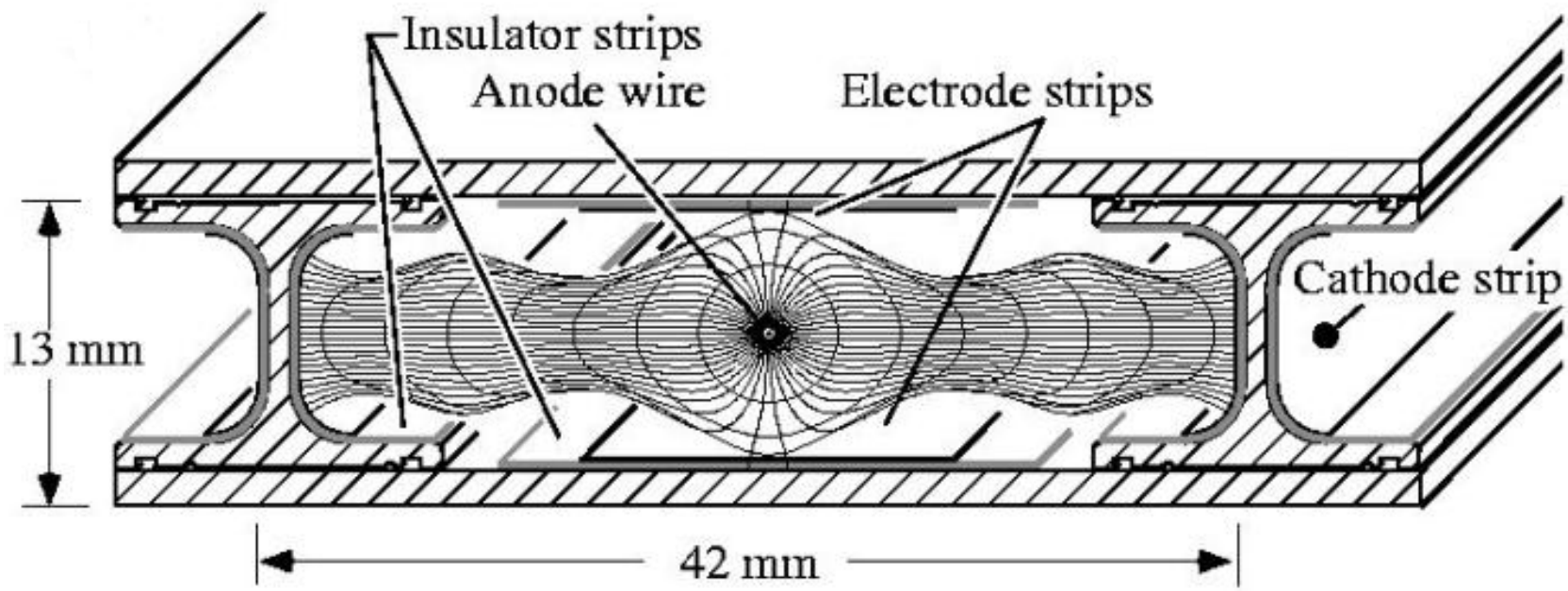

- **1 Anode:** 50 μm gold-plated stainless steel wire
- **2 Field shaping strips:** Aluminium strip
- **2 Cathodes:** Aluminium strip on I-beam
- An/Strip/Cath at +3.6 kV / +1.8 kV / -1.2 kV
- aluminium drift cell wall set to 0 V
- tube cross section of $13 \times 42\,\mathrm{mm}^2$
- individual tubes protect against damage from broken wire
- 1.5 mm thick drift drift cell wall decouples from low energy $e^{\pm}$

CMS Drift Tube Drift Velocity

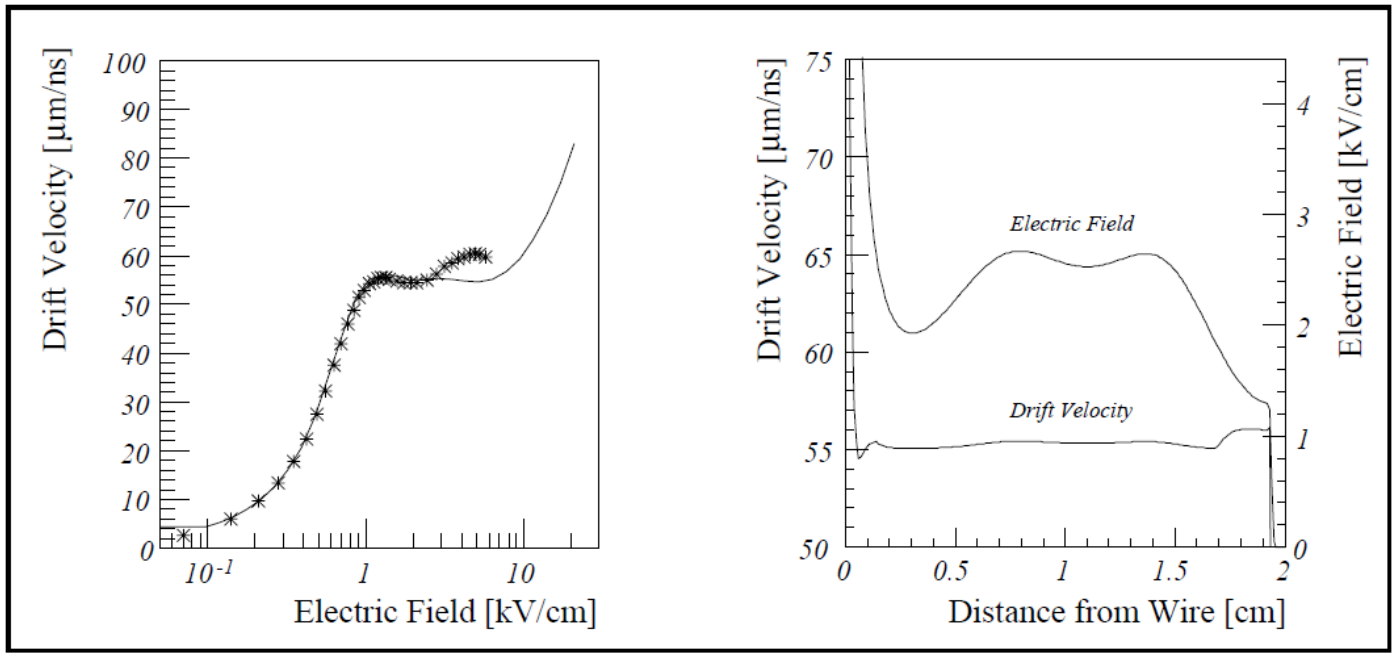

Fig. 3.2.5: a) (left) drift velocity vs. electric field for simulations and measurement with the final gas choice (Ar/CO_2 85/15); b) (right) drift velocity across the drift cell; it can be seen that a good linearity is present in the entire cell.

- Ar/CO_2 gas mixture (85/15) (Gain $= 10^5$)
- uniform drift field of $\approx 1.5\,kV/cm$
- v_{drift} saturation between 1 and $2\,kV/cm$
- linear relationship t_{drift} and distance

CMS Drift Tube System

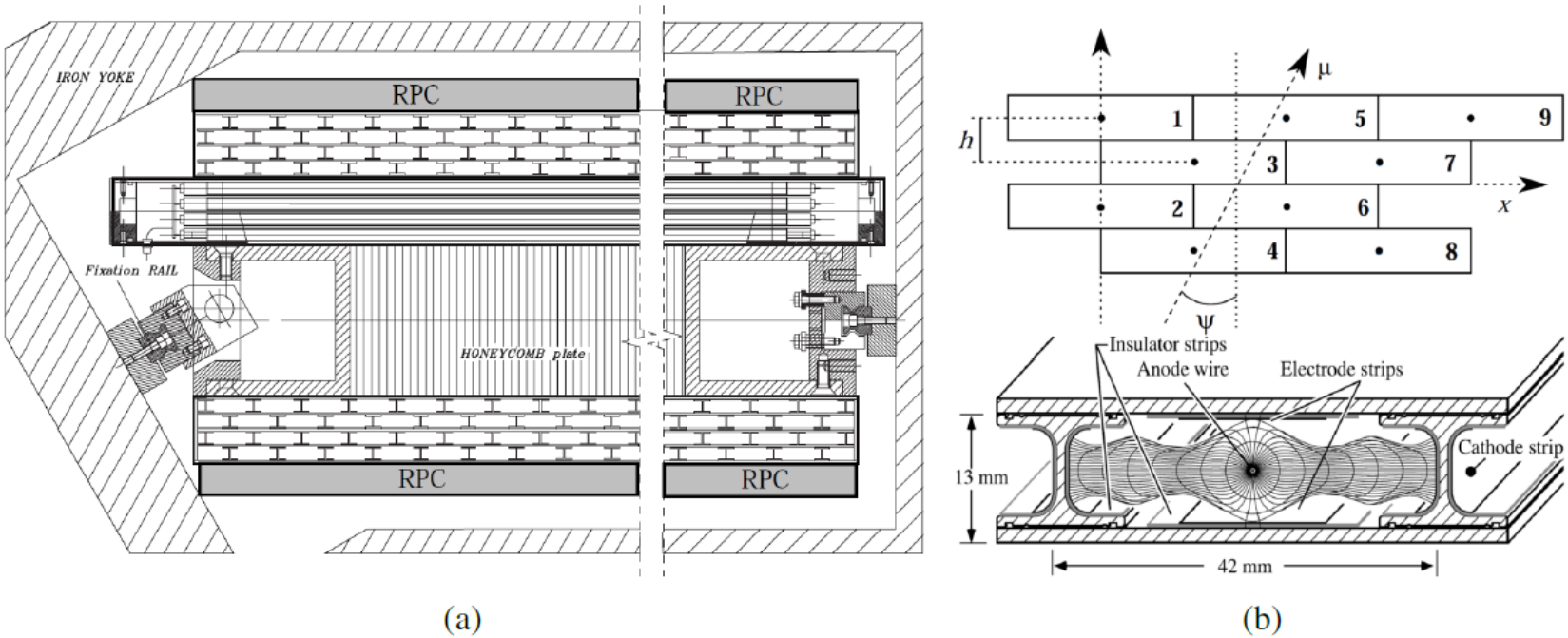

(a) (b)

Figure 3.8: (a) Cross section of a DT chamber with RPCs attached both on top and and at the bottom. The two superlayers measuring the ϕ coordinate are perpendicular to the plane of the figure and are at the bottom and at the top of the chamber. The superlayer measuring the η-coordinate is in the middle, above the honeycomb plate separating the two ϕ-superlayers. (b) Bottom: A Drift Tube cell and its complexly shaped electric field inside. (b) Top: The hit pattern of a muon passing through a superlayer [138, 141].

Mean Timer Algorithm

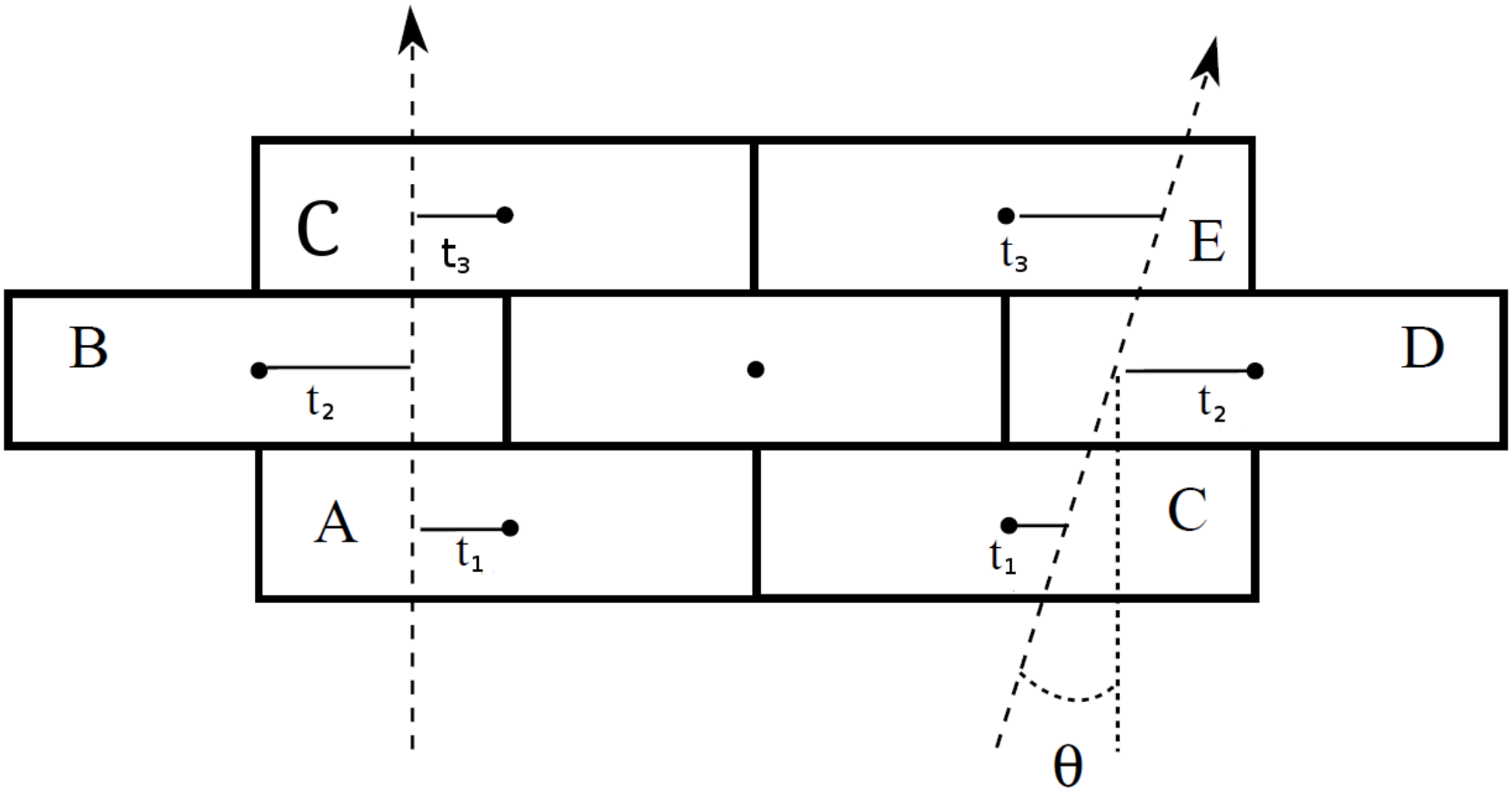

max drift time in one DT cell obeys to the following relation:

$$t_{max} = \frac{1}{2}(t_1 + 2t_2 + t_3)$$

Mean Timer Algorithm

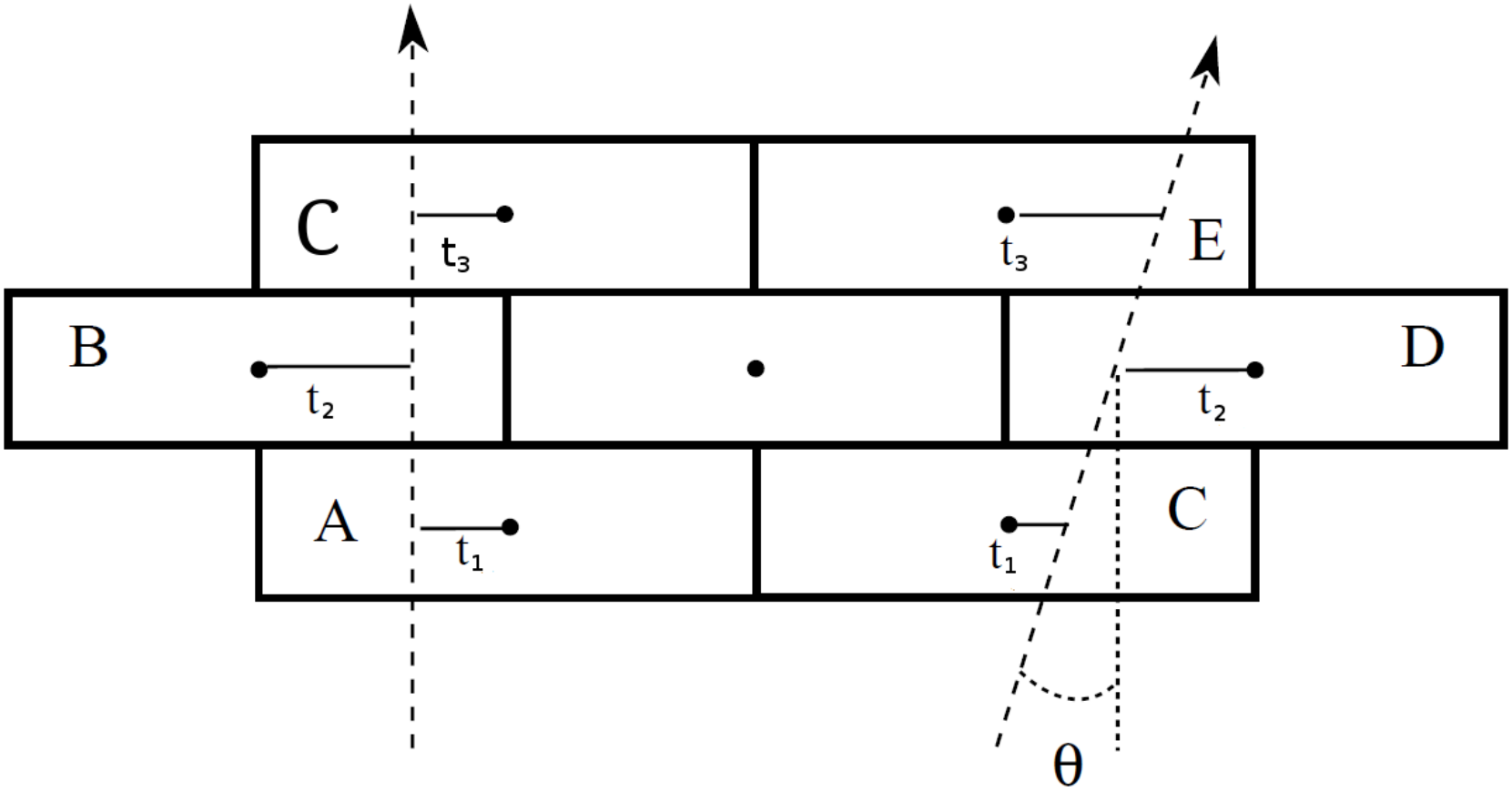

e.g. $400\,ns = \frac{1}{2}(150\,ns + 2 \cdot 250\,ns + 150\,ns)$

Mean Timer Algorithm

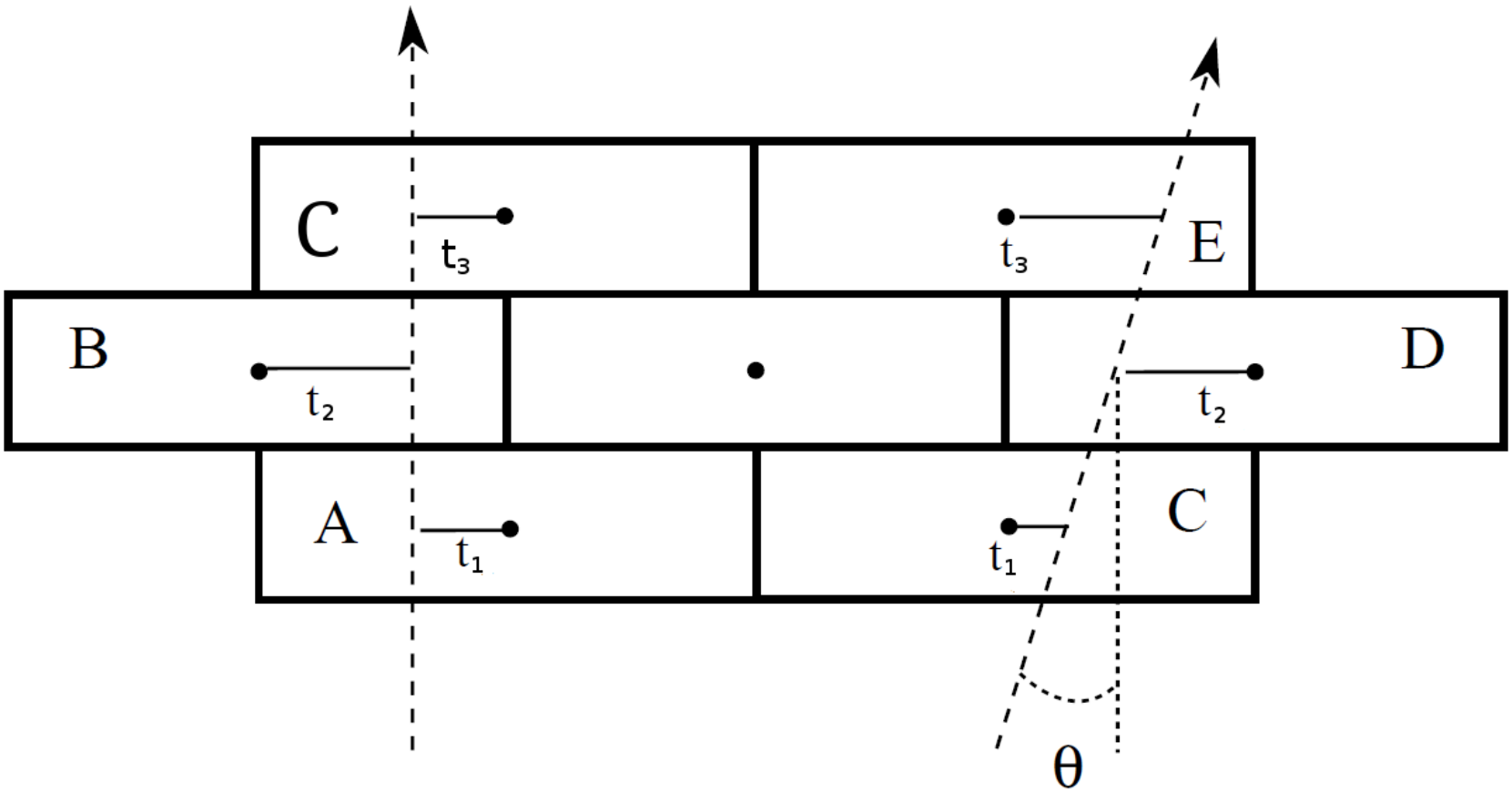

in reality we do not measure the exact drift times
only the differences between the times in the three cells:

$$t_A = t_1 - t_1 = 0, \qquad t_B = t_2 - t_1 \qquad t_C = t_3 - t_1$$

$$400\,ns = \frac{1}{2}(t_1 + 2 \cdot (t_B + t_1) + (t_C + t_1)) \quad \Rightarrow \quad t_1 \quad \Rightarrow \quad t_2, t_3$$

CMS Drift Tube System

DT System in numbers:

- 5 barrel "wheels", with 4 stations each
- $0.0 < |\eta| < 1.2$
- 250 chambers, each consisting of 3 SL
- 1 SL consisting of 4 layers of 60-70 cells
- in total 172k sensitive wires
- wires are 2.4 m long and 50 μm diameter
- $t_{\text{max}} = 380\,\text{ns}$ in Ar/CO_2 (85/15)
- $d_{\text{max}} = 21\,\text{mm}$
- $v_{\text{drift}} = 55.5\,\mu\text{m/ns}$

CMS Drift Tube System

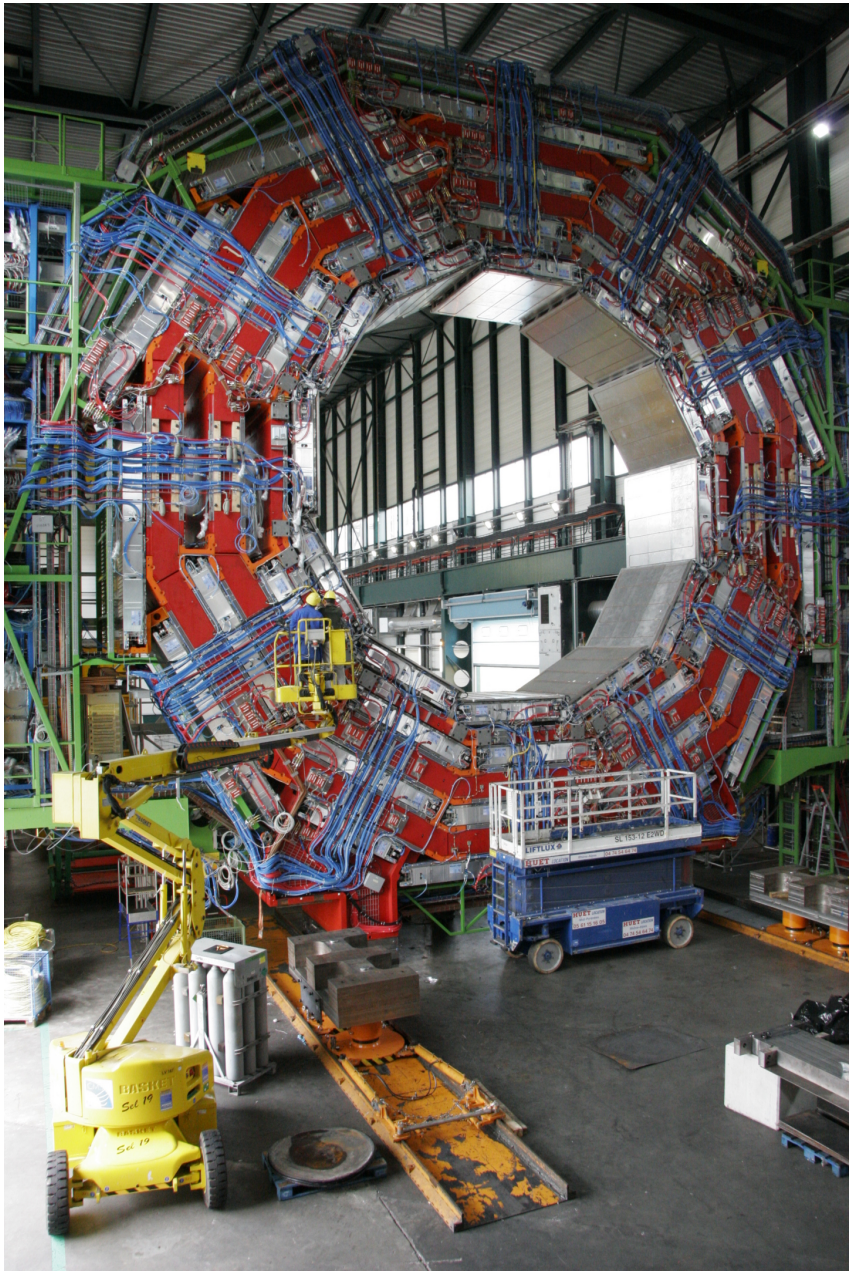

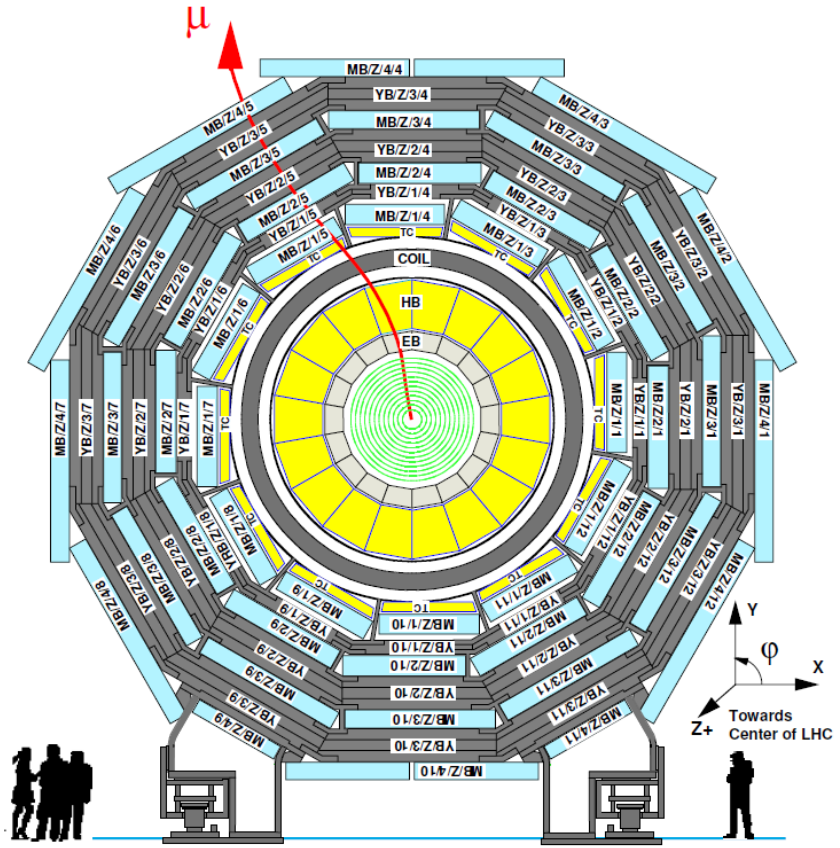

- 5 wheels
- 4 stations
- 12 sectors (60°)
- overlap in φ

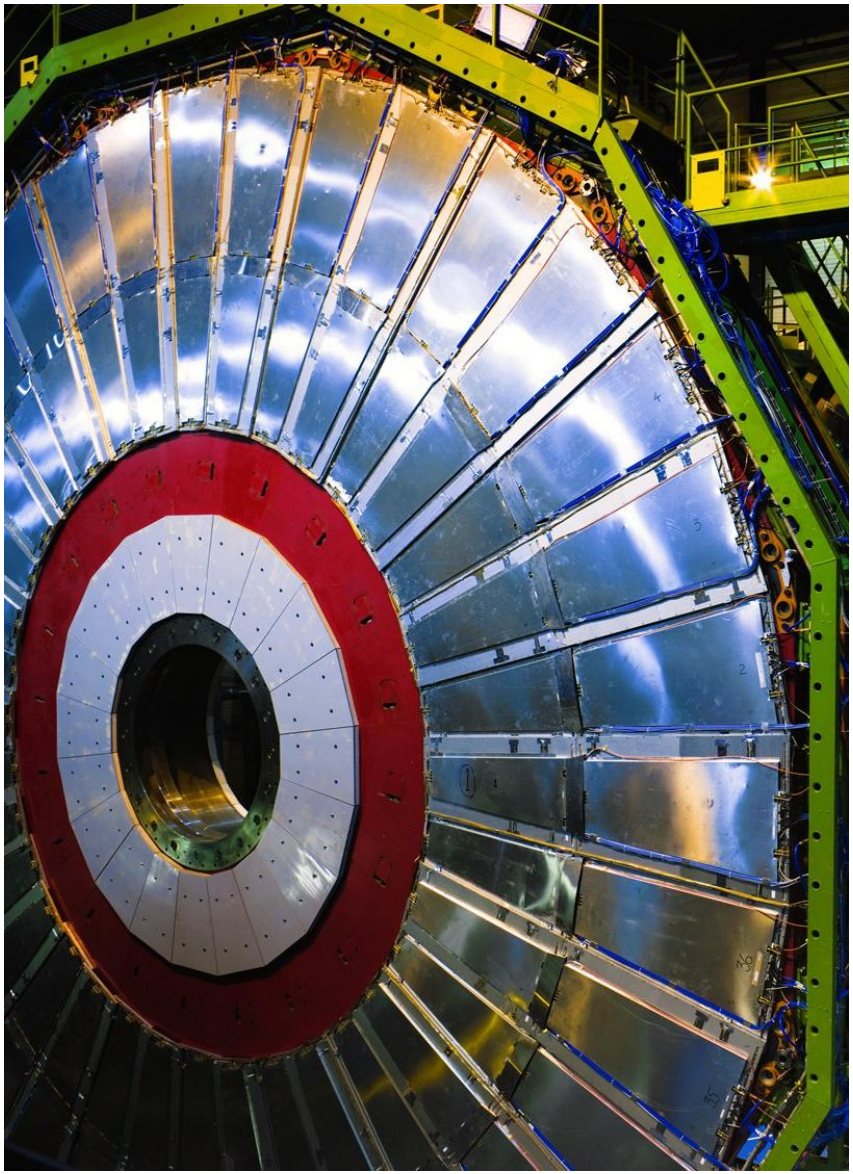

Resistive Plate Chamber detector

Position Resolution/Time resolution

Up to now we discussed gas detectors for tracking applications. Wire chambers can reach tracking precisions down to 50 micrometers at rates up to <1MHz/cm^2.

What about time resolution of wire chambers ?

It takes the electrons some time to move from thir point of creation to the wire. The fluctuation in this primary charge deposit together with diffusion limits the time resolution of wire chambers to about 5ns (3ns for the LHCb trigger chambers).

By using a parallel plate geometry with high field, where the avalanche is starting immediately after the charge deposit, the timing fluctuation of the arriving electrons can be eliminated and time resolutions down to 50ps can be achieved !

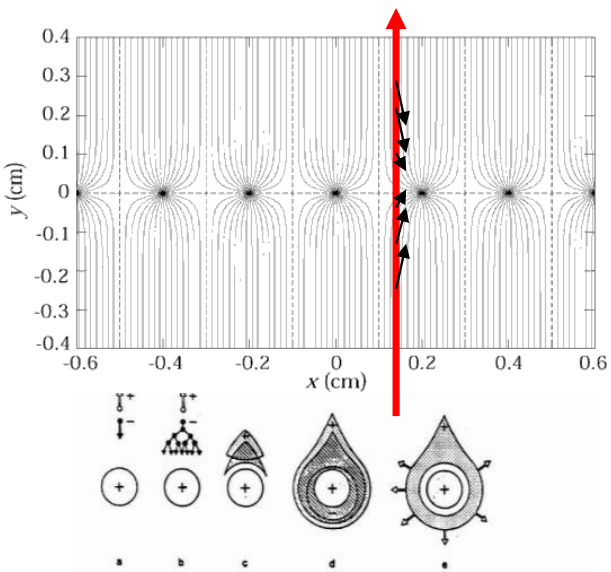

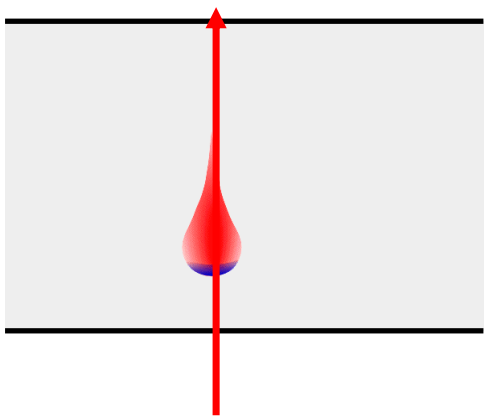

Resistive Plate Chambers (RPCs)

Keuffel 'Spark' Counter:

High voltage between two metal plates. Charged particle leaves a trail of electrons and ions in the gap and causes a discharge (Spark).

→Excellent Time Resolution(<100ps).

Discharged electrodes must be recharged → Dead time of several ms.

Parallel Plate Avalanche Chambers (PPAC):

At more moderate electric fields the primary charges produce avalanches without forming a conducting channel between the electrodes. No Spark → induced signal on the electrodes. Higher rate capability.

However, the smallest imperfections on the metal surface cause sparks and breakdown.
→ Very small (few cm^2) and unstable devices.

In a wire chamber, the high electric field (100-300kV/cm) that produces the avalanche exists only close to the wire. The fields on the cathode planes area rather small 1-5kV/cm.

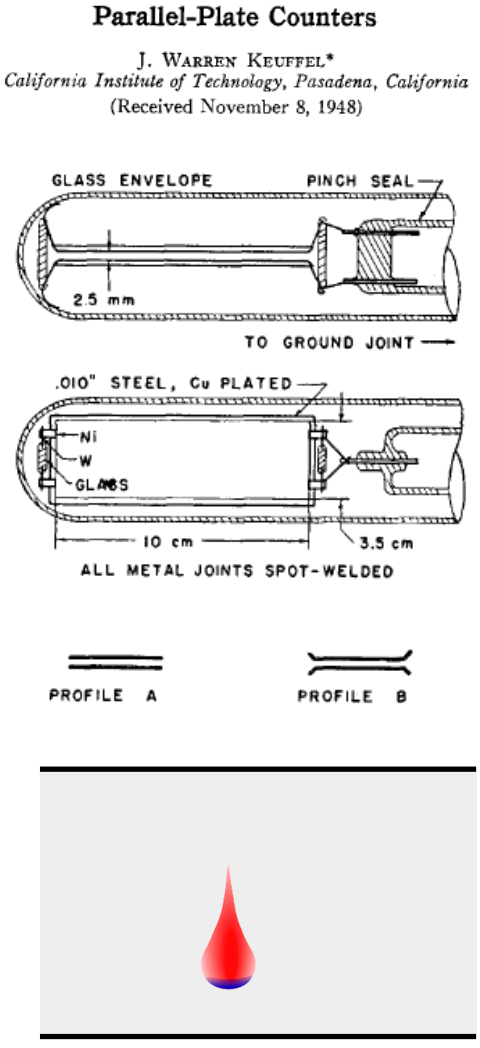
Parallel-Plate Counters

J. Warren Keuffel*
California Institute of Technology, Pasadena, California
(Received November 8, 1948)

GLASS ENVELOPE
PINCH SEAL
2.5 mm
TO GROUND JOINT
.010" STEEL, Cu PLATED
Ni
W
GLASS
10 cm
3.5 cm
ALL METAL JOINTS SPOT-WELDED
PROFILE A
PROFILE B

Resistive Plate Chambers (RPCs)

→ Place resistive plates in front of the metal electrodes.

No spark can develop because the resistivity together with the capacitance (tau ~ $\varepsilon * \rho$) will only allow a very localized 'discharge'. The rest of the entire surface stays completely unaffected.

→ Large area detectors are possible !

Resistive plates from Bakelite ($\rho = 10^{10}$-10^{12} Ωcm) or window glass ($\rho = 10^{12}$-10^{13} Ωcm).

Gas gap: 0.25-2mm.
Electric Fields 50-100kV/cm.
Time resolutions: 50ps (100kV/cm), 1ns(50kV/cm)

Application: Trigger Detectors, Time of Flight (TOF)

Resistivity limits the rate capability: Time to remove avalanche charge from the surface of the resistive plate is (tau ~ $\varepsilon * \rho$) = ms to s.

Rate limit of kHz/cm^2 for 10^{10} Ωcm.

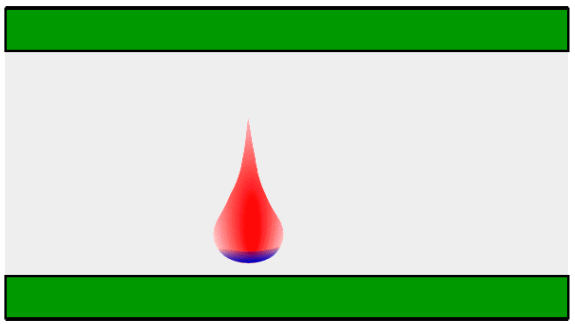

RPC Detection Principle

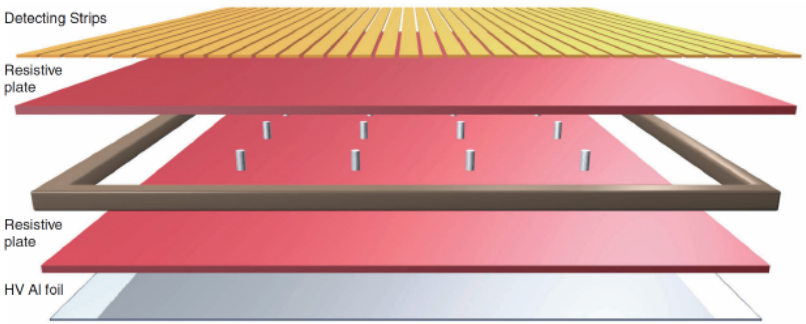

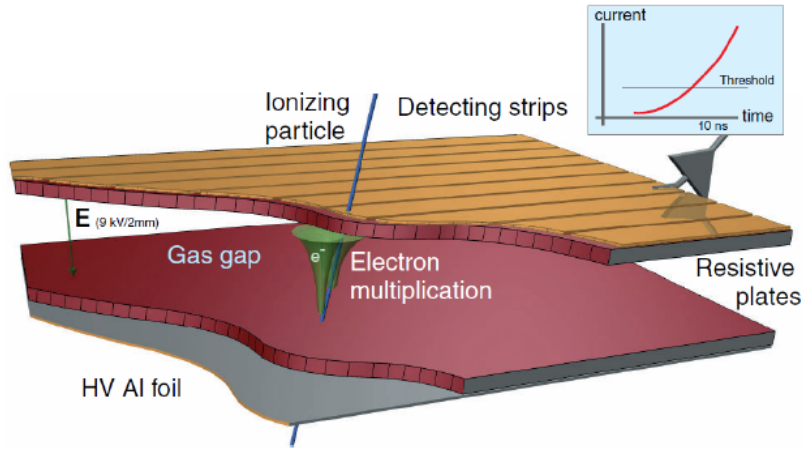

- Relatively new detector (1981–1988) developed by Santonico, Cardarelli (INFN Roma)
- Low cost alternative to fast large area scintillator detectors (expensive PM-tubes)
- Good time resolution, high efficiency, moderate spatial resolution

- 2 parallel plates with high resistivity
- small gas gap ($\sim$ atm. pressure)
- high electric field ($\sim 50\,\mathrm{kV/cm}$)
- immediate multiplication of ionization e^-
- signal picked up by strips through capacitive coupling

RPC Streamer mode vs Avalanche mode

NORMAL AVALANCHE

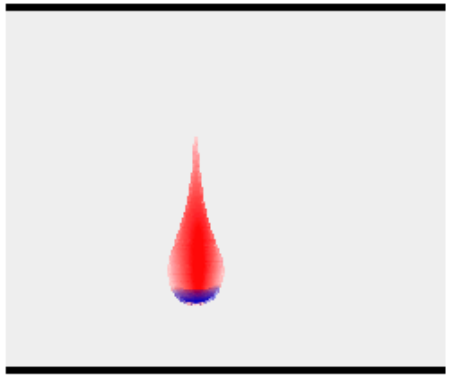

PHOTON MEDIATED BACKWARD PROPAGATION: STREAMER

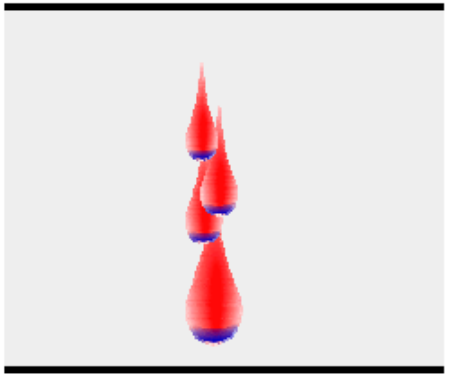

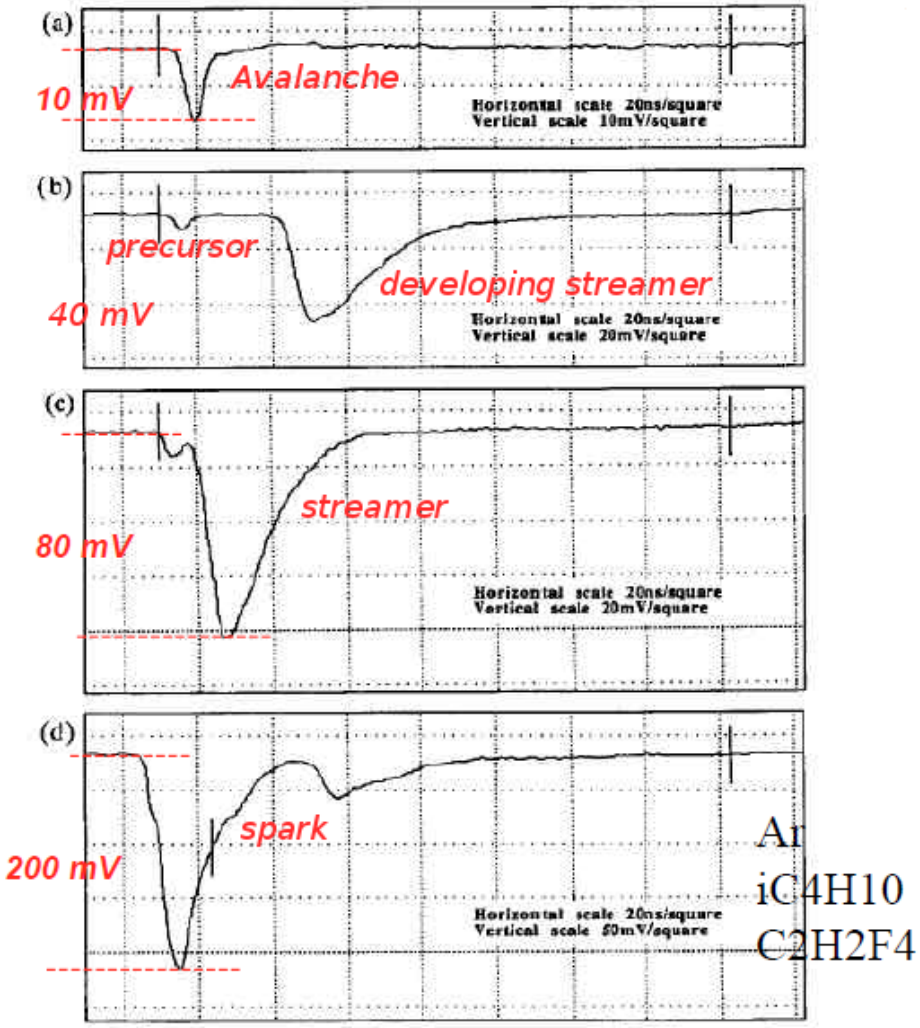

R. Cardarelli, V. Makeev, R. Santonico, Nucl. Instr. and Meth. A382(1996)470

The initiating **primary avalanche** generates photons which in turn generate numereous secondary avalanches. The electrons of the **secondary avalanches** are pulled by the strong electric field into the positively charged trail of the primary avalanche, creating a **streamer** (= a fast growing thin conductive channel). If a streamer connects the two electrodes, an arc is formed and the electrodes are discharged. **Lightning:** the arc is only visible when a conducting channel has been established between two clouds at different potential.

RPC Avalance mode requirements

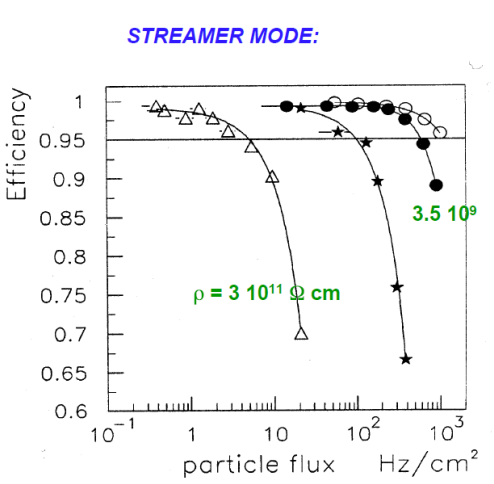

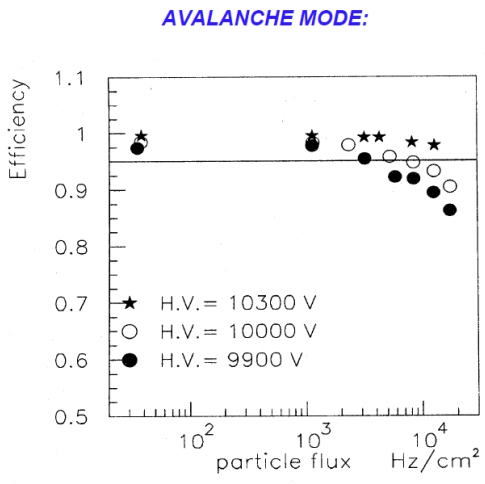

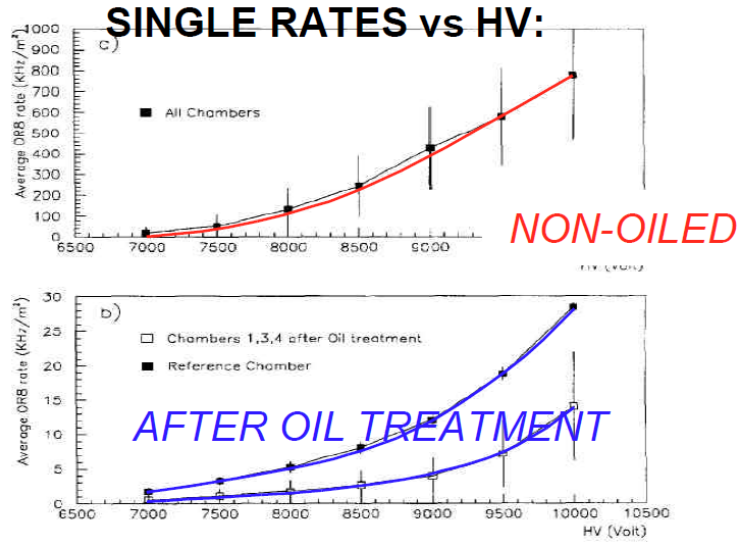

Requirements

- At LHC RPCs need to be operated in Avalanche mode to cope with the high particle rates
- RPCs needed to operate for 10 years at high efficiency therefore integrated charge need to be reduced
- RPCs operate at high electric fields, to avoid noise from random discharges a polished surface is required

Lessons learnt

- Babar :: RPCs had problems with oiling: droplets creating high electric fields or even conductive channels
- Babar :: RPCs had problems with rising bulk resisitivity due to temperature changes and irradiation
- CMS :: No oiling resulted in high noise rates. New oiling defined for LHC RPCs
- CMS :: Humified gas to keep bakelite plates humified (bakelite plates drying out have increased resisitivity)

RPC Single and Double Gap Layout

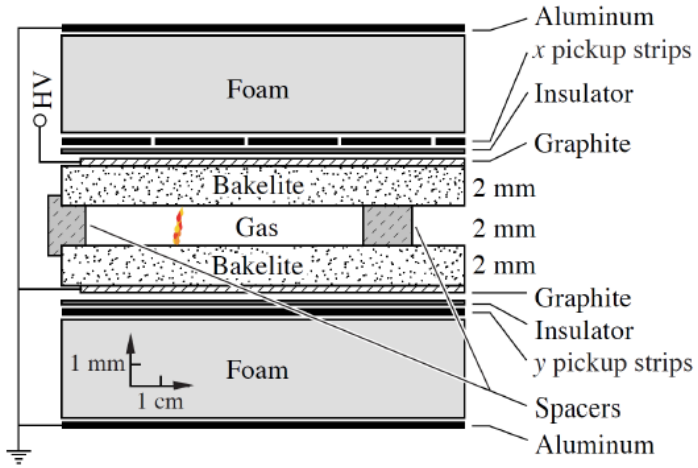

(a) Babar single gap RPC

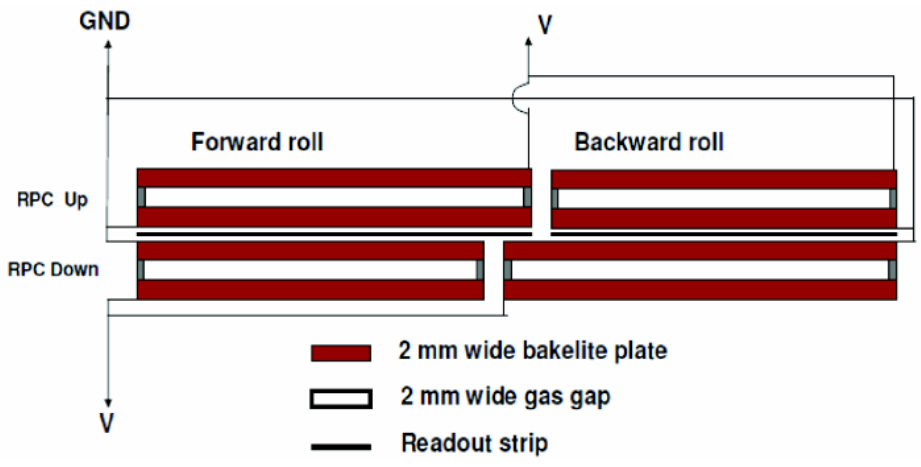

(b) CMS double gap RPC

Figure 5.2: A cross section of the BaBar single gap RPC with two layers of readout strips (left) [5] and a simple sketch of the layout of the double gap RPC installed in the barrel of CMS (right) [233].

Single Gap RPC

- Ar + i-C_4H_{10} & $C_2H_2F_4$
- Large signal ($\sim$ 300 mV, 10–100 pC)
- No need for Electronic Amplification
- Rate Capability of 40–100 Hz/cm^2 (for Bakelite, depends on ρ material)

Double Gap RPC

- $C_2H_2F_4$ (85–97%) + i-C_4H_{10} (2–5%) + SF_6 (0.1–10%)
- Small signal ($\sim$ 1 mV, 10 pC)
- Need Electronics for Amplification
- Rate Capability up to 1 kHz/cm^2

RPC Double Gap Layout

- Aluminium honeycomb frame
- Front End Electronics connected with coaxial cables to strips
- Strips run in between two gas gaps
- Gas gap coated with graphite (Surface Resisitivity of $10^5\,\Omega/\square$)
- High Voltage connected to graphite
- Gas gap made of 2 mm Bakelite (Bulk Resisitivity of $1\text{–}6\cdot 10^{10}\,\Omega$cm)
- Bakelite plates separated by 2 mm (gas gap) by means of spacers ($\varnothing$ 1 cm) on a 10 cm $\times$ 10 cm grid
- Gas gaps and strips wrapped in Cupper foil (Faraday cage)
- Mylar foils used as insulator
- Cupper pipes for cooling (Electronics)
- gas pipes, distributors, and in- & outlets

RPC Assembly Procedure

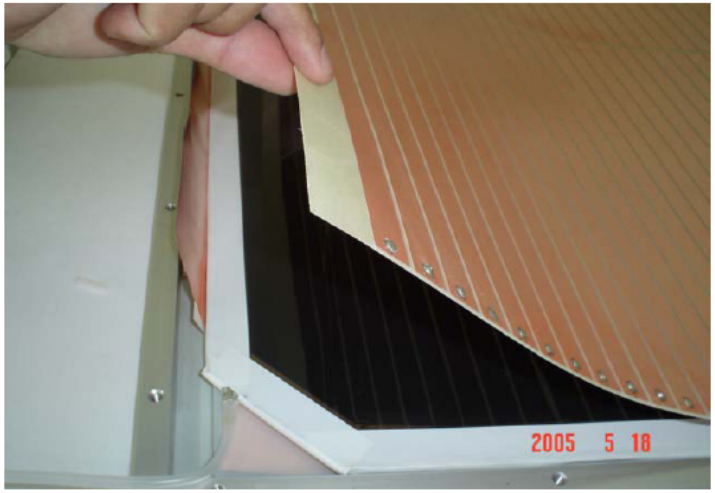

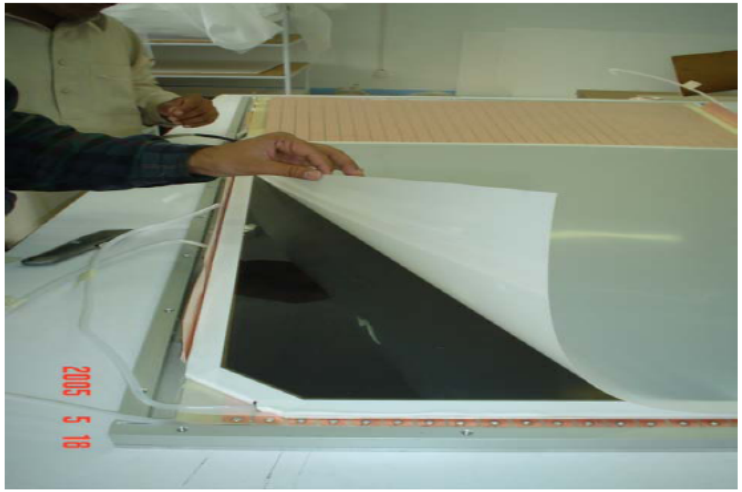

RPC Assembly Procedure

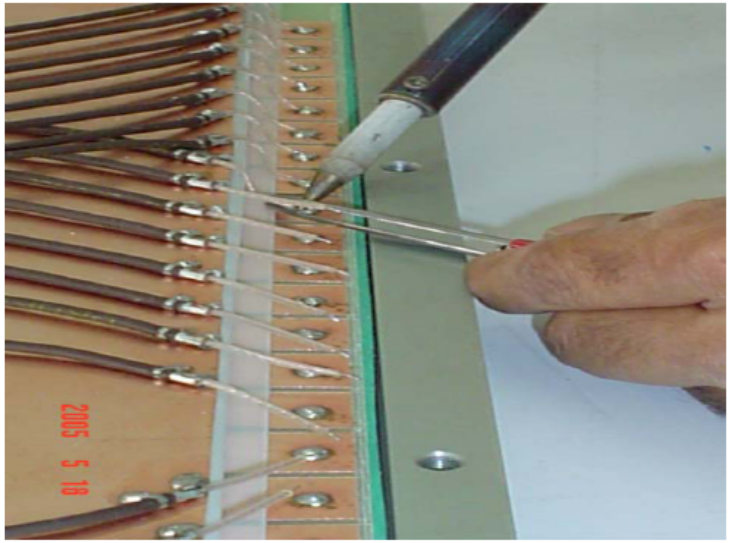

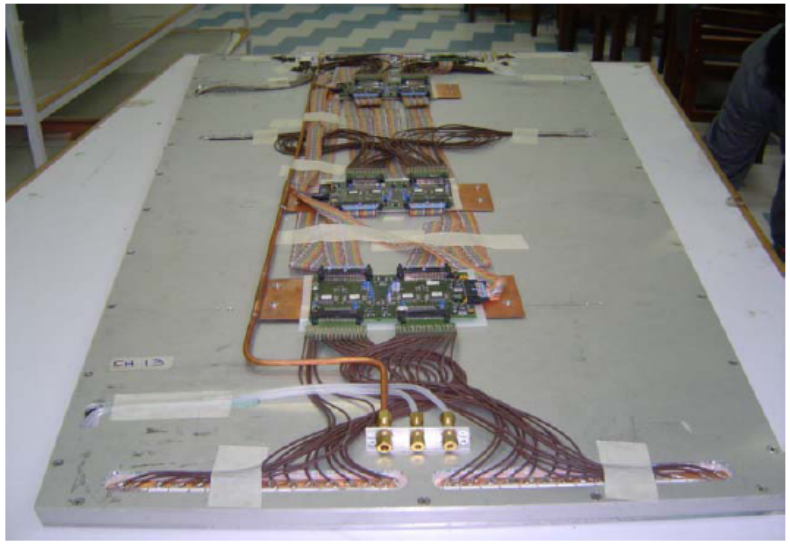

RPC Simplified Electric Model

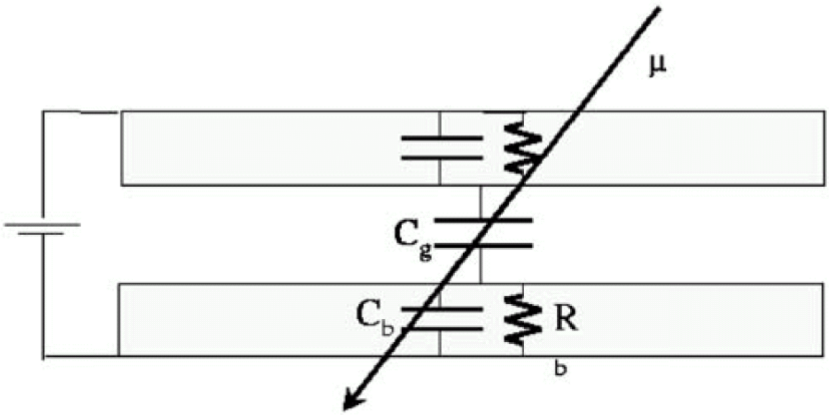

- Capacitors: C_b and C_g: $C = \epsilon_0 \epsilon_r \frac{A}{d}$
- Bakelite is resistive: $R_b = \rho \frac{d}{A}$

- RC-circuit: $\tau = RC = \rho\epsilon \approx 10\,\text{ms}$
- independent of area (A) or electrode thickness (d)
- dead time due to recharge is $\tau_{\text{recharge}} \approx 10\,\text{ms}$
- Larger resitivity ρ results in longer time for recharging the bakelite
- High rate capability needs bakelite of low-resisitivity!

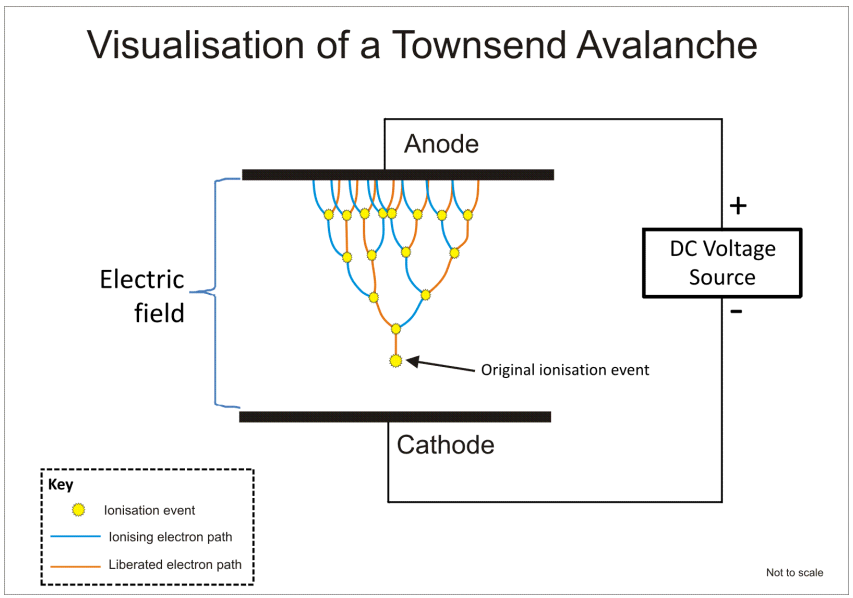

- Townsend: $I = I_0 \exp\left[(\alpha - \beta)x\right]$
- $x = v_d \cdot t = \mu \cdot E \cdot t$ and $\eta = \alpha - \beta$
- $I = I_0 \exp\left(\frac{t}{\tau}\right)$
- $\tau_{\text{avalanche}} = (v_d \cdot \eta)^{-1} \approx 1\,\text{ns}$
- $\tau_{\text{avalanche}} \ll \tau_{\text{recharge}}$
- discharge snuffed $\Rightarrow$ limited discharge
- rest of detector stays sensitive: dead area $\approx$ few cm^2

RPC Rate Capability

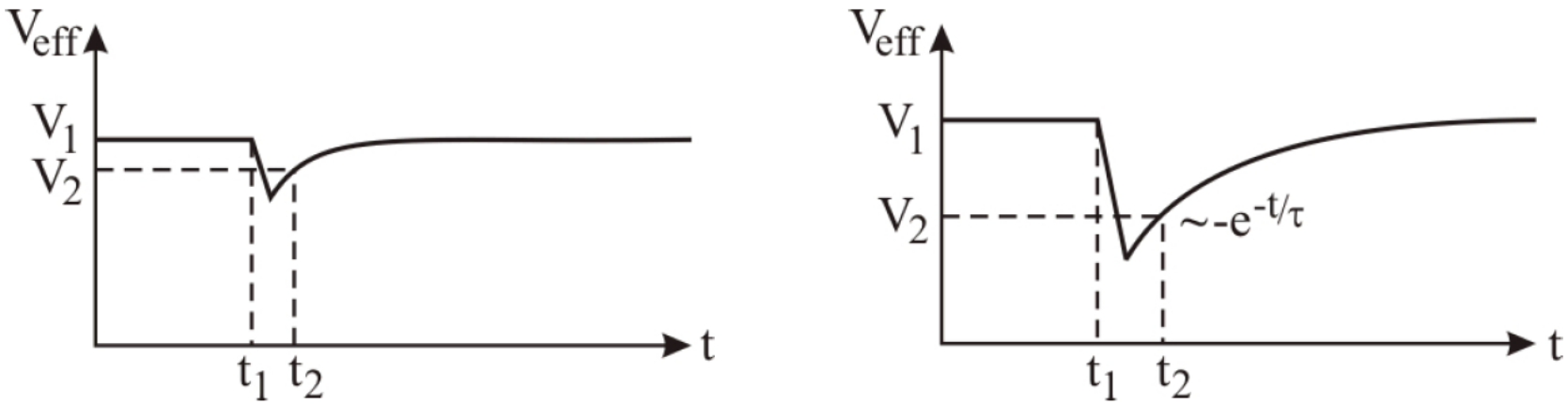

Figure 5.5: The voltage drop due to an avalanche (left) and a streamer (right) at time t_1. A second charged particle passing through the gas gap at t_2 experiences a different effective voltage V_2. In case of the avalanche the effective voltage is high enough to produce an avalanche, while in case of the streamer, the effective voltage is to low to create an avalanche and the detector is inefficient.

RPC Electric Model

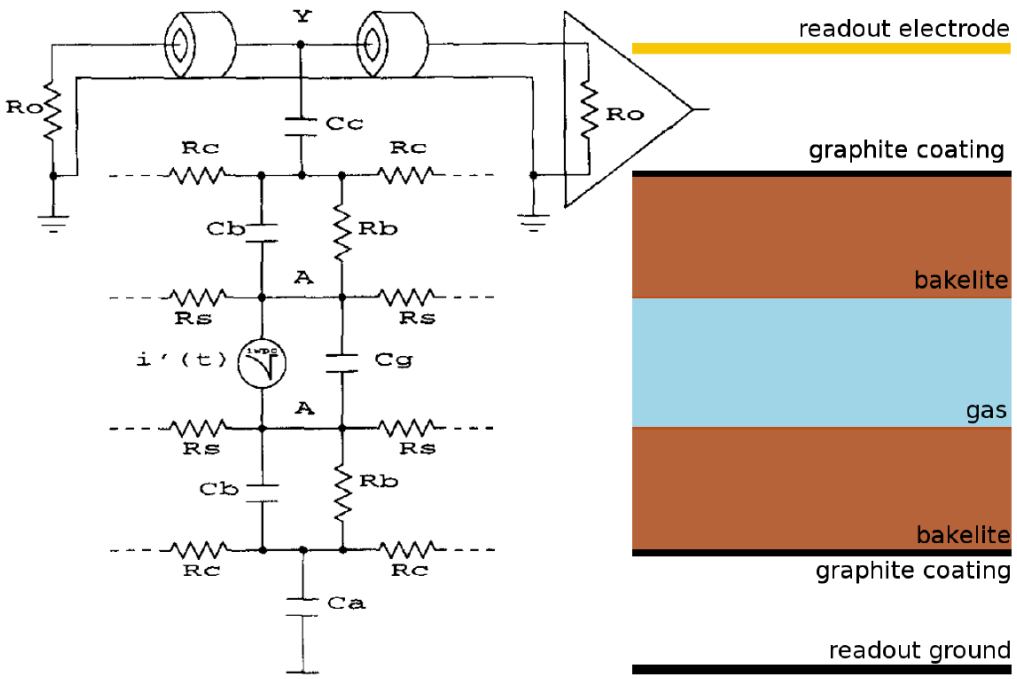

Coupled Signal

- Surface resistance of bakelite (R_s)
- Surface resistivity of graphite coating (R_c)
- Read out strips capacitively coupled (C_c) to the coating
- Coating act as high-pass filter
- $f_c = \frac{1}{2\pi R_c C_c} \approx 0.5\,\text{MHz}$
- $1\,\text{ns signal} \Rightarrow f \approx 2 \cdot 10^7\,\text{GHz}$

RPC Front End Board

Front End Board

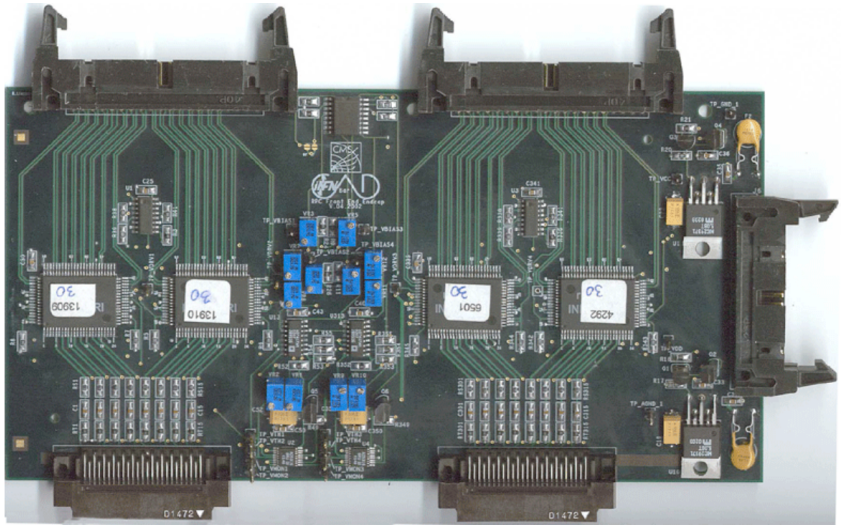

- Front-End electronics have chips with CFD
- New pulse with length of 100 ns (mask reflections)
- Dead time of 3 BX for a fired strip

Constant Fraction Discriminator (CFD)

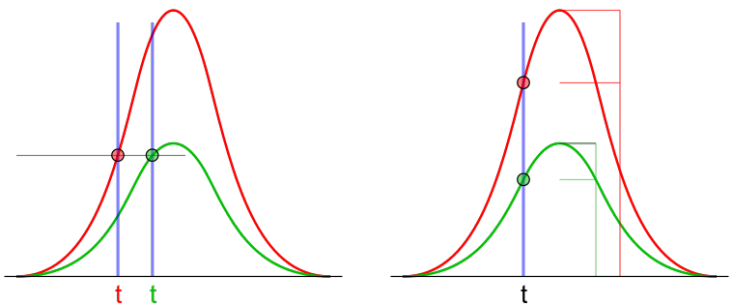

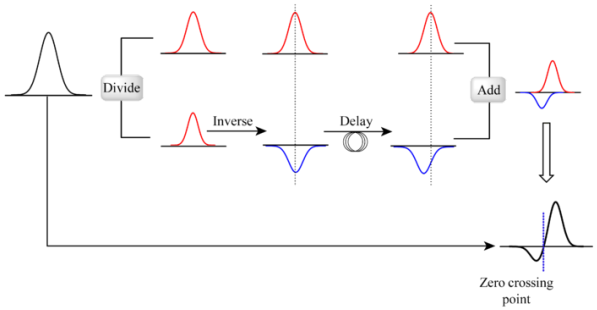

RPC Front End Board

Constant FractionDiscriminator (CFD)

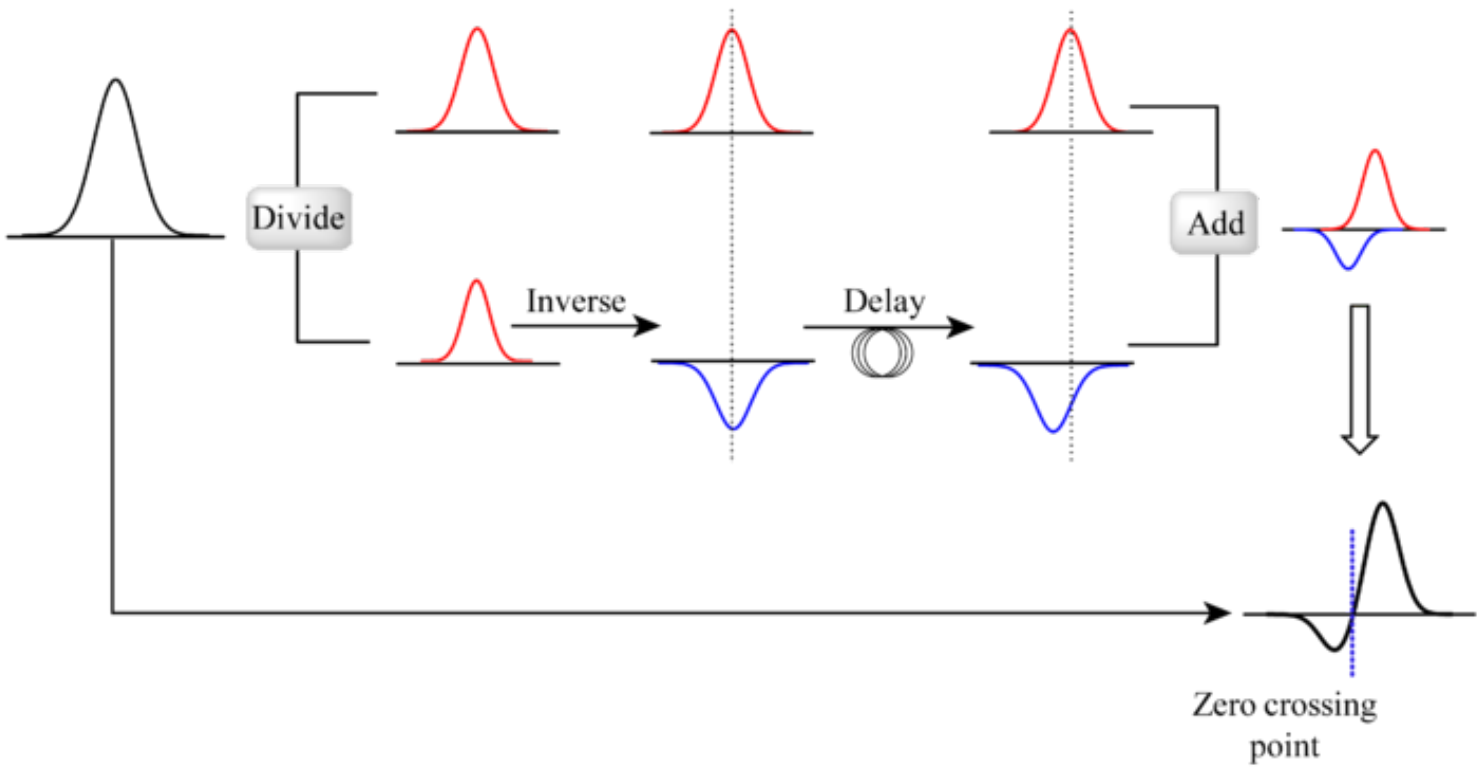

RPC Simulation

- Simulation starting with the generatio of primary ion-electron clusters and ending with the calculation of the induced current on the pick-up electrodes
- Induced charge on the electrodes:

$$q_{\text{ind}}(x = g) = \frac{k}{\eta g} \sum_{\text{clusters}} q_e n_0 M k \left[e^{\eta(g - x_0)} - 1 \right]$$

  - q_e being the electron charge $(-e)$
  - η being the effective Townsend coefficient
  - g the gap width
  - x_0 the initial distance between cluster and anode
  - n_0 the initial number of electrons in the cluster
  - M the avalanche gain fluctuation factor (from a Polya distribution) describing the stochastic fluctuations of the exponential growth of the avalanche
  - k a geometrical factor (not all charge being read out by pick-up electrodes
- Induced charge is core observable of the simulation
- Induced current follows from Ramo-Shockley theorem:

$$i_{\text{ind}}(t) = -q_{\text{ind}} \left(t = \frac{x}{v_d} \right) \cdot \vec{v}_d \cdot \vec{E}_w$$

  - $\vec{v}_d$ the drift velocity
  - $\vec{E}_w$ the weighting field

RPC Simulation

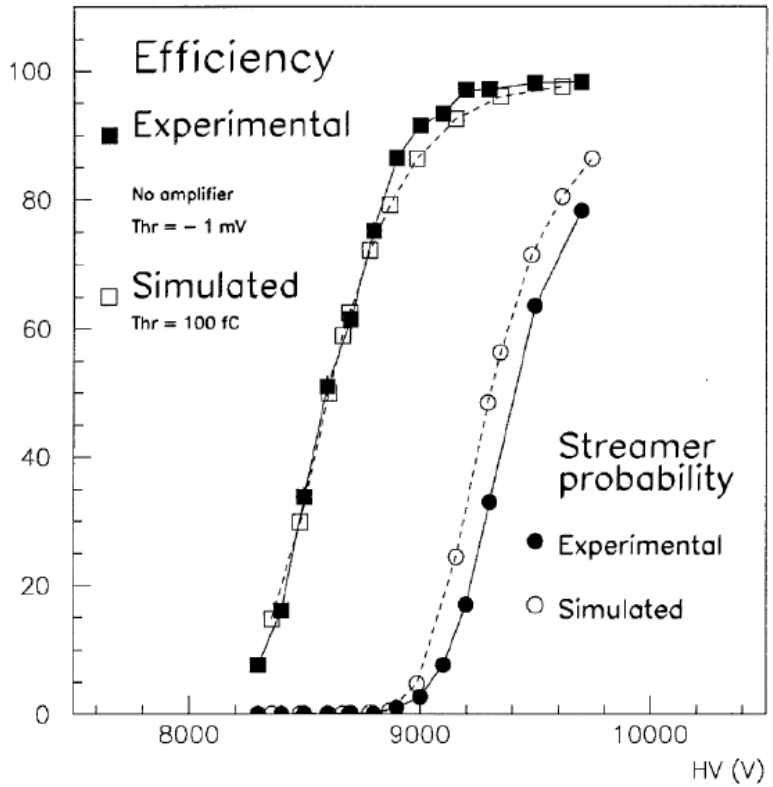

Figure 5.7: Simulated and experimental detection efficiency and streamer probability for a single 2 mm gap RPC with a 90/10 $C_2H_2F_4$/i-C_4H_{10} mixture. Figure taken from Reference [241].

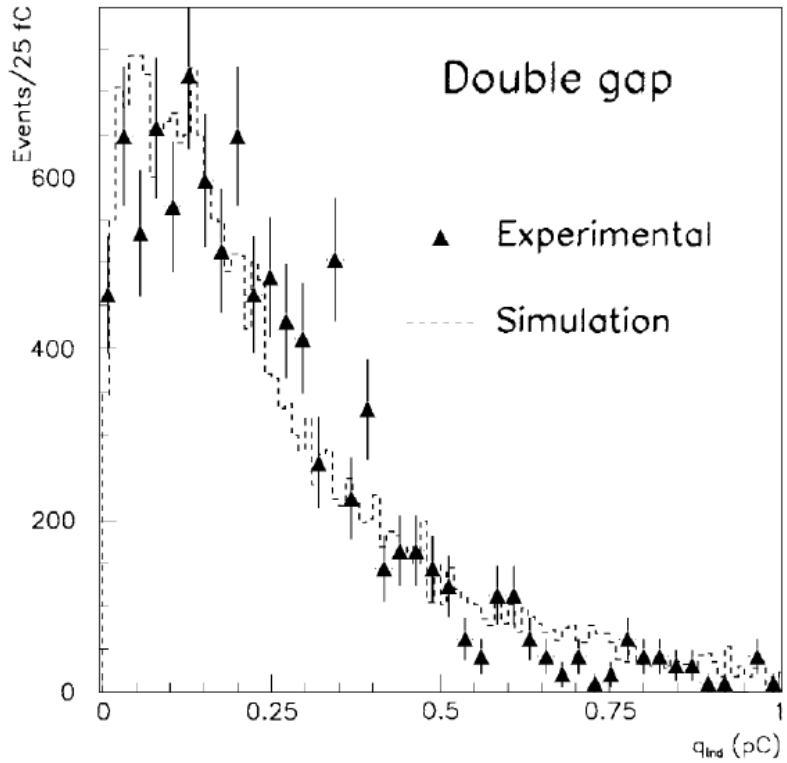

Figure 5.8: Simulated and experimental charge distributions for a 2 mm double gap RPC with a 90/10 $C_2H_2F_4$/i-C_4H_{10} mixture. Figure taken from Reference [241].

- Description of steamers require more detailed simulations considering space charge screening

RPC gas gap width

- **High detection efficiency** and **small time resolution** are governed by **width of the gas gap** and the **composition of the gas mixture**
- Simulations were used to determine optimal gas gap width
- Number of primary clusters generated by the ionizing particle per unith lenght $\lambda \approx 5.5\,\mathrm{mm}^{-1} \Rightarrow$ minimal gas gap width

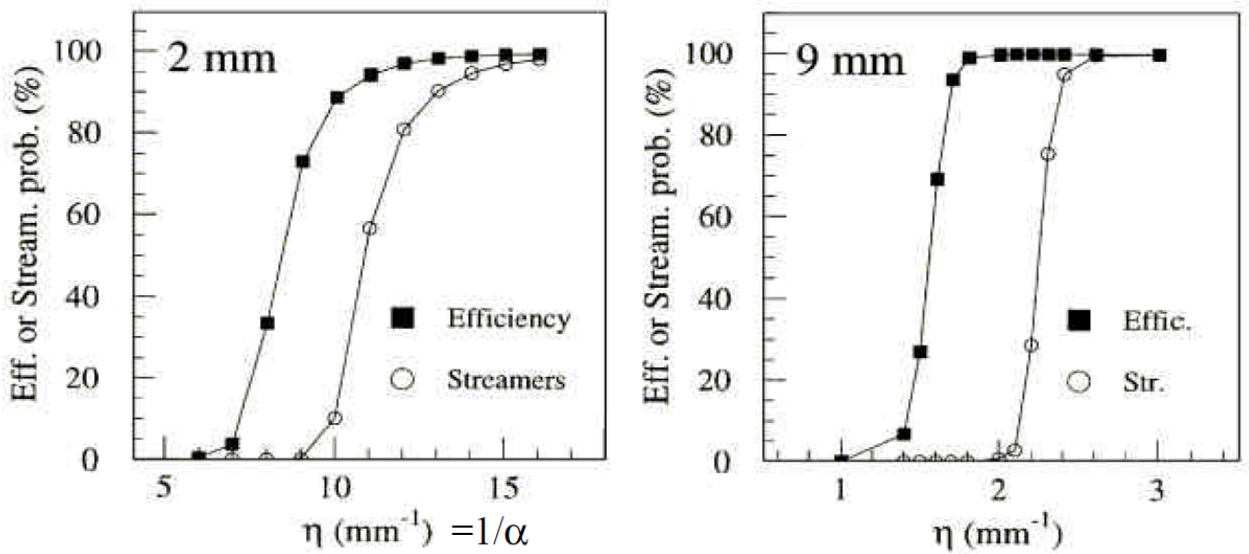

- Large gap provides better efficiency plateau but worse time resolution
- 2 mm gas gap was found to be a good compromise between detection efficiency $> 98\,\%$ at a time resolution of 2 ns

RPC Gas Mixture

- 95.2 % Freon (R134a – $C_2H_2F_4$)
- 4.5 % Isobuthane (i-C_4H_{10})
- 0.3 % Sulfur Hexafluoride (SF_6)

SF_6

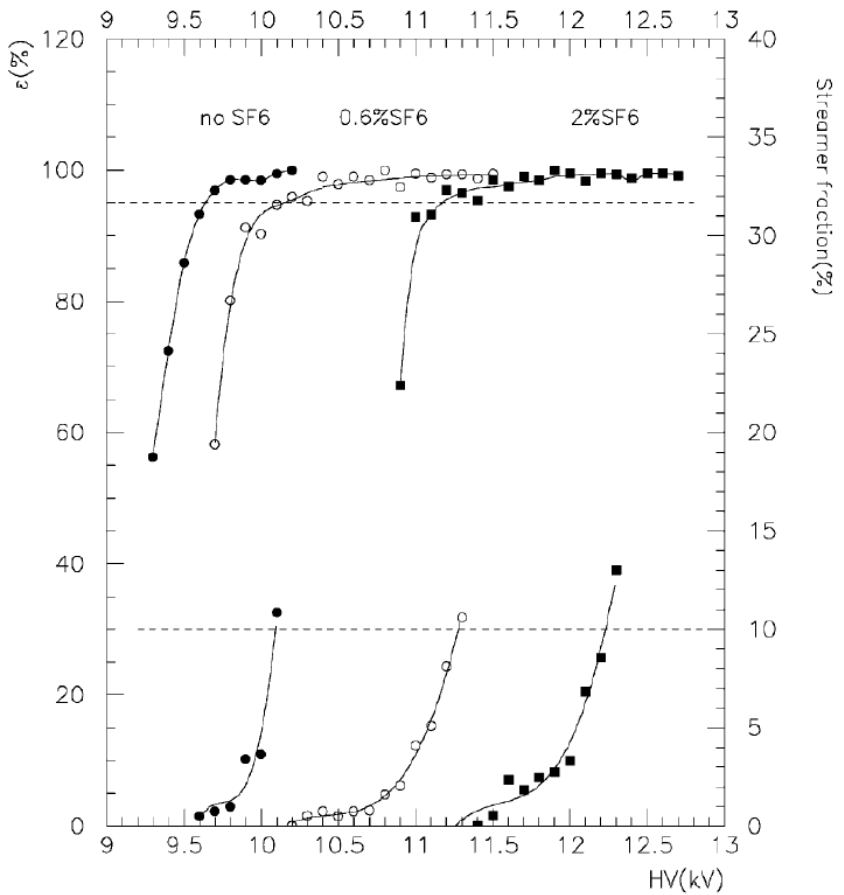

Freon

- high electron drift velocity ($\rightarrow$ timing!)
- limited ozon-depletion power
- new refrigerant replacing CFCs (Cl$\rightarrow$F)
- low cost, easy to find
- non-negligible greenhouse effect (only discovered later $\rightarrow$ replace in 2020)
- high density (high primary ionization)

Isobuthane

- absorb UV-photons
- transverse growth of avalanche deteriorates spatial resolution, reduces rate capability and limits detector lifetime
- max 5.5 % (flammable gas limit)

Sulfur Hexafluoride

- streamer suppression
- water vapour added to obtain relative humidity of 40–50 % (bakelite)

RPC effect of pressure and temperature

Gas density and **Bakelite resisitivity** depend on environment

Bakelite resisitivity

- **Bakelite resisitivity** depends on **temperature** and **humidity** (variations of factor 10)
- Low resistivity is key parameter to limit the discharge and hence to maintain high rate-capability
- $\Rightarrow$ stabilize **temperature** and **humidity**

Gas density

- Gas & Plasma physics: reduced Electric field E/p to describe density effect
- Townsend coefficient $\alpha \propto v_d \propto 1/\text{density} \Rightarrow \alpha/p = f(E/p)$
- Korff approximation:

$$\frac{\alpha}{p} = A \exp\left(-\frac{B}{E/p}\right)$$

RPC Temperature effect

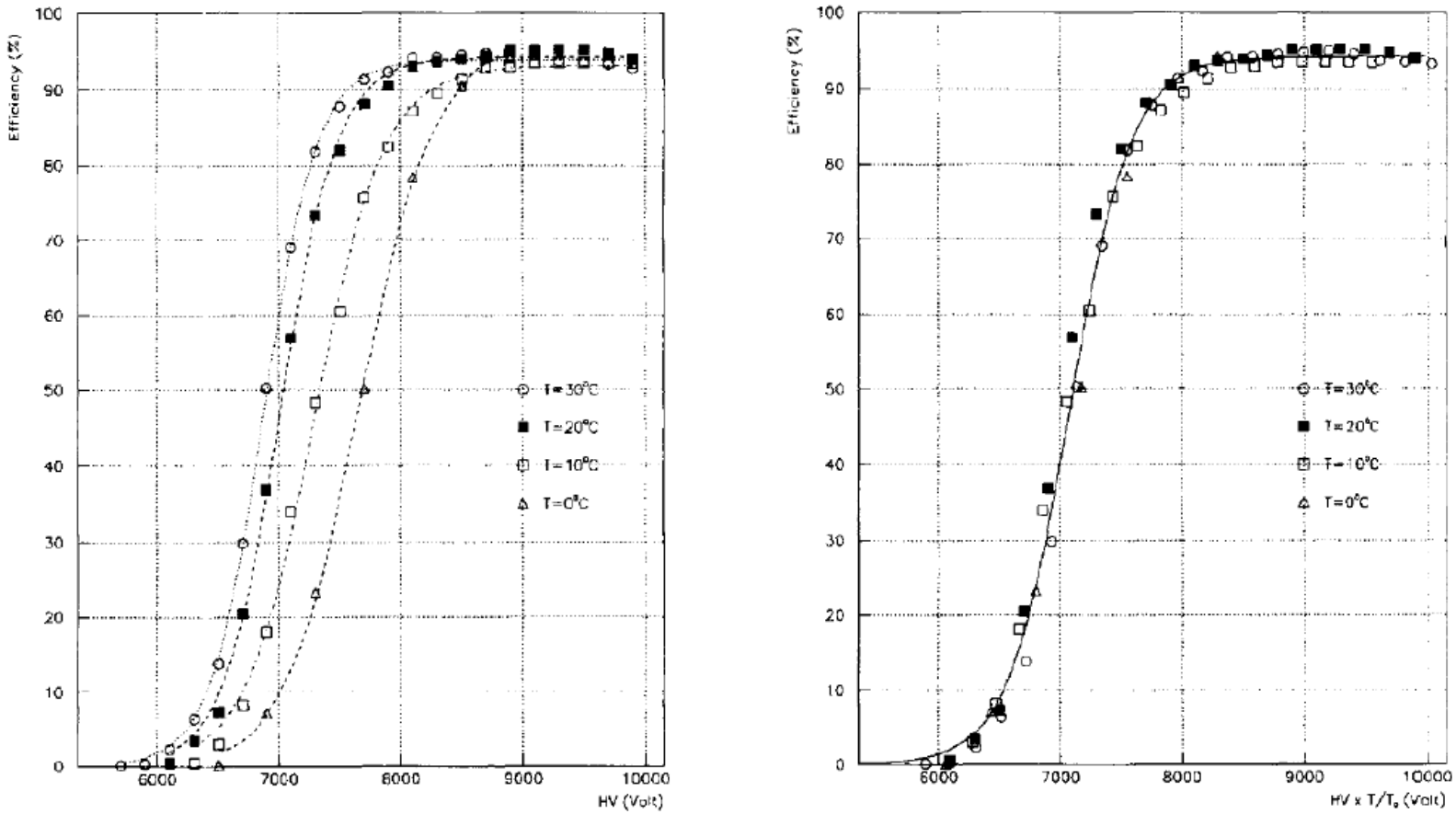

Figure 5.11: Efficiency for RPCs operated at 0, 10, 20 and 30°C as a function of their operating voltage (left) and as a function of a temperature corrected voltage $T/T_0 \cdot \mathrm{HV}$, with $T_0 = 293\,\mathrm{K}$. The RPC was a double-gap RPC with gas gaps of 2 mm and a 58/40/2 Argon/Butane/Freon (CF_3Br) gas mixture was used. Figure taken from Reference [267].

RPC Pressure effect

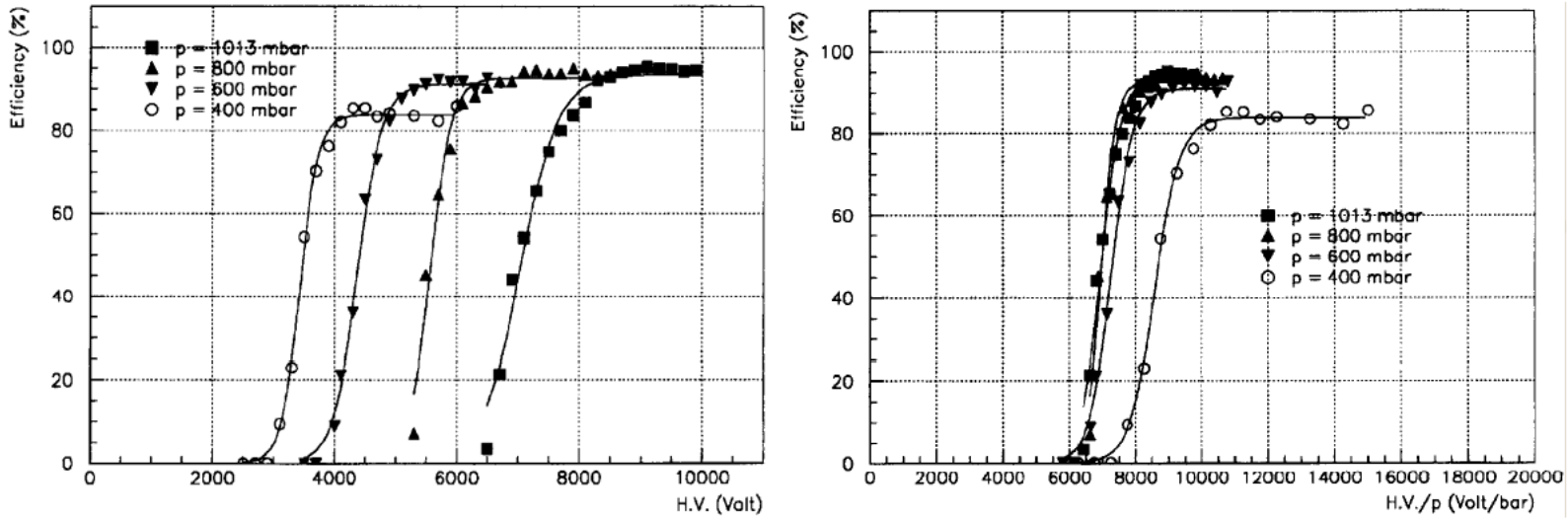

Figure 5.12: Efficiency for RPCs operated at 1013, 800, 600 and 400 mbar as a function of their operating voltage (left) and as a function of a pressure corrected voltage HV/p. The RPC was a double-gap RPC with gas gaps of 2 mm and a 58/40/2 Argon/Butane/Freon (CF_3Br) gas mixture was used. Figure taken from Reference [268].

Correction to reference temperature and reference pressure

- Temperature correction :: T/T_0 leads to unified efficiency curve
- Pressure correction :: p_0/p correction is not perfect.
- Since $\alpha \propto \exp p/E$ an additional term $\propto \ln p/p_0$ would be better
- First approximation:

$$HV_{\text{eff}} = HV_{\text{app}} \cdot \frac{p_0}{p} \cdot \frac{T}{T_0}$$

CMS RPC System

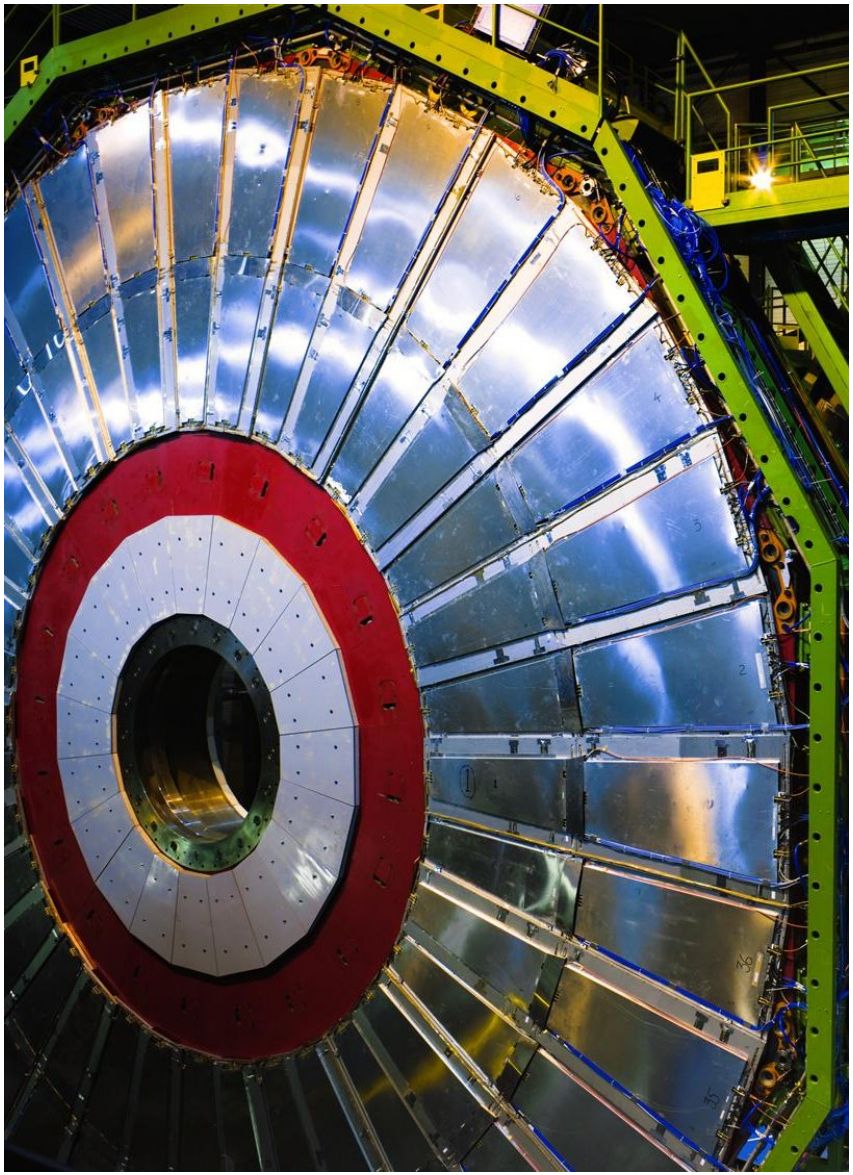

RPC System in numbers:

- Barrel and 2 Endcap regions ($|\eta| < 1.6$)
- 4 stations (4 concentric cylinders in the barrel, 4 disks in the endcap)
- Barrel: 480 chambers ($2285\,\mathrm{m}^2$)
- Endcap: 2×288 chambers ($895.6\,\mathrm{m}^2$)
- Barrel: 80640 strips
- Endcap: 42792 strips
- Total: 123432 strips

CMS RPC System

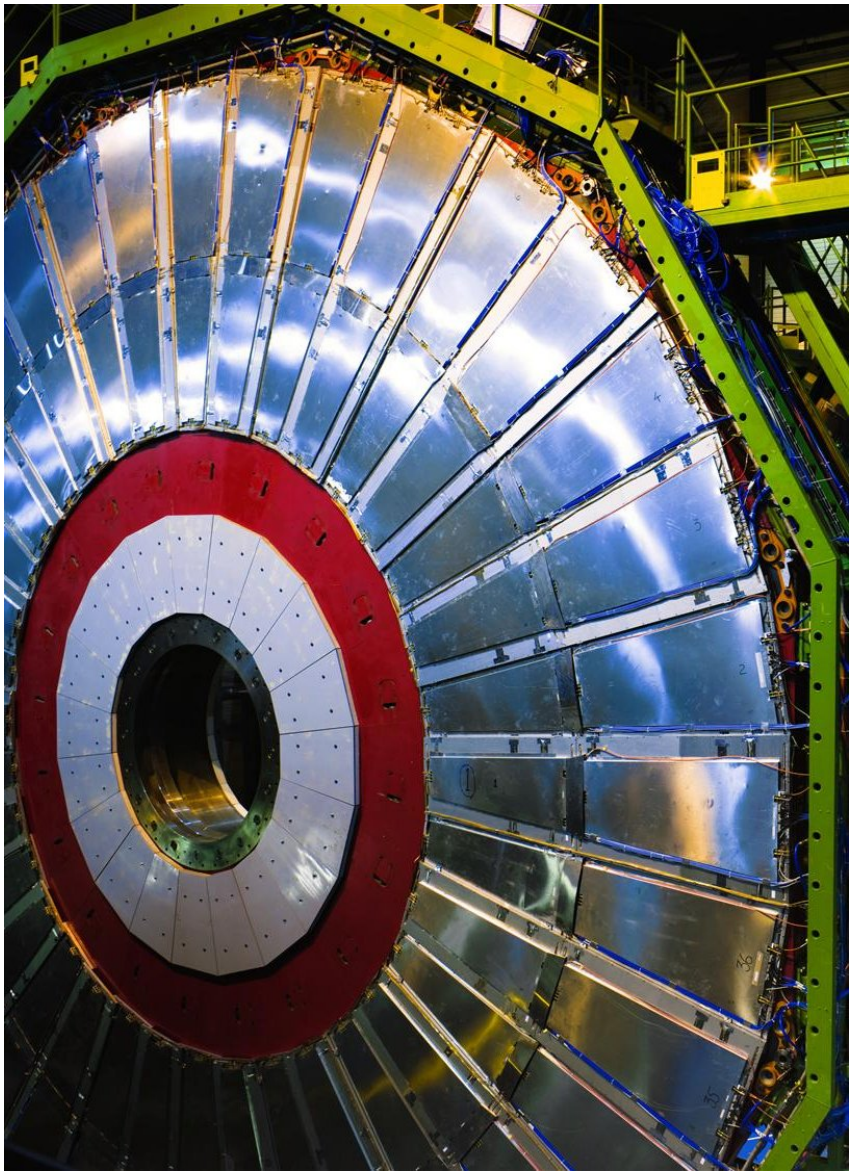

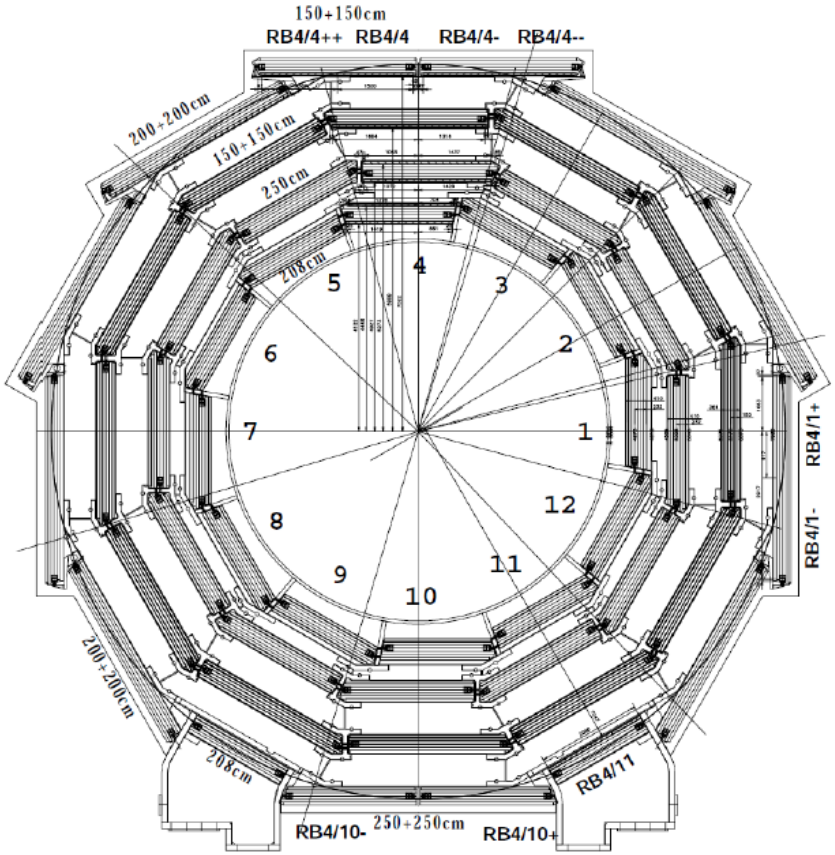

RPC Barrel

- 5 wheels
- 4 stations
- 12 sectors (30°)
- overlap in φ

CMS RPC System

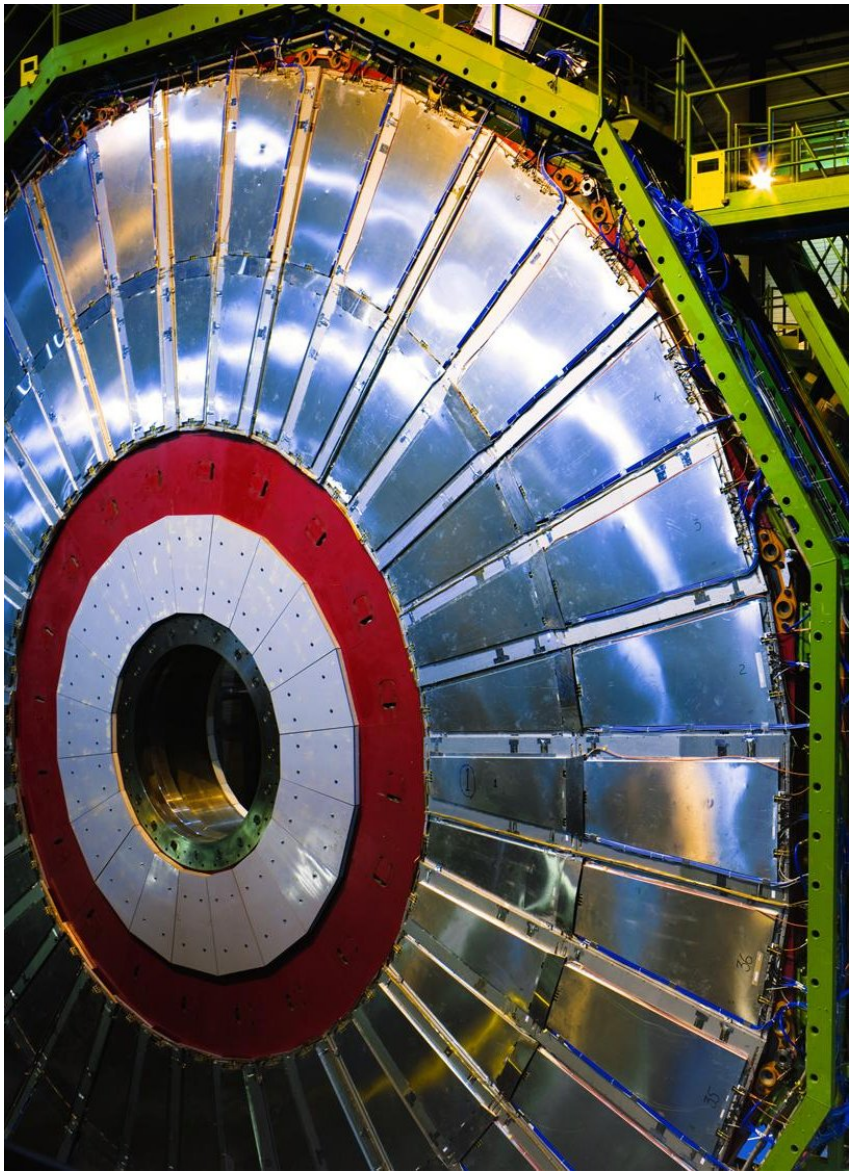

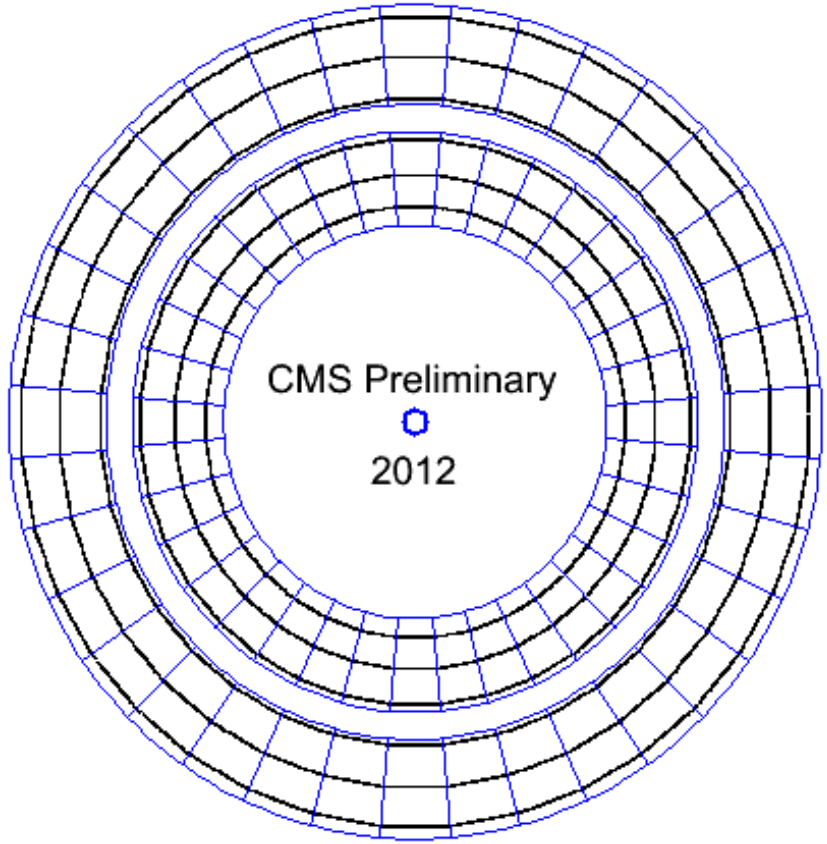

RPC Endcap

- 8 Disks
- 4 stations
- 6 sectors (60°)
- complete coverage in φ

Muon Alignment :: System

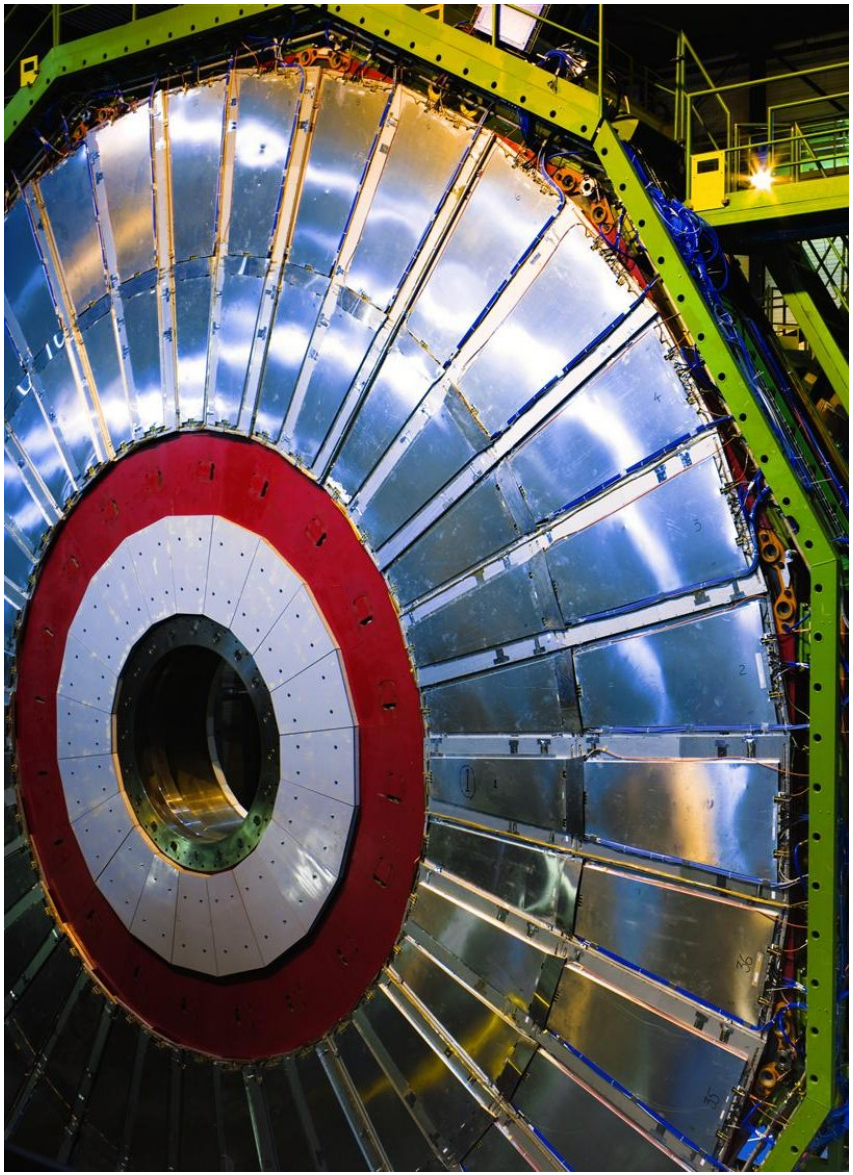

Muon Alignment System

Muon Alignment :: System

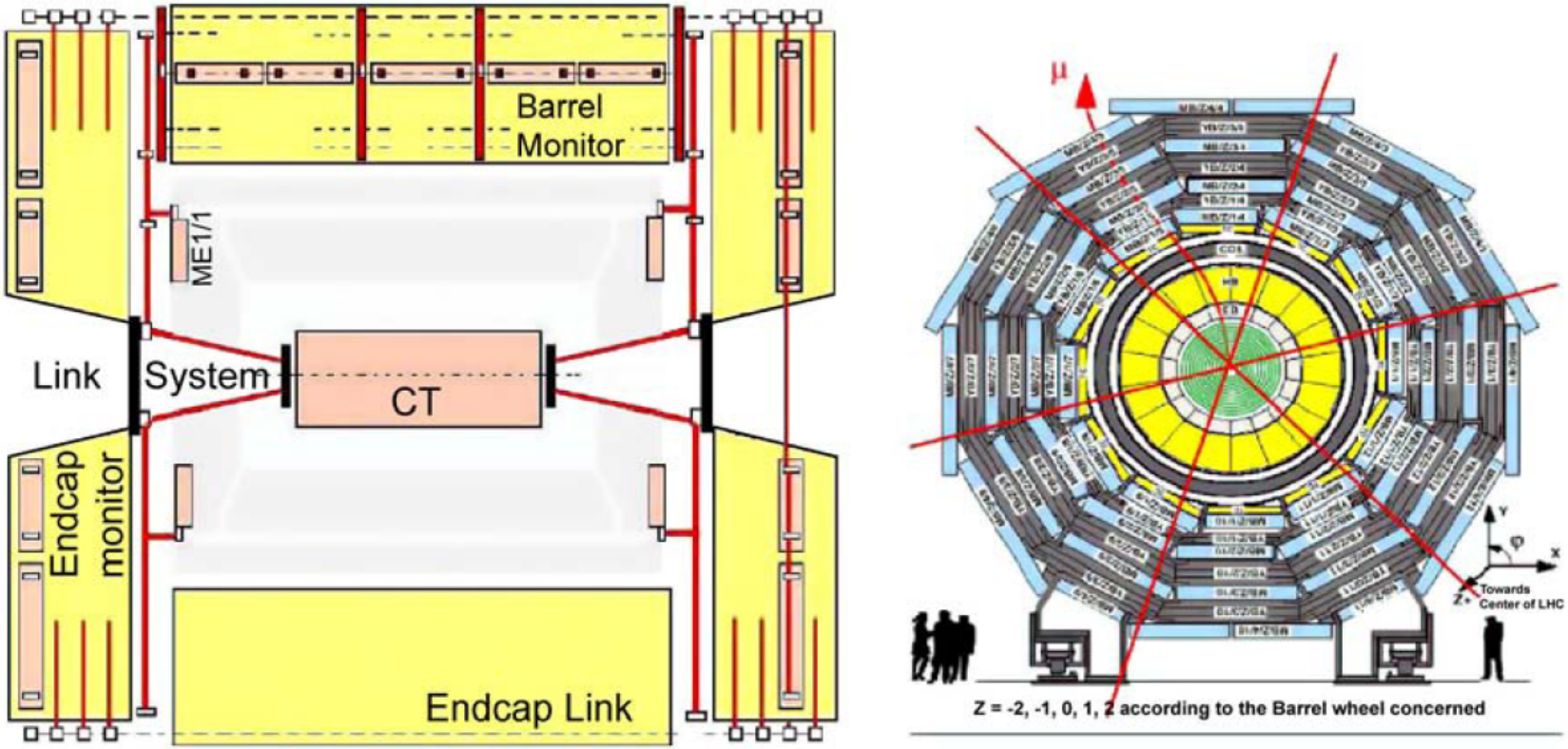

Figure 7.86: Schematic view of the alignment system. Left panel: longitudinal view of CMS. The continuous and dotted lines show different optical light paths. Right panel: transverse view of the barrel muon detector. The crossing lines indicate the r-z alignment planes with 60° staggering in ϕ.

Muon Alignment :: Forces on Endcap Disks

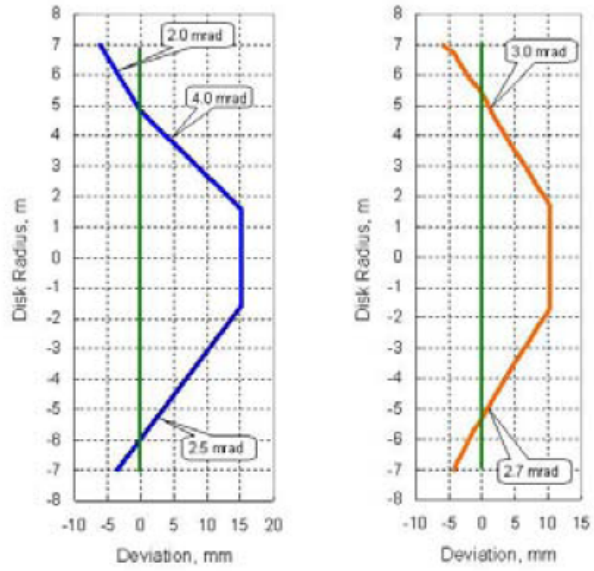

Figure 7.93: Comparison of the YE+1 disk deformations in the r-z plane at full magnetic field (4 T) measured by the alignment system (left panel) and predictions from finite element analysis (right panel). The vertical lines correspond to 0 magnetic field.

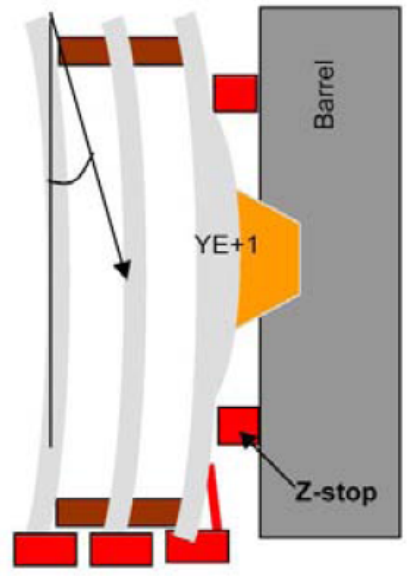

Figure 7.94: Current understanding of disk deformation due to magnetic forces based on alignment system measurements. The z-stops (red) prevent the disks from getting pushed into each other. Note that the indicated bending angle is exaggerated for illustrative purposes. Its measured magnitude is 2.5 mrad.

Magnetic Force on the endcaps is approx 7000 ton $\gg$ 900 ton of the individual endcap elements

Sources

- H.-C. Schultz-Coulon & J. Stachel — Physics of Particle Detectors [course notes] — http://www.kip.uni-heidelberg.de/~coulon/Lectures/Detectors/
- Werner Riegler — Fundamentals of Particle Detectors and Developments in Detector Technologies for future Experiments https://indico.cern.ch/event/24765/
- F. Sauli — Gaseous detectors Principles, Performance and Limitations — https://indico.cern.ch/event/124394/
- R. Veenhof — Gaseous detectors Principles, Performance and Limitations — https://indico.cern.ch/event/124394/
- A. Sharma — Resistive Plate Chambers: State of the Art for LHC — https://indico.cern.ch/event/a033218/
- Tim Cox — CSC Local Reconstruction — https://indico.cern.ch/event/210563/
- CMS Muon TDR — http://cds.cern.ch/record/343814
- CMS Trigger TDR — http://cds.cern.ch/record/706847
- The CMS experiment at the LHC — http://iopscience.iop.org/1748-0221/3/08/S08004
- The performance of the CMS muon detector in proton-proton collisions at $\sqrt{s} = 7$ TeV at the LHC — http://iopscience.iop.org/1748-0221/8/11/P11002